AN ADVANCED NON-INTRUSIVE LOAD MONITORING TECHNIQUE AND ITS APPLICATION IN SMART GRID BUILDING ENERGY MANAGEMENT SYSTEMS

A Dissertation
Presented to
The Academic Faculty

By

Dawei He

In Partial Fulfillment
of the Requirements for the Degree
Doctor of Philosophy in Electrical and Computer Engineering in the
School of Electrical and Computer Engineering

Georgia Institute of Technology

May 2016

AN ADVANCED NON-INTRUSIVE LOAD MONITORING TECHNIQUE AND ITS APPLICATION IN SMART GRID BUILDING ENERGY MANAGEMENT SYSTEMS

Approved by:

Dr. Thomas G. Habetler, Advisor
School of Electrical and Computer Engineering
Georgia Institute of Technology

Dr. David G. Taylor
School of Electrical and Computer Engineering
Georgia Institute of Technology

Dr. Ronald G. Harley
School of Electrical and Computer Engineering
Georgia Institute of Technology

Dr. Maryam Saeedifard
School of Electrical and Computer Engineering
Georgia Institute of Technology

Dr. Lei Zhu
School of Mechanical Engineering
Georgia Institute of Technology

Date Approved: Dec 15, 2015

This dissertation is dedicated to

my families and friends

ACKNOWLEDGEMENTS

Many people have come into my life, helped and supported me in every way during my study at Georgia Tech. Without you, it would not have been possible for me to finish this long journey.

I would like to express my deepest gratitude to my advisor, Dr. Thomas G. Habetler. His constant support and guidance have been invaluable. He has helped me grow technically and professionally. His patience, understanding, and humor have made this journey a much easier one for me.

I have the greatest respect and gratitude to all the faculty members and staff, from inside or outside of Georgia Tech, whom I have had the privilege to work with. I owe a lot to and Ronald G. Harley, who generously helped me on all kinds of problems in my life. I would also like to thank Dr. José A. Restrepo, who generously offered me his hardware experience. I would like to thank Dr. Yi Yang for her invaluable help and technical advices throughout my PhD study. Dr. Deepak M. Divan, Dr. Miroslav M. Begovic, and Dr. Santiago Grijalva are faculty members in the power group who have inspired me so much and brought to me different angles of power engineering. I would like to thank, Dr. Lei Zhu, Dr. Maryam Saeedifard and Dr. David G. Taylor for serving on my PhD proposal and defense committee and providing me with insightful suggestions. I would also like to extend my gratitude to Ms. Deborah King for being so patient and helping me with the numerous room reservations and lab orders.

My friends and student colleagues at Georgia Tech, especially those in the power group, have been an enormous source of energy, support, and inspiration. I would like to thank all of you for all the great moments. Dongbo Zhao, Siwei Cheng, Jiaqi Liang, Yi Du, Jing Dai,

Pinjia Zhang, Qin Sun, Yao Duan, Liang Du, Zhenyu Tan, Liangyi Sun, Hao Chen, Nan Liu, Evangelos Farantatos, Dustin Howard, Diogenes Molina, Frank Kreikebaum, Sangtaek Han, Zhaoyu Wang, R. Prasad Kandula, Rohit Moghe, Jorge E. Hernández, and Debrup Das are a few friends among the many who I want to express my special thanks for their help, friendship, and kindness.

I would like to thank my parents, Chunlong He and Jing Du, my girlfriend, Xiaobei Jiao who have always believed in me and gave me my strength and confidence in the early stage of my life.

Finally, I would like to thank all my best friends, Qianyao Xu, Mingxuan Li and Xiao Zhang, who has always been there for me, given me support during the most difficult time, and come along with me in every step through the entire journey.

TABLE OF CONTENTS

Page

LIST OF TABLE

LIST OF FIGURES

LIST OF ABBREVIATIONS

AC	Average current
ACD	Adaptive Critic Design
APP	Appliances
CART	Classification and regression tree
CCFL	Cold cathode fluorescent lamp
CCM	Continuous conduction mode
CDF	Cumulative distribution function
CF	Crest factor
CFHSMM	Conditional factorial hidden semi-Markov model
CrM	Critical conduction mode
DCM	Discontinuous conduction mode
DNA	Deoxyribonucleic acid
DOE	Department of energy
DR	Demand response
DSM	Demand Side Management
EE	Energy efficiency
EI	Eigenvalues of current waveforms
EMI	Electro-magnetic interference
EN	Envelope of the current waveforms
FDD	Fault detection an diagnosis
FFT	Fast fourier transform
FHMM	Factorial hidden markov model

FSM	Finite state machine
GFI	Ground Fault Interrupter
GCR	Global classification rate
GLR	General logistic regression
GMM	Gaussian mixture model
HMM	Hidden markov model
HVAC	Heating, ventilating and air conditioning
IA	Instantaneous admittance
ICA	Independent component analysis
IEC	International electro-technical commission
IOT	Internet of thing
IP	Instantaneous power
LASSO	Least absolute shrinkage and selection operator
LCD	Liquid-crystal-display
LED	Light-emitting diode
M	Complex structures loads
MCU	Multi-computing unit
MEL	Miscellaneous electrical loads
MFD	Multiple function devices
NILM	Non-Intrusive Load Monitoring
NP	Electronic loads without a power factor correction circuit
NREL	National renewable energy laboratory
P	Electronic loads with a power factor correction circuit
PAR	Peak-to-average ratio

PAC	Phase angle controllable loads
PC	Peak current
PCA	Principle component analysis
PCB	Printable circuit board
PCs	Personal computers
PEL	Plug-in electrical loads
PFC	Power factor correction
P&Q	Active and reactive power
PNNL	Pacific northwest national laboratory
PWM	Pulse width modulation
R	Resistive predominant loads
RF	Random forest
SOM	Self-organize map
SVD	Singular value decomposition
SVM	Support vector machine
T	Linear power supply using transformer to boost voltage
THD	Total harmonic distortion
X	Reactive predominant loads

SUMMARY

The objective of the proposed research is to develop an intelligent load modeling, identification, and prediction technology to provide granular load energy consumption and performance details and drive building energy reduction, demand reduction, and proactive equipment maintenance.

Electricity consumption in commercial and residential sectors accounts for about 70% of the total electricity generation in United States. Buildings are the most important consumers, and contribute to over 80% of the consumptions in these two sectors. To reduce electrical energy spending and carbon emission, several studies from Pacific Northwest National Lab (PNNL) and National Renewable Energy Lab (NREL) prove that if equipped with the proper technologies, a commercial or a residential building can potentially improve energy savings of buildings by up to about 10% to 30% of their usage. However, the market acceptance of these new technologies today is still not sufficient, and the reason is generally acknowledged to be the lack of solution to quantify the contributions of these new technologies to the energy savings, and the invisibility of the loads in buildings.

A non-intrusive load monitoring (NILM) system is proposed in this dissertation, which can identify every individual load in buildings and record the energy consumption, time-of-day variations and other relevant statistics of the identified load, with no access to the individual component.

The challenge of such a non-intrusive load monitoring is to find features that are unique for a particular load and then to match a measured feature of an unknown load against a database or library of known. Many problems exist in this procedure and the proposed research is going to focus on three directions to overcome the bottlenecks. They are

respectively fundamental load studies for a model-driven feature extraction, adaptive identification algorithms for load space extendibility, and the practical simplifications for the real industrial applications. The simulation results show the great potentials of this new technology in building energy monitoring and management.

CHAPTER 1 INTRODUCTION AND OBJECTIVES OF RESEARCH

1.1 Background of Building Energy Management and Research Motivation

The annual energy review prepared by the Energy Information Administration showed that the total electricity generation of the United States has grown up to 4.5 trillion kilowatt hours by 2011 [1], shown in Figure 1.1. The commercial sector and the residential sector consume 34.94% and 35.63%, respectively, of the total generation. Buildings are the most important consumers and contribute over 80% of consumptions of these two sectors. Recently, several studies from PNNL and NREL [2, 3] proved that if equipped with the proper technologies, a commercial or a residential building can potentially improve the energy savings by up to 10% to 30% of the usage. Therefore, there is still enough impetus from both the government and the customers to improve the building energy efficiency.

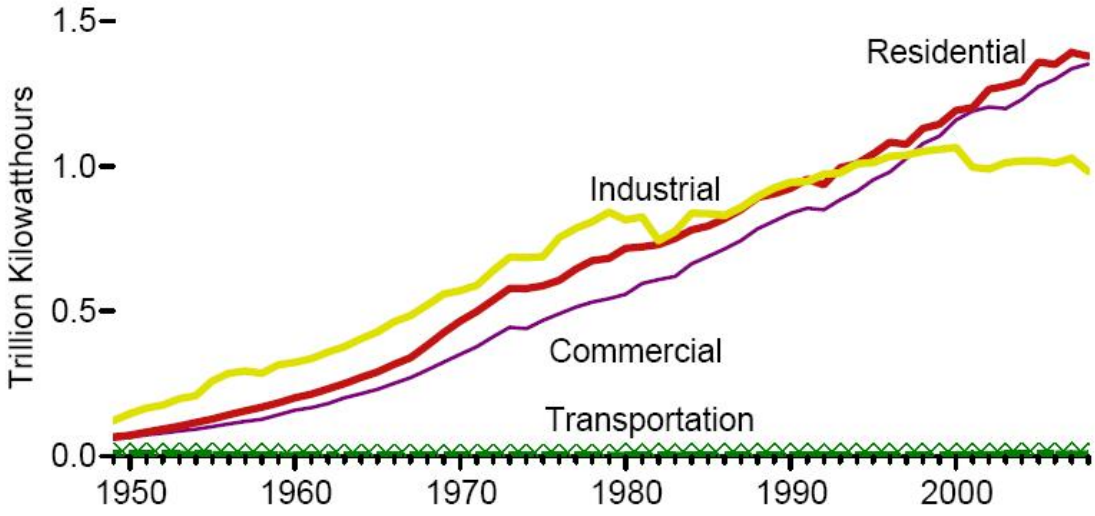

Figure 1.1 USA electricity retail sale by sectors from 1949 to 2011 [1].

The building-energy-management industry has already attracted millions of investments during the past decade, and some emerging technologies like daylight harvesting systems [4] and window shade systems [5] have already been commercialized. However, the market acceptance of these technologies is still at a relative low level, and some new players like Google and Microsoft have decided to exit the game after several years' test. A generally acknowledged reason of such a situation is the limited visibility of the contributions of these new products. A clear example is the programmable thermostats, which are used by less than 50% of home owners as a result of the lack of a clear analysis of the energy savings [6]. The majority of loads connected to a building today remain unidentified.

On the other hand, referring to the survey released by the Department of Energy (DOE) [7], 71% of customers reported changing their energy consumption as a result of accessing their energy usage information. Actually, in addition to benefiting those customers, a thorough understanding of the energy usage in a building benefits the infrastructure manager and the local utilities in many ways at the same time [8-10]. Therefore, it is necessary to develop such a monitoring technique to understand the energy consumption and wellness status of a building in an automatic and low-cost manner.

The traditional solution for building energy monitoring is usually based on the installation of large numbers of sensors [11-14]. The outlets or strips proposed by Intel [15], Belkin [16], and Google [7] are all able to provide the power-consumption information of every individual load after they are labeled as one type of load manually. This method is generally called *intrusive* monitoring [17]. This product needs pre-installation and pre-education before it can work properly. In this work, an attractive alternative called *non-intrusive* load monitoring, which equips the traditional monitoring system with intelligence to identify the loads, is presented [18]. To sum up, a non-intrusive load monitoring (NILM)

system can identify every individual load in buildings and record the energy consumption, time-of-day variations and other relevant statistics of the identified load, with no access to the individual component.

1.2 Introduction of Non-intrusive Load Monitoring (NILM)

The concept of NILM was first proposed in the 1980s [19, 20]. A conceptual framework of NILM system is shown in Figure 1.1. Generally, a NILM system is composed of five components, i.e., a data-acquisition module, a data preprocessor, a feature-extraction module, an identification or disaggregation module, and a load-management module.

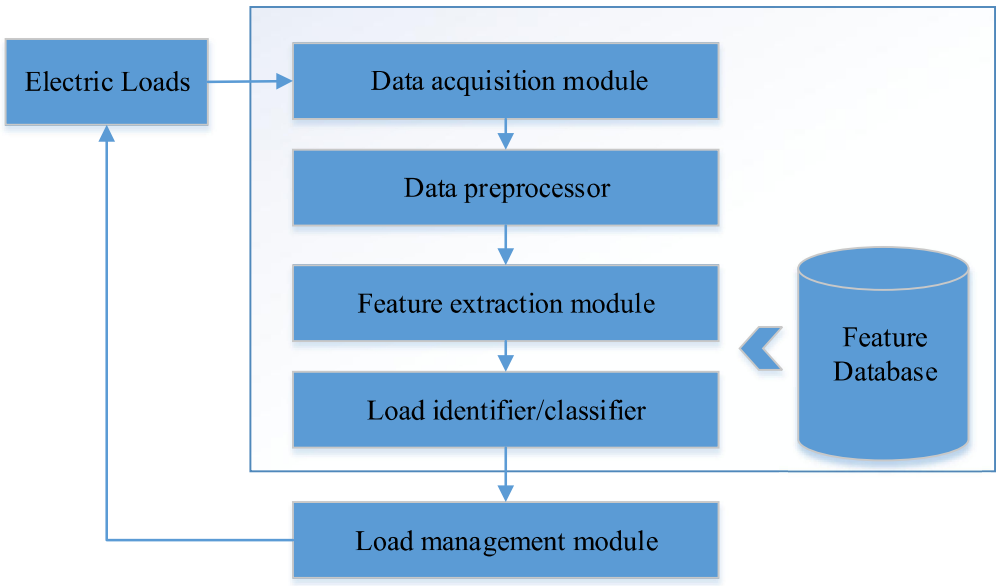

Figure 1.2 System structure for the non-intrusive load monitoring technology.

In a NILM system, the data-acquisition module and the data-preprocessing module are implemented based on the fundamental theory of digital signal processing. Two common ways to realize data measurement are (1) To insert an intermediate monitoring device between the socket and the appliance and then record its operation in a high sampling

frequency (over 1 kHz) and (2) To install the sensors at the main service entrance metering point in a low sampling frequency (below 1Hz).

The feature-extraction module and the identification or disaggregation module are usually regarded as the two more important parts of NILM, and these two modules require the knowledge of computational intelligence and machine learning. Over 90% of the works in NILM focus on these two modules [6, 21].

Using the information generated from the identification or disaggregation module, the load-management module provides granular load-energy consumption and performance details to drive building energy intensity reduction, demand reduction, energy optimization, and proactive equipment maintenance.

1.3 The Electrical Loads in the Residential and Commercial Sectors

Loads in commercial and residential buildings are commonly classified into space conditioning loads, water heating loads, ventilation loads, major appliances, lighting loads and miscellaneous electric loads, as shown in Figure 1.3 [22].

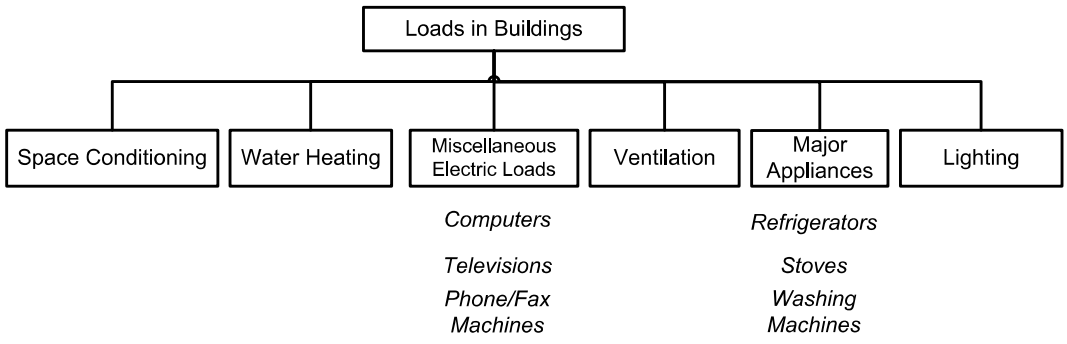

Figure 1.3 Classification of loads in commercial and residential buildings [22].

From the Annual Energy Outlook 2010 by the Energy Information Administration, the electrical energy consumption splits for commercial buildings and residential buildings are listed in Table 1.1 and Table 1.2 [22]. From the tables, lighting, space heating and cooling, water heating, and ventilation account for 70% of total electric energy consumption. Many industrial players have invested large amount of money on the energy savings of these high power electric loads [23-27]. This work will stand on these works and focus on the demand response or efficiency for the sake of utilities. Besides, the energy consumption of the miscellaneous electrical loads (MELs) can also constitute 30%-40% of the remaining energy use, which should not be overlooked. MELs, which can be also called plug-in electrical loads (PELs), are the small and diverse collection of energy-consuming devices, including what are commonly known as plug loads [28].

Table 1.1 Electric energy consumption for commercial buildings [22].

Loads in Commercial Buildings	**Electric Energy Usage**
Lighting	31.53%
Space Heating	4.73%
Space Cooling	15.99%
Water Heating	3.60%
Ventilation	8.56%
Electronics	9.46%
Cooking	0.90%
Refrigeration	5.18%
Computers	4.73%
Others	12.84%
Adjustment	2.48%

The energy potential of MELs can achieve 60-70% whole-house energy savings, and this percentage is likely to increase in the future as home electronics become even more sophisticated and their use becomes more widespread [29, 30]. Both these two groups of

loads will be studied while with different research targets in this dissertation.

Table 1.2 Electric energy consumption for residential buildings [22].

Loads in Commercial Buildings	Electric Energy Usage
Clothes Dryers	3.95%
Clothes Washers	0.34%
Color Television	4.48%
Cooking	2.90%
Dishwashers	1.30%
FA Furnace Fans	0.98%
Freezers	1.31%
Lighting	6.07%
Computer Monitors	0.39%
Desktop PCs / Laptops	1.40%
Refrigeration	4.84%
Space Heating	25.67%
Space Cooling	12.59%
Water Heating	10.67%
Home Audio Eq.	0.53%
Microwave Ovens	0.70%
Set-top Box	1.69%
All Other End Uses	19.56%

1.4 Opportunities for Non-intrusive Load Monitoring

The large portion of the total electricity consumption of buildings offers great opportunities for NILM to manage energy usage and consumption, reduce energy wasted by the vampire loads, and regulate the major high power electric loads for a demand response or energy efficiency program. There are a large number of ongoing NILM works for many purposes including energy saving, building fault detection, and demand response.

1.4.1 Energy Savings by PELs Identification

Energy auditing is one of the original targets for NILM. Recently, instead of the major high power loads, defined in Chapter 1.3, those vampire loads attracts more attentions because of their increasing amount of energy consumptions [31-33]. Several alliances and

standards on PELs management have been established.

Energy Star [34], as one of the alliances, indicates that standby PELs consumes more than 100 billion kilowatt hours annually and contributes to more than $10 billion in annual energy costs in United States. Proper PELs consumption management can result in as much as 75% standby power savings [35, 36] and 40 million tons of carbon emission reduction expected per year in United States [37].

Building America, a recent effort by DOE, has started to identify and reduce PELs consumption [38] and aims at 50% energy savings in new homes by 2015.

Comparing to the other major high power loads such as water heating and space conditioning appliances, PELs possess great and unique potentials to be efficiently managed in buildings since they can be directly controlled (e.g., turned ON/OFF) by the switches in power strips, main sockets, and power outlets in which PELs are plugged into [39].

To achieve the energy saving target, the energy auditing of these PELs becomes very important. Establishing a two-way communication between each household appliance and the customer-end (PC, Tablet, or Cellphone) is one way to realize this objective [40, 41]. However it might not be feasible in the real applications because most existing appliances don't have communication capability [42]. As an alternative, some smart outlets equipped with communication capability are introduced by many industry members and have been accepted by the customers, such as Belkin WeMo [16]. However, these smart outlets are still lack of the capability to identify the plugged load automatically. A manually labeling is required for all the existing products as for now. According to the survey from [43], over 80% of the customers will not change the label, even though some new loads are plugged in. This greatly increases the error rate of the energy auditing service. Therefore some automatic load identification solutions are highly expected.

1.4.2 Demand Response by Smart Meter Data Disaggregation

Different from the PELs management, many industrial providers like Siemens, Eaton, Schneider, etc. [23-27] have commercialized many energy auditing products for the major high power loads in commercial buildings. Their products actually have the capability to monitor these loads 7 days, 24 hours with a panoramic view. Therefore, the opportunities here are not in energy auditing but in collaboration with utilities on their demand response (DR) and energy efficiency (EE) program. Recently, many utilities in U.S. released the energy efficiency and demand response program for the residential customers [44-47]. Many efforts have been devoted to the demand-side management (DSM) of electric loads in residential and commercial buildings [48-56]. DSM of electric loads typically aims at improving system reliability, dynamic pricing [57], reducing energy consumption [58, 59], and introducing advanced real-time control [60-62], and load balancing [63, 64].

Typical demand response in buildings to reduce energy consumption during peak energy-consumption hours is achieved by a centralized building automation system with time scheduling. A number of such building automation systems have been designed and are available, such as “Lawrence Berkeley National Laboratory’s automated demand response system [65], and Pacific Northwest National Laboratory’s facility energy decision system (FEDS) [66].

However, from the perspective of the utilities, the baseline load modeling and auditing are the pre-requisite and should be conducted first by utilities to achieve their DR and EE programs [67]. Same as PELs monitoring, a direct idea is to establish a two-way communication between the loads and the well-developed central system to collect the usage and identity information. Many IOT eco-system providers like Apple [40], Google [68], and IBM [69] are targeting this market rapidly. However it is still too expensive and unrealistic

to embed communication accessories into the existing major high power loads in a short term and most loads today do not have communication capabilities [10]. Besides, from the perspective of utilities, only large and regularly repeatable using loads can be used as DR or EE [70], and meanwhile the utilities have large amount of smart meter data [71]. Naturally, NILM attracts their attentions again because NILM only utilizes the power signal at the main breaker level to estimate the states and power consumptions of the individual loads.

1.4.3 Fault Detection of Large Loads such as HVAC System

Nowadays, the heating, ventilating and air conditioning (HVAC) system accounts for over 45% of the energy consumption in buildings, and takes billions of kilowatt-hours every year [22]. It has been reported that 14% of the U.S. primary energy is consumed by the HVAC for commercial and industrial buildings and 32% of the electricity generated is consumed by the HVAC in commercial buildings [72]. Two biggest concerns of HVAC system are comfort and cost-efficiency [73]. The comfort is first considered by consumers, especially in specific locations such as the hospital and food storage room. As to the application in the general commercial and industrial buildings, the cost of the HVAC system can be another important factor, and most consumers are likely to choose the cost-effective ones. Most consumers are concentrating on the price of buying and installing an HVAC and air-conditioning system, while they often neglect that the cost in the future [74]. Actually, it may cost more due to the cost of energy consumption and high frequency requirements for maintenance, especially for some special applications like data center. The cost of maintenance is the major contributors for data center operation. In this way, a smart fault detection technology for the HVAC systems has been expected for many years. With a proper fault detection system, the imperfect operation can be figured out and the cost can be greatly saved by adjusting the HVAC to the perfect state [75-80].

1.5 Challenges of PELs Identification

In the aspect of PELs management, the measuring device is usually capable to reach each individual load and record every detailed change of the current and voltage of the load. The sampling frequency is usually higher than 1.92 kHz. The core idea of PELs management is to apply advanced digital signal processing technology on the raw data, generating a group of frequency domain and time domain features, to train the identifier based on the different pattern recognition algorithms. Theoretically, it should provide more information and therefore guarantee a better identification results than low sampling rate solution. However, several challenges exit and the study of high sampling based solution has been seen no progress for a long time.

In detail, despite the large set of features, there is still no a complete set of robust, widely accepted load features such that the variability of these features within classes is small whereas the interclass difference is large. It is not even known whether the existing features are really useful and efficient. As a result, when the input sample is a load whose model or operating status is not covered in the training set, the incorrect identification frequently occurs.

Besides, the load space is too large which results in the difficulty to define a universal load space of interest. What is worse, with the development of consumer electronics industry, new types, brands and models of appliances are emerging at a fast speed. This further increases the difficulty for load identification. Taking the TV as an example, the technique of the TV from ten years' ago is totally different from what is used for today, as shown in Figure 1.4.

Finally, the amount of data available for training is limited. No one can measure all the types of loads all around world to set-up a complete training dataset. This also impedes the

identifier to do a feasible learning.

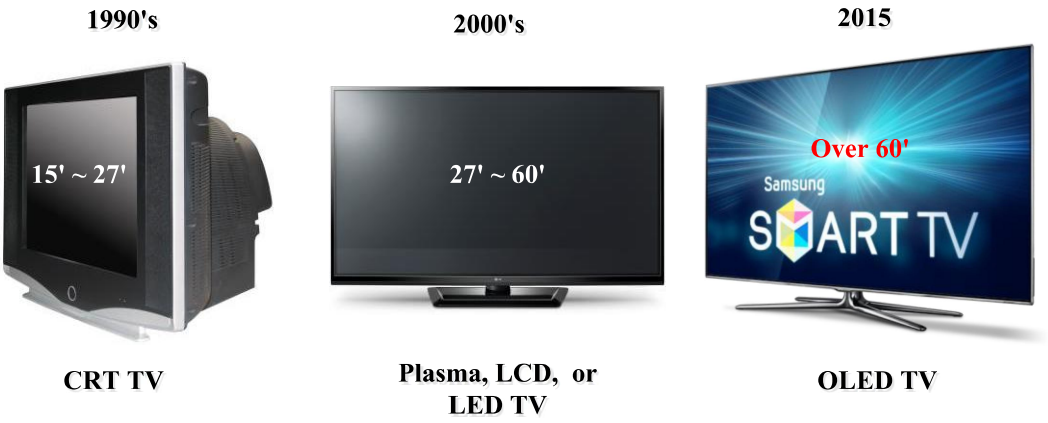

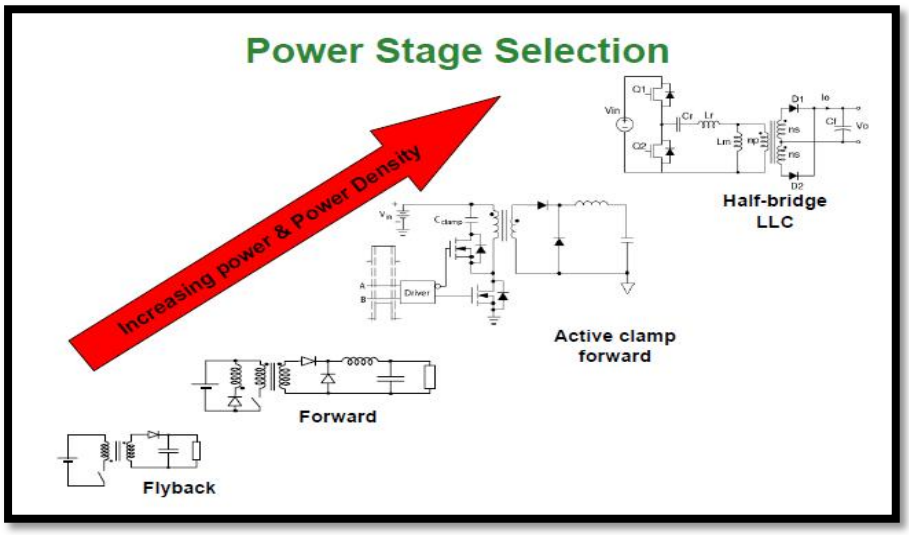

Figure 1.4 The technology trend of TV industry.

1.6 Challenges of the Major High Power Load Monitoring

In the aspect of the major high power loads monitoring, the measuring device is usually the smart meter, which records the real/reactive power of the entire home every five or fifteen minutes. Therefore it is a low sampling frequency solution. The smart meter is installed in the main service entrance of each residential home or building. The core idea is

to detect the power-change events and utilizes the change of real and reactive power to disaggregate the load underlying an event. However, the exiting solutions meet difficulties in distinguishing between loads with similar power consumption. In addition, it is still a challenge for most of studies to deal with the situation where two appliances change their states simultaneously, which is very likely to happen. These two theoretical challenges come from the nature characteristics of the low sampling data, which lose a large amount of useful information, as shown in Figure 1.5.

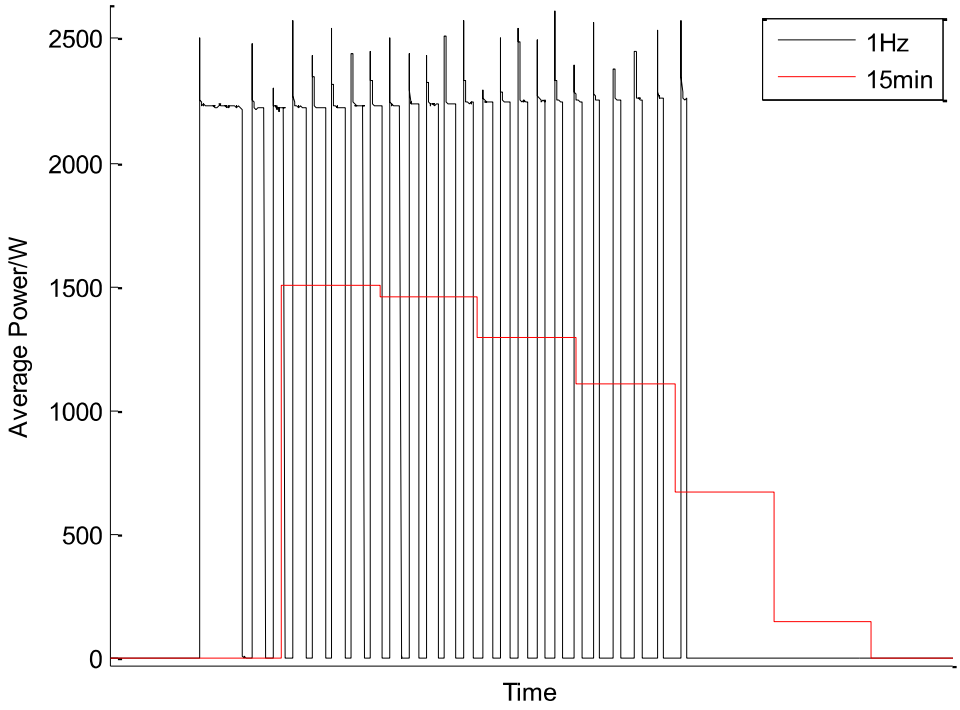

Figure 1.5 The difference between 1Hz and 15 minutes resolution data.

Moreover, from the perspective of the practical application, most existing solutions need supervised learning, i.e., individual load waveforms are required to estimate the parameters in the algorithm [81]. The user is also required to record the usage information

manually for a period of time at the beginning of the installation. The usage information is used to train the disaggregation module, which is typically not available for the real application. Although some existing works have proposed learning algorithms that do not need individual load waveforms, these algorithms still need generic load models (i.e., a priori load knowledge) or manual waveform selection [82, 83]. This challenge also makes the ground test for existing solutions very difficult.

Finally, the computation effort of the solution is too high for most of the algorithm. Since most of the measuring devices are only equipped with the basic multi-computing unit (MCU) and communication module [6]. It is impossible for the installed device to implement such an over complex algorithm. This also prevents the development of low-sampling frequency based solution.

1.7 Challenges of the Fault Detection of the HVAC System

There are a good number of papers and books concerning on the fault detection of HVAC with various approaches [84, 85]. One noticeable characteristic of these conventional conditioning monitoring methods is that they rely on a relatively extensive network of sensors [86-88]. Many of the methods have five or more temperature sensors, as well as pressure sensors [89], mass-flow sensors [90], and relative humidity sensors [91]. Even though these mechanical sensors can provide valuable information about the state of an air-conditioning system, their use in a conditioning monitoring method must be considered in the context of their cost and rate of failure.

The idea of NILM based fault detection of the HVAC system is to measure the currents and the voltages at the terminals of the electromechanical device, and then identify faulty mechanical behavior on the basis of these observations [92]. This represents an interesting and potentially viable alternative comparing to the traditional solutions. In effect, these

methods either use a signal-based approach, in which *a priori* knowledge is used to relate mechanical faults to particular features observed in the electrical sensor output, or a model-based approach, in which the observed inputs and outputs of the system are used to characterize the behavior of the system and determine the existence of any faults.

However, the existing NILM based fault detection solutions suffer from the following challenges which impede their applications in the real industry [92]. Firstly, the motors used in HVAC system are typically designed to be good energy conversion systems. They are not usually intended to be used as transducers, which makes it much harder to develop reliable conditioning monitoring methods. Moreover, there are mechanical faults which have no observable effect on the electrical variables because of effects like noise or scaling problems, such as arise for loads coupled through gearboxes. Finally, wide variety of mechanical changes is being mapped into a relatively small number of electrical variables, i.e. currents and voltages. This mapping can make fault isolation more difficult, since different types of mechanical faults sometimes have identical effects on the electrical variables. To deal with these problems, a comprehensive study on the physical model of the HVAC system is required.

1.8 Objectives of Research

Different applications of non-intrusive load monitoring can benefit different stakeholders. The objectives this research is trying to provide a complete non-intrusive load monitoring solution vertically for various customers, as shown in Figure 1.6.

In the aspect of residential customer, many studies have investigated the effects of providing consumers with feedback on their electricity consumption [93]. They suggest that the greatest savings result from appliance-specific feedback. Based on the survey [94-96], the most important reason why appliance information facilitates greater energy reductions is

that the technology enables automated personalized recommendations. Therefore this work targets a high-frequency load identification solution able to detect as much as loads by introducing an adaptive online learning mechanism. This new technology will automatically study the new loads by itself without the help from the customers.

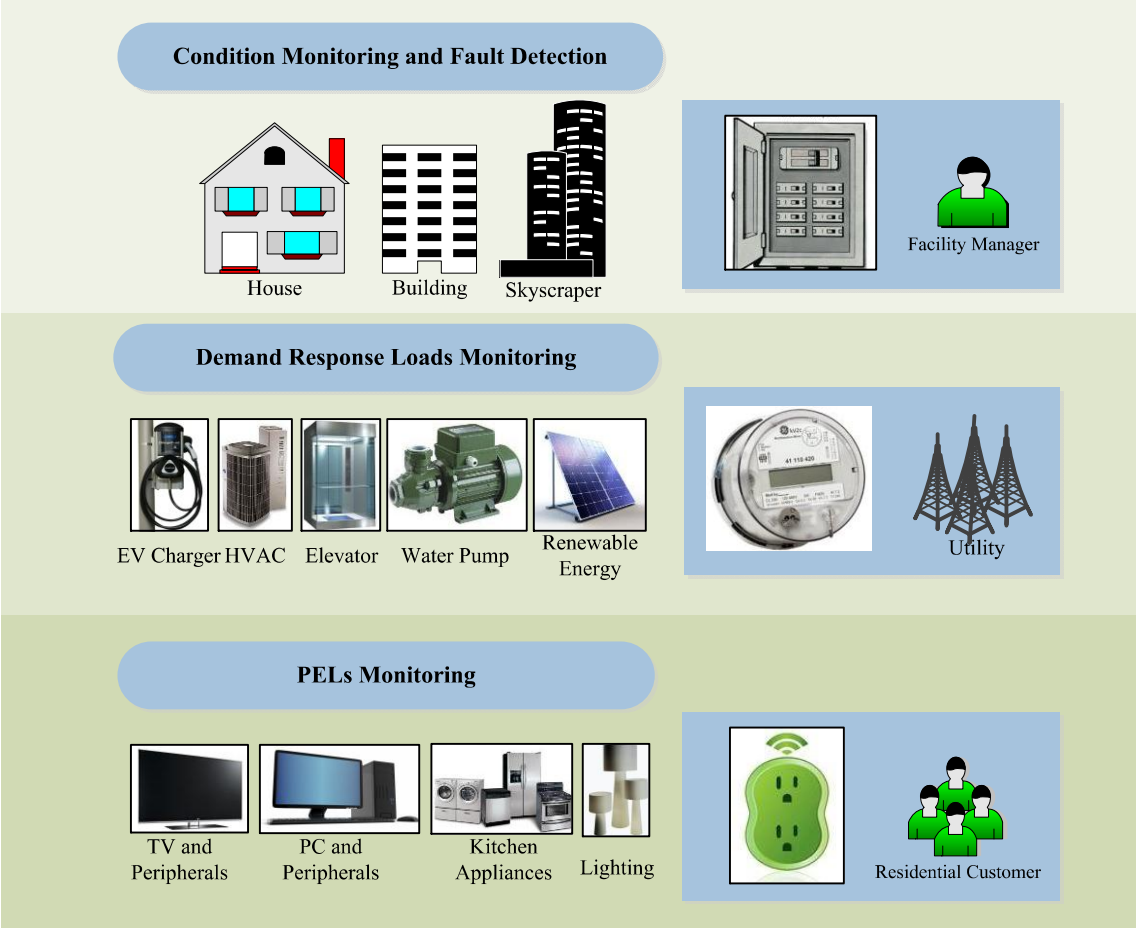

Figure 1.6 The research directions of NILM in this dissertation.

In the respect of utilities, the smart meter data disaggregation has the potential to improve the DR and EE marketing – by improving market segmentation, diversifying programs, and transforming program development and evaluation. Strategic use of historical energy consumption patterns would allow program designers to target individual consumers as well as whole communities with more specific recommendations and offers. For example,

knowing which consumers or consumer groups (residents, residential communities, businesses, or business sectors) are using energy through air conditioning, pool pumps, or old refrigerators, would allow program designers to target the most appropriate audiences with specific rebates and usage tips. The objective of this work is to using the smart meter data to disaggregate those demand responsive loads (air-conditioner, stove, washer/dryer, etc.) to improve the ability to predict energy demand annually and seasonally for utilities. Moreover, by conducting a statistical analysis on the disaggregated data, it also improves our understanding of energy consumption patterns, and this can be used to improve the representation of human behaviors in energy models. This may help policy makers better evaluate utility energy efficiency programs, and allow for better allocation of funds.

In the aspect of the facility manager, the fault detection technology is highly expected to improve the comfort level, energy savings as well as the system reliability of the buildings. HVAC system as most important the appliances, its maintenance and diagnosis will be studied in this work. The target of the research is to provide several diagnostic techniques based upon the output of electrical sensors installed in the HVAC systems. Such methods measure the currents and the voltages of the HVAC systems, and then identify the faulty mechanical behavior on the basis of these observations.

In detail, the proposed research is going to focus on four major works.

1. **Model-driven Feature Extraction**: A fundamental study on front-end electronic circuit topology and electrical operation principles of the majority of loads are presented. This study looks at the available features from the model-drive perspective and therefore brings a more robust and efficient feature space. Some new features are also introduced.

2. **Adaptive-learning Identification Algorithm**: A random forest based algorithm is introduced here to cope with the online requirements. This new algorithms promise the future application of NILM in building energy industry.
3. **Human-Behavior based Load Disaggregation Algorithm**: A Hidden Markov Model (HMM) algorithm is introduced to deal with load disaggregation for smart meter data. To cope with the challenges of disaggregation, some human behavior based features are incorporated into the algorithm to promise the performance of the solution.
4. **Electrical Measurement Based HVAC Fault Detection**: The physical model of the HVAC system is well studied to form the basis of the work. The frequency domain features are applied to act at the index for different condition for HVAC system. The traditional non-intrusive fault detection works for electric motors are seamlessly integrated in the proposed work.

1.9 Dissertation Outline

The rest of this dissertation is organized as follows:

Chapter 2 provides a comprehensive literature review on the existing methods and techniques pertinent to the proposed research.

Chapter 3 proposes a load space and feature study based on the survey of front-end electronic circuit and electrical operation principles for different loads. This study firstly provides a new taxonomy for current load space and then extracts a high-efficient feature set for the following study.

Chapter 4 introduces a high-sampling frequency based load identification solution. The random forest algorithm is applied to realize an adaptive online learning mechanism. This new mechanism allows the identifier to study the loads automatically as the usage of the

customer. It is a more practical application for future energy auditing service.

Chapter 5 applies the Factorial Hidden Markov Model (FHMM) to the 15-minute resolution smart meter data. The human-behavior features and an unsupervised learning module are presented as well for the load disaggregation work. This work successfully disaggregates the large loads used in the residential home.

Chapter 6 proposes an electrical measurement based fault detection technique for HVAC. The air-flow blockage fault and refrigerant leakage fault are studied. A front-end high sampling frequency measurement is implemented. The speed/torque estimation algorithm from traditional motor parameter estimation is applied. The physical model of the air-conditioner is studied. Finally, a statistical analysis is provided to establish the relationship between the observed condition index and the two studied faults.

Chapter 7 provides the conclusions and contributions of this dissertation work and recommendations for future investigations.

CHAPTER 2 REVIEW OF LITERATURE

2.1 Chapter Overview

The current research topics in NILM are shown in Figure 2.1. This chapter provides a literature review on topics pertinent to this dissertation work, including: (1) the existing solution for high sampling frequency load identification, (2) the existing solution for low sampling frequency load disaggregation, (3) the existing solution for air-conditioner air-flow detection and refrigerant leakage/undercharge detection.

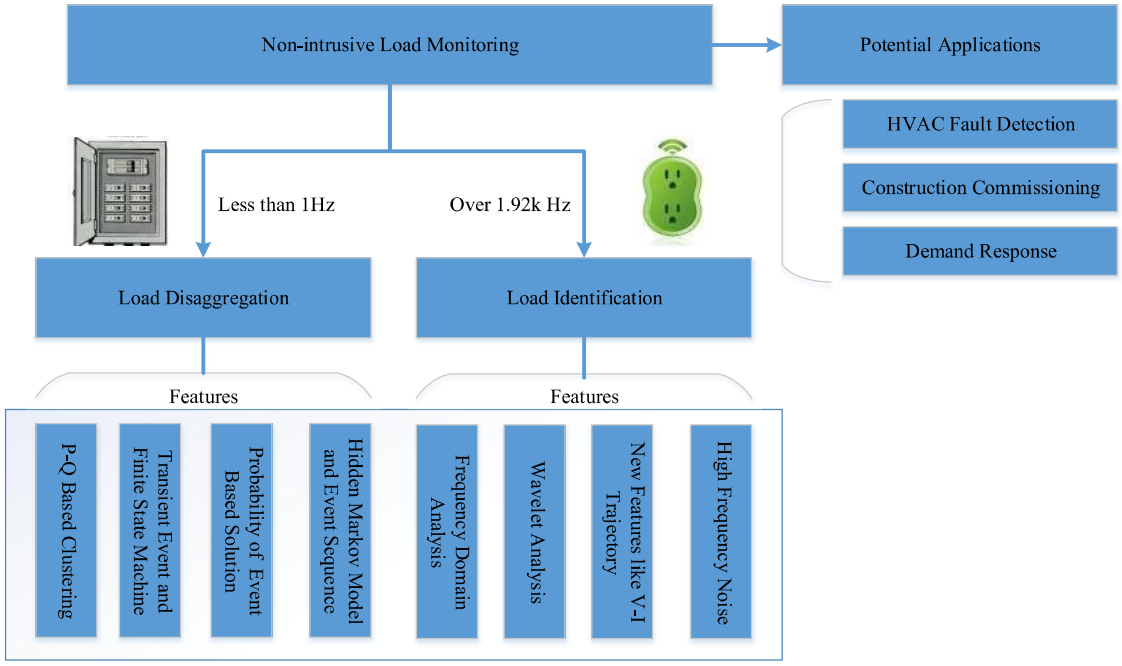

Figure 2.1 Research topic summary of the study on non-intrusive load monitoring.

2.2 High Sampling Frequency Based Load Identification

Even though the study of the load identification based on the high sampling rate has been dropped by many manufactures in NILM industry, the contributions of these previous

studies are still of great importance for the new applications and solutions.

S. Leeb, the group leader of MIT after Dr. Hart changed their focus by introducing high-frequency harmonics as the major features in [97-99], shown in Figure 2.2. The concept of a spectral envelope is introduced as well [100]. This method successfully solves the problems mentioned in [101], and is able to detect numerous appliances including the variable loads. However, as a tradeoff, an excessive training is required. Moreover, it is still not known why these high-frequency harmonic features are distinct and whether these differences only exist in the sampled load sets. Therefore it is difficult to prove that the method is widely feasible.

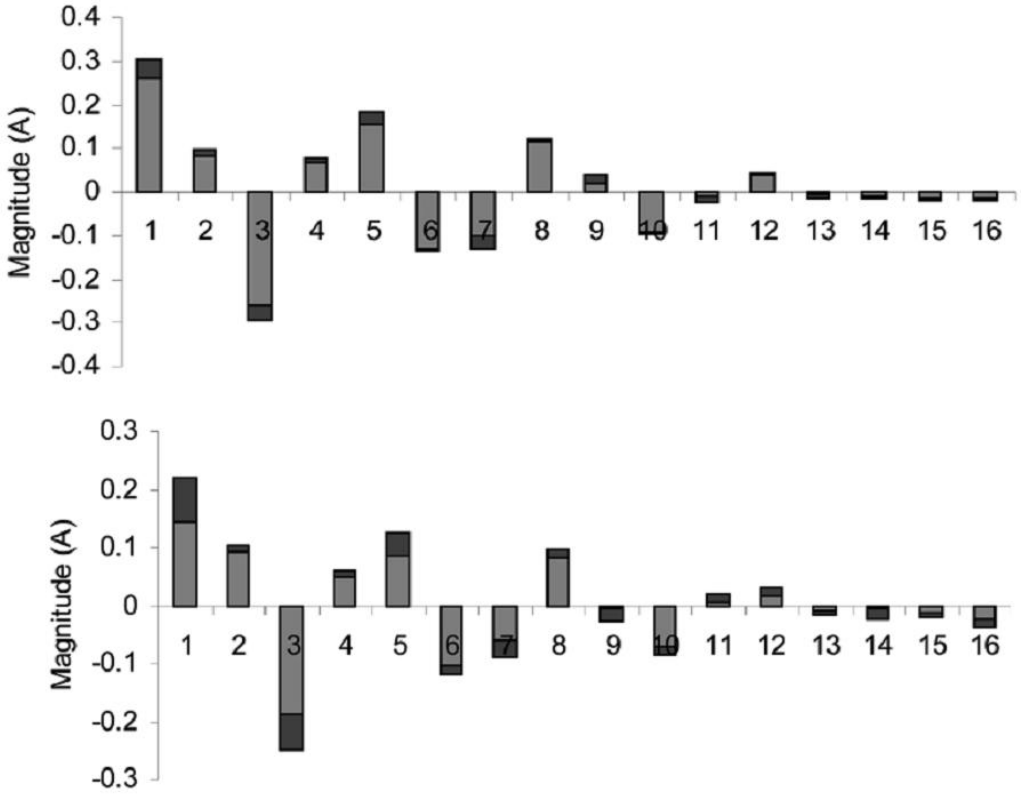

Figure 2.2 Harmonic signatures of monitor (upper) and CPU (lower). The fluctuations are shown by black bars [97].

Apart from traditional FFT analysis, S. Patel takes the FFT noise as a feature [102, 103]

which is a completely new solution to NILM, shown in Figure 2.3. By monitoring the electric noise in a socket for transient signals, it is reported to be able to detect most appliances connected to the sockets of the household. The results in terms of detection accuracy were comparable to those of other groups. Even though the new noise-based technology appears to be more reliable than the previous technology, several open questions remain. First, the appliance signature may depend on the household electrical wiring. Second, it is not clear how the EMI from neighboring environment will influence the detection process. Third, overlaps between the EMI signatures are inevitable. Fourth, mere detection of appliances is not sufficient for the load monitoring purposes.

Chan [104] have proposed to use a wavelet transform instead of the FFT to extract features, shown in Figure 2.4. The motivation is that the wavelets allow simultaneous time and frequency information localization, whereas the time localization with the conventional FFT is not possible. It is demonstrated that the wavelet features of several consumer electronics are quite distinct. However, there are still no attempts to use these features in a real NILM algorithm so far.

The geometrical features of waveforms from different appliances have been explored in [105, 106], shown in Figure 2.5. The main novelty is to use an I-V trajectory curve. Even though the use of I-V curves looks like a promising direction, the authors have never offered a working algorithm for NILM based on these features. A recent work from the same group proposed to use several different features simultaneously to increase the algorithm accuracy, in which the geometrical feature exploration was applied [107]. In [107], a committee decision procedure is proposed.

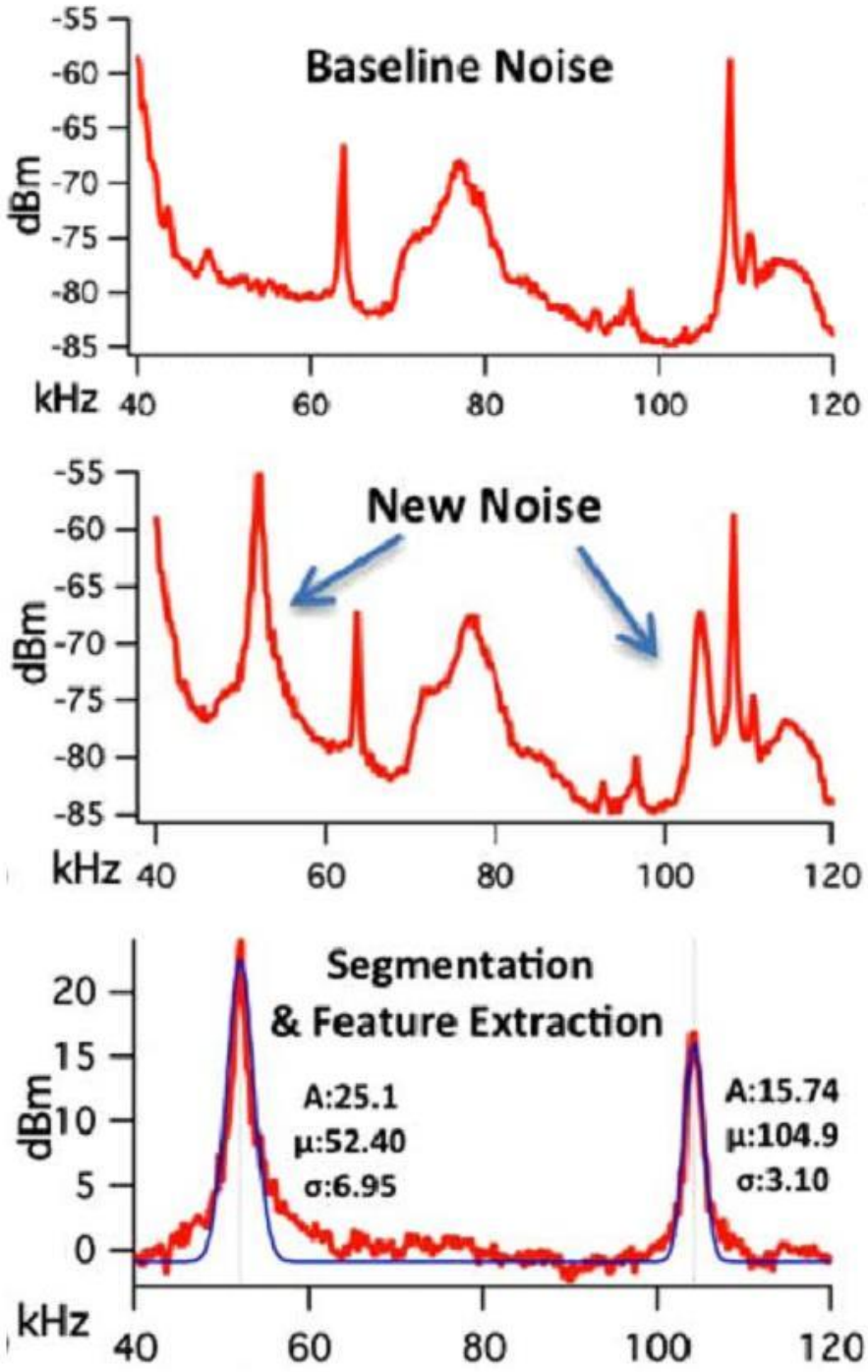

Figure 2.3 Background noise observed in a socket (upper panel). A new SMPS device is turned on, producing additive EMI (middle panel). After background subtraction the new signal features are extracted. The features are amplitude (A), mean (μ) and variance (σ) of the Gaussian fit [103].

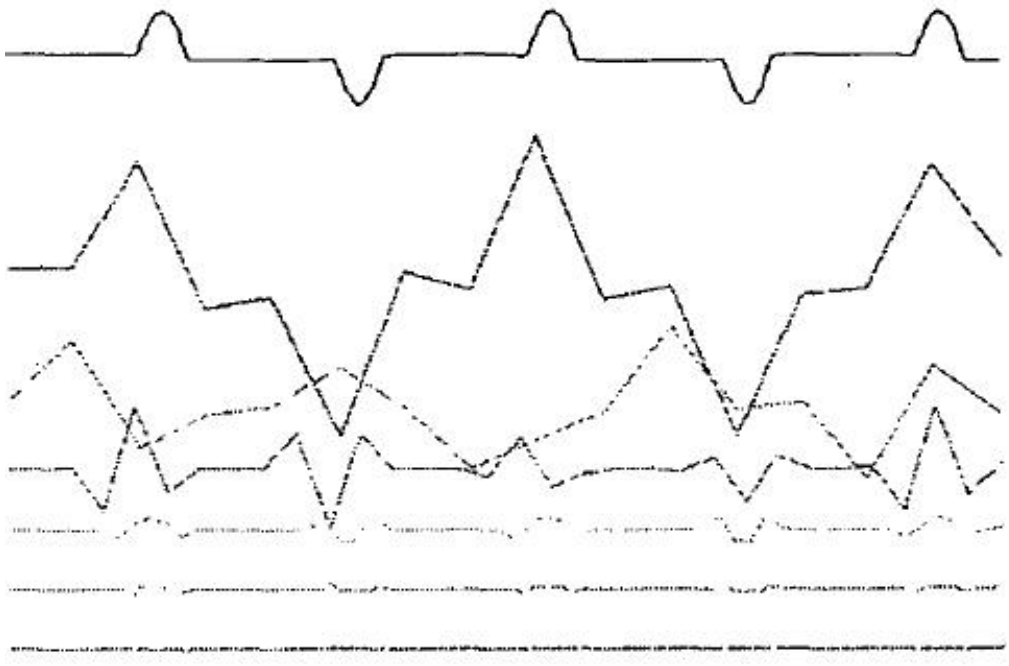

Figure 2.4 Wavelet decomposition of PC current waveform [104].

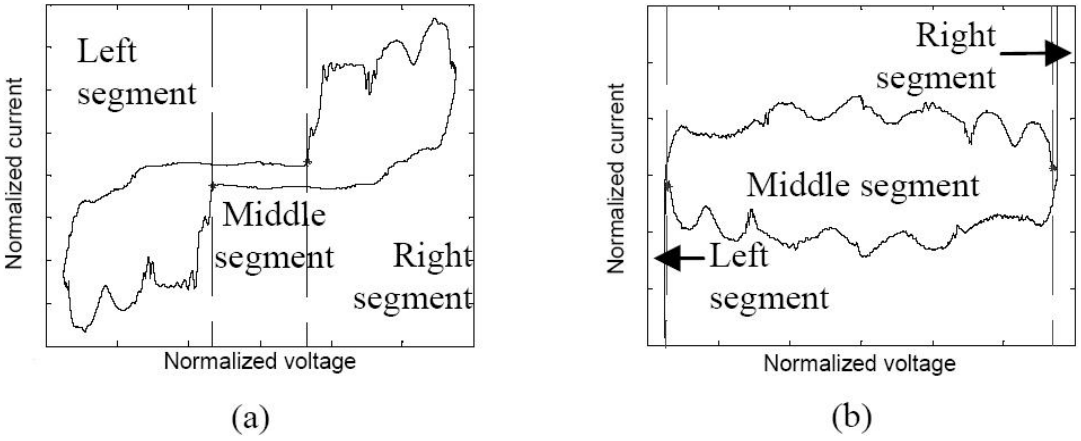

Figure 2.5 (a) The trajectories of a laptop, (b) a desktop PC operating in standby mode [105].

2.3 Low Sampling Frequency based Load Disaggregation

The ultimate objective of NILM described by MIT in 1980s [20] is simply to install one smart sensor in the metering point recording the real power at a as 1ow as possible frequency, shown in Figure 2.6.

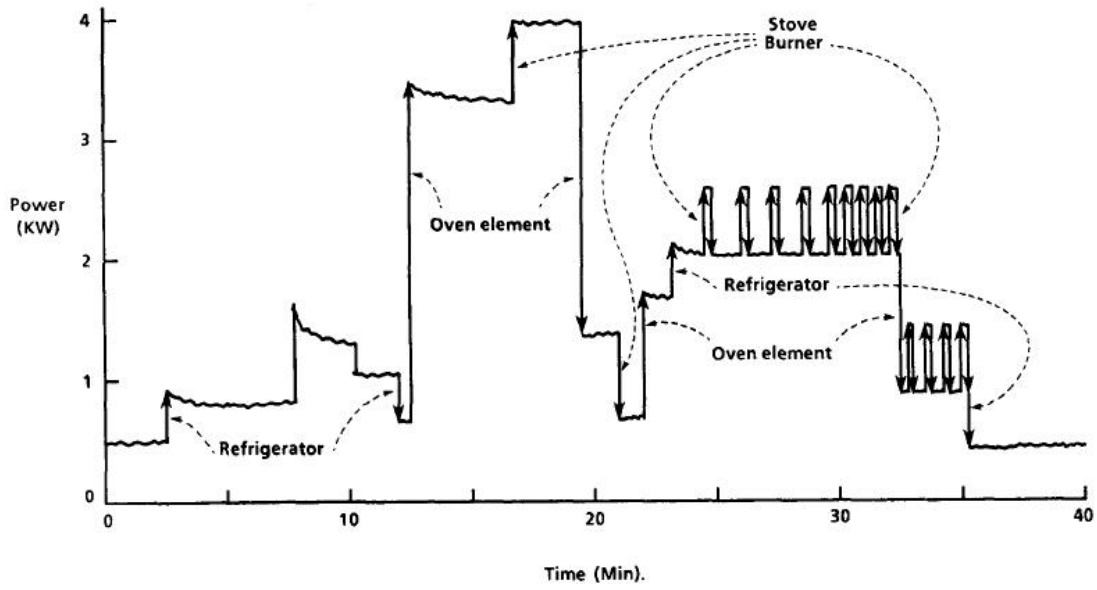

Figure 2.6 Power vs. time plot shows step changes due to individual appliance events [20].

In this work, four categories of appliances were defined by the authors, i.e., permanent consumer devices, on-off appliances, finite state machines (FSM) and continuously variable consumer devices. This study formed the basis of their following 20 years of study. Permanent consumer devices and on-off appliances were considered in detail in [20], by using the changes of real power and reactive power as the main features, shown in Figure 2.7. Later, a time-order FSM method is proposed in [108] and [109] to tackle with the FSM load identification, shown in Figure 2.8. In [110], the shapes of the transient events were introduced to find the solution to continuously variable consumer devices, as shown in Figure 2.9. Even though these studies comprehensively contributed to the NILM study, the

authors themselves summarized the problems and limitations of their methods in their recent studies [111], i.e., the appliances consuming similar power may not be separated, and the poor repeatability of transient events.

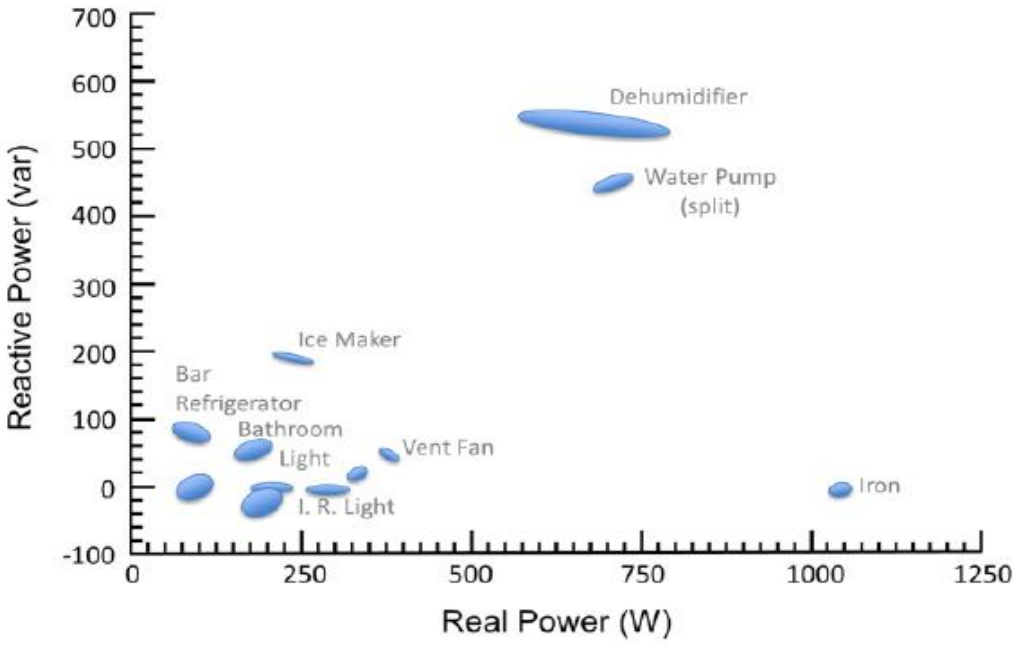

Figure 2.7 Complex power space and appliance clusters [20].

Similarly to the work did in MIT, Sultanem did an independent research at the same time. In his work, he proposed to use normalized real and reactive changes in power draw as the two major features. This algorithm successfully overcame the mismatch problem in MIT's study [112].

Cole and Albicki from University of Rochester proposed in [113] and [114] to use the significant spikes in power draw as the new features as shown in Figure 2.10. However, it bears the same drawbacks of the poor repeatability of transient events as stated in [111]. After this work, the research on MIT's original proposal seems stopped even though there is still no answer to these problems.

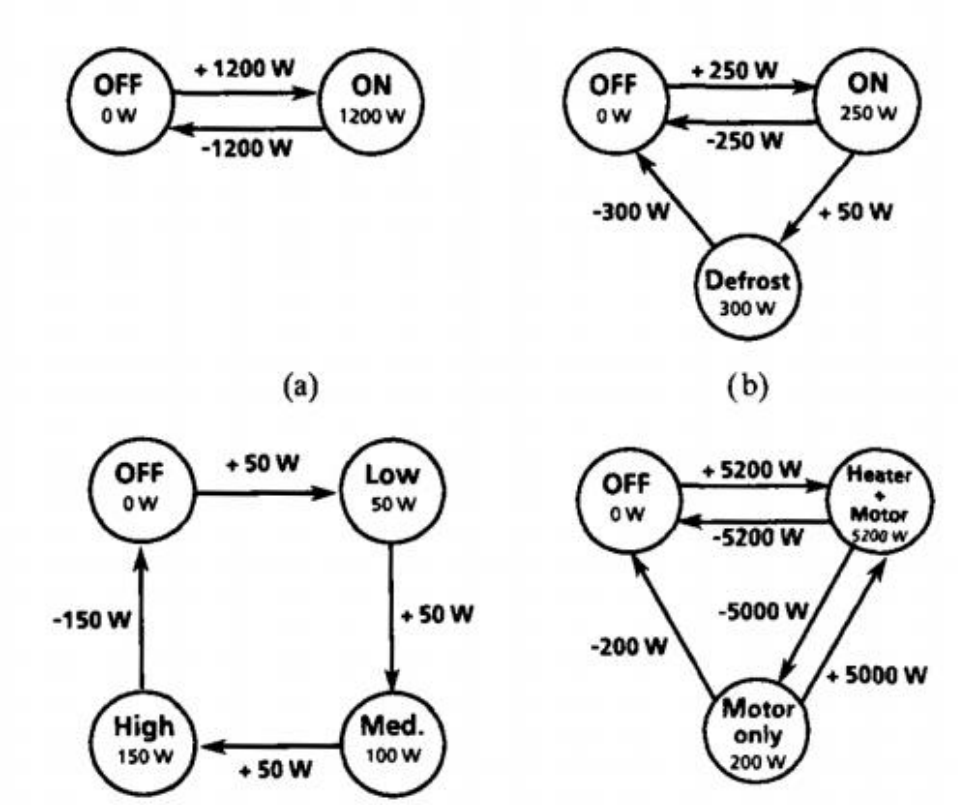

Figure 2.8 Finite-state appliance models: (a) generic 1200 W two-state appliance, e.g., toaster; (b) refrigerator with defrost state; (c) "three-way" lamp; (d) clothes dryer [109].

Until recently, another group from computer science area started this study again and came back to the origin point of this study, only taking the changes of real power into consideration. However, some modern machine learning and statistics methods were introduced this time [115].

The approach developed by Concordia University in [116] relied on the changes in real power and some appliance-specific decision rules to detect those large appliances such as water heaters. Although the method achieved an estimated accuracy of 80%, it only can be used to reliably detect just two appliances. In [117], the authors improved their work by using changes in real power and signal smoothing technology to detect on-off events.

Reportedly, this method was able to detect the water heater, the refrigerator, the clothes washer, the stove, the clothes dryer, the dishwasher, and the baseboard heater with an accuracy of up to 90%. However, the necessity to develop appliance-specific decision rules, required by the method, makes it hardly applicable for consumer electronics.

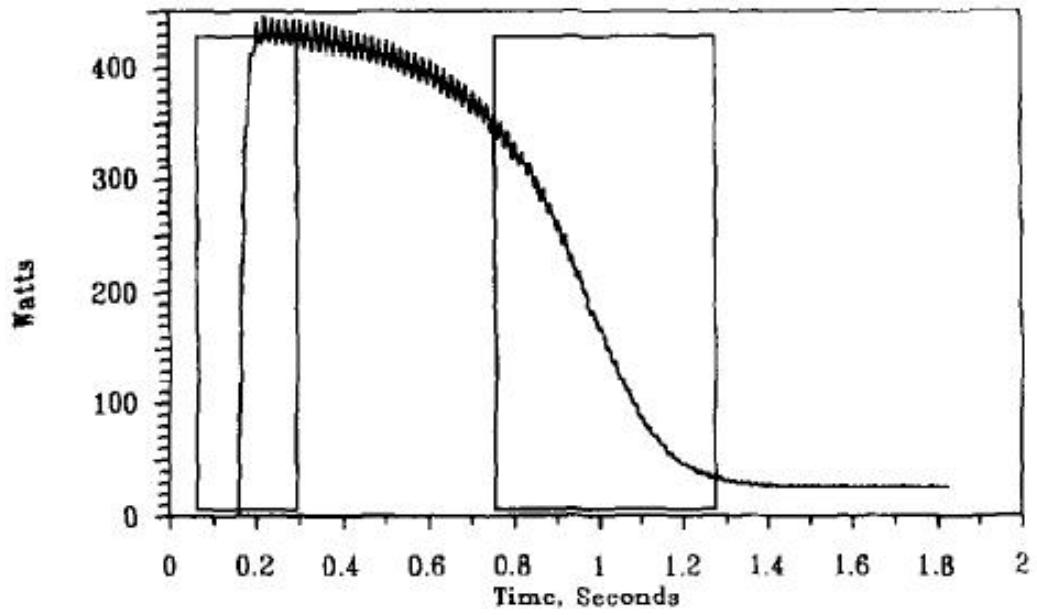

Figure 2.9 Measure induction motor real power transient [100].

Unlike most of the other methods, the NILM method proposed by Baranski and Voss [118-120] created a frequency analysis based on the historical data, and only those frequent power changes were considered further as the feature. However, the proposed genetic algorithm was a simulation method that may or may not provide the optimal solution.

In [83], Kolter firstly applied the factorial Hidden Markov Model (FHMM), which was comprehensively applied in DNA decoding and image identification, into NILM problem, as shown in Figure 2.10. Since then, HMM has become the state-of-the-art model for load disaggregation and much work has been done to develop HMM based NILM systems:

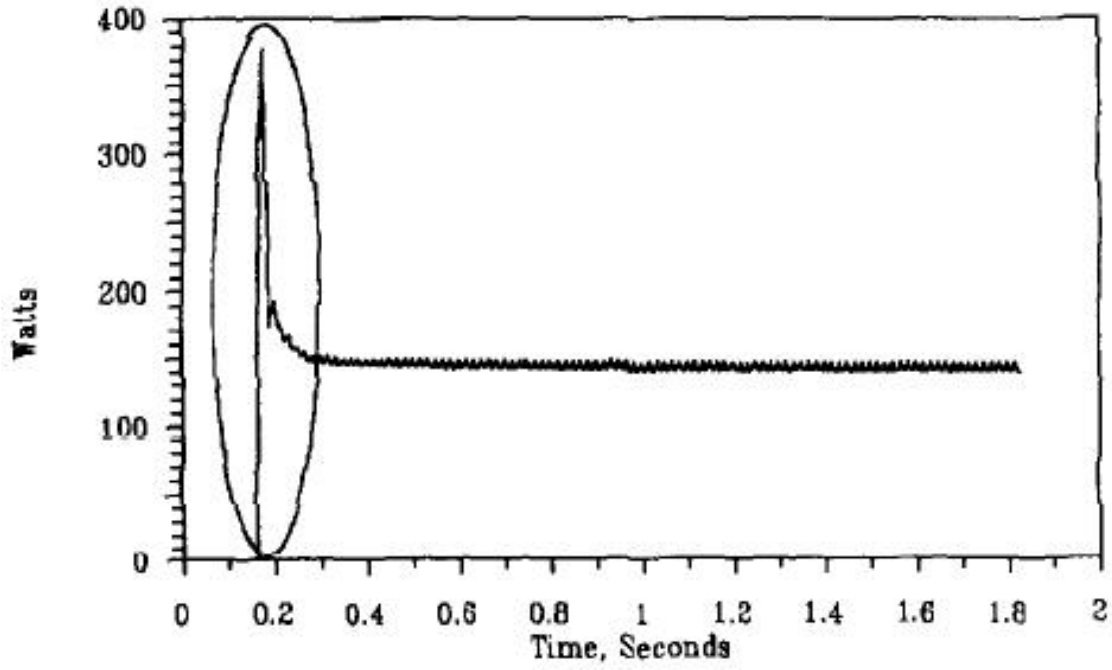

Figure 2.10 Instant start lamp power [100].

In 2011, H. Kim considered the on-duration time of the appliances, and proposed the conditional factorial hidden semi-Markov model (CFHSMM). The reported accuracy is 83%. However, the simulated annealing algorithm used in this paper suffers from the low efficiency problem [121]. In the same year, Sundeep Pattern contributed to the FHMM study by improving the data preprocessing techniques of FHMM [122]. The residual data were also preserved and analyzed. Oliver Parson changed FHMM to a supervised training by using certain prior knowledge to improve the training efficiency in 2012 [123, 124]. However, the FHMM method is still a novel method for NILM problems, and it bears lots of problems at the moment.

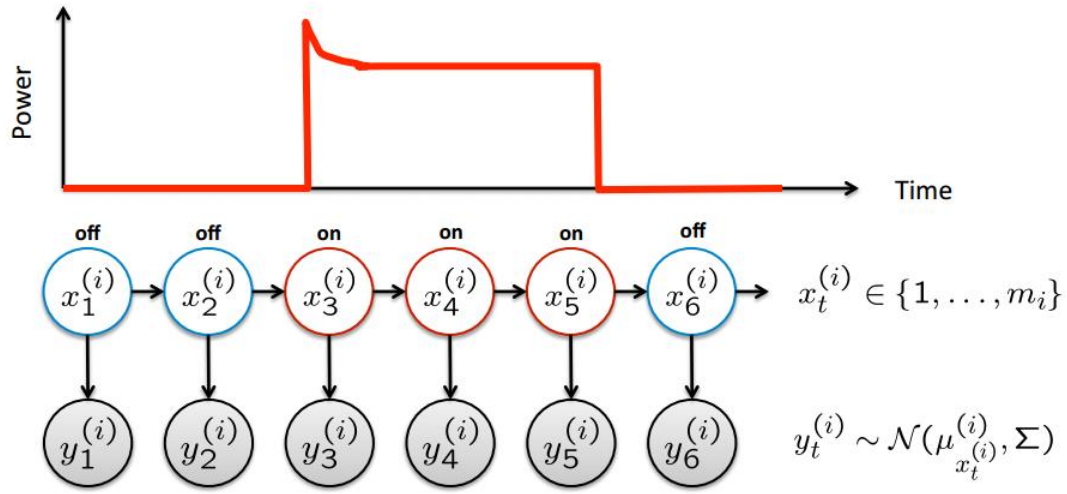

Figure 2.11 HMM model of the kitchen outlets [83].

2.4 Non-intrusive Fault Detection of the HVAC System

It is acknowledged by most of the researchers in this area that traditional application of NILM in energy auditing has seen no great progress in recent years. Most of researchers are trying to find a more specific application with a more reasonable load set. The fault detection application used in construction area is proposed by several studies as the preliminary attempts to jump out of the deadlock of current NILM study.

A group of CMU researchers from civil engineering has recently pursued NILM to benefit construction commissioning. Based on their released paper, they believe this will be a synergetic relationship between NILM and the building commissioning process. They started their work from the data acquisition [125] to the feature extraction and then the algorithm development [126]. However, no recent progress has been released after that.

At the same time, some civil engineering researchers from MIT also started to use NILM technology to help verify the working status of the building loads, like water pump, HVAC system and elevator systems [127, 128]. Their works mainly focus on using the

change of working power and the stator current of the motors to verify the conditions of these loads as shown in Figure 2.12. The idea is really attractive, nevertheless most of their works actually are not in a 'non-intrusive' environment. This work will focus on the conditioning monitoring of air conditioner, therefore the review of existing work on two typical faults in air-conditioning system is provided below.

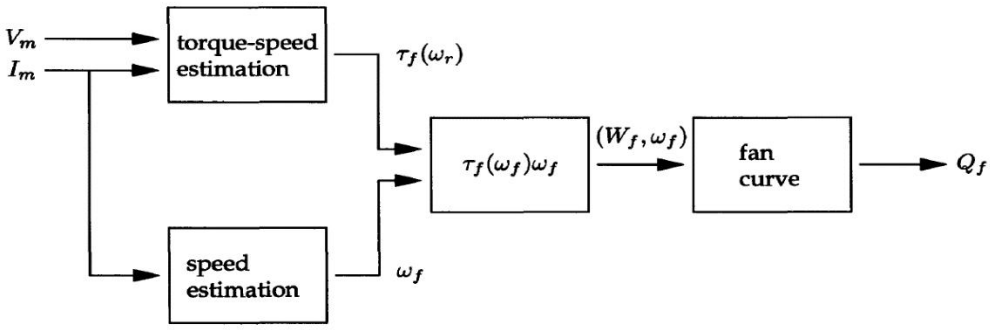

Figure 2.12 Flowchat of the air-flow estimation method [128].

2.4.1 Conventional Solutions for Air-flow Leakage Detection

To detect the air-flow faults, numerous methods based on mechanical sensor measurements have been proposed in the literature. Anemometers are commonly employed to estimate airflow in ducts, with propellers measuring the rotational speed of their blades, or with hot-wire types, and both methods measure the air speed directly [129]. However, the sensitivity and single-point measurement are the main weaknesses of these methods. An indirect approach measures the dynamic air pressure p_w instead of the air speed. It exploits the relationship of $V = \sqrt{\frac{2p_w}{\rho}}$ (where ρ is the air density) which, however, is similarly limited by the single-point measurement problem [130]. A flow plate or true-flow grid [131] is used to compensate the above drawbacks, through measuring the average air pressure by

inserting a series of tubes into the duct. Pressure measurements of relatively high accuracy can be used [131]. However, due to the high cost, difficulty to install and sensitivity to bias, these methods have not seen widespread utilization so far. Other less common approaches are demonstrated in [132], where CO_2 or ozone is injected at one point in a duct and the concentration is measured on the other side of pipe line to determine the flow of air. In [133], the acoustic spectrum and transfer function of duct are measured by sensors and exploited for pinpointing any blockage.

Most of these conventional methods above are either not reliable enough or expensive. Recently, a new idea has been proposed [127, 134] that is based on the measurements of the currents and the voltages of the HVAC systems, and then identify faulty mechanical behavior on the basis of these observations. The principal benefit associated with the use of these electrically-based fault detection techniques is that electrical instrumentation is often easier to install, more reliable, and less expensive than comparable mechanical instrumentation, and at the same time smart sensors have been widely utilized in today's energy management system. However the work in [127] as a preliminary attempt still bears the drawbacks and thus is difficult to be utilized in the practical application.

2.4.2 Conventional Solutions for Refrigerant Leakage Detection

Refrigerant undercharge or overcharge may cause severe effect on compressor lifetime, latent heat capacity or even environment.

The mass of refrigerant is specified for the expected cooling capacity. Too little refrigerant will cause the superheat in the evaporator, thus reduce the heat absorption capacity, while too much refrigerant will result in higher pressure than rated, which will cause other undesirable effect on the components. The possible causes for undercharge fault are leakage and mal-installation. Release of chlorofluorocarbons is well-known for its

destructive power to ozone layer, and the reduced cooling capacity will increase the power loss and thus lower the energy consumption efficiency.

A large amount of literatures have focused on the effect of refrigerant undercharge fault detection, in [135], a 3-ton system with undercharge fault is studied. The author revealed that the performance deteriorate quickly when the refrigerant charge falls below 10% of its rated level. Paper [136] provided a persuasive conclusion for the undercharge detection that the sensitive parameters to the charge level are the degree of superheat at the evaporator outlet, the degree of sub-cooling at the condenser outlet and the discharge pressure. Refrigerant undercharge FDD method is used in [137], where the leaks in supermarket refrigeration system were analyzed. However, most of these methods related to faults detection need a great number of sensors for temperature or pressure measurement, which largely reduced the convenience and accuracy.

2.5 Chapter Summary

This chapter provides a comprehensive literature review on topics pertinent to this dissertation. First, the existing solutions for high sampling frequency load identification are introduced. An adaptive self-learning technique has been suggested by several researchers as a promising technique to realize the energy auditing goal. Next, the existing solutions for low sampling frequency load disaggregation are reviewed. The human-behavior features are suggested in the training procedure. An unsupervised solution is also mandated for a real application. Finally, the existing conditioning monitoring solutions for HVAC based on mechanical sensor measurement is introduced. Based on this literature review, the rest of this dissertation proposes a complete non-intrusive load monitoring solution vertically for different level applications.

CHAPTER 3 FUNDAMENTAL STUDY OF ELECTRIC LOAD AND FEATURE EXTRACTION

3.1 Chapter Overview

The huge load space comparing with the limited measurement capability and the lack of knowledge on the existing feature sets act as the two dominant challenges for high sampling frequency load identification today. This chapter starts from a survey on the market and the standards of the PELs loads to generate a load space with a hierarchical taxonomy that can represent the majority of loads in the real world. The data collection metrics and data management tool are introduced. Furthermore, with the collected data, a comprehensive study on front-end power supply circuit topologies and electrical operation principles of the collected loads is presented. This forms the basis of the proposed taxonomy from the power electronics' point of view. Under the proposed taxonomy, a complete model-driven hierarchical feature extraction method is presented, and the features extracted from this method prove much simpler and more feasible in differentiating the subtle differences between similar loads.

3.2 Data Collection and Preprocessing

3.2.1 Load Space Definition

The first step to building an NILM system is to construct a database with a pre-defined load space. Usually, the selection of the loads to be identified is based on their usage frequency, total contributions to building energy consumption and energy saving potentials. To obtain a more generalized load space, this work also takes several standards including 80 PLUS [138], Energy Star [34], and IEC 61000-3-2 [139] into consideration in the selection

process. To date, this work has included a total of 42 load types, and 5 to 7 brands per type, as the set to be studied. The constructed database covers over 90% of appliances used in the commercial and residential buildings. The detailed load list is shown in Table 3.1. In addition, the database describes every load type in five categories, (1) Load type, (2) Brand (with top five market share), (3) Operating characteristics, (4) Front-end circuit topologies, and (5) Operating states. The database structure for a space heater is shown in Table 3.2.

Table 3.1 A list of the loads to be studied.

Load Category	**Loads Name**
Large Loads (>1kw)	HVAC, space heater, water heat, coffee maker, furnace, oven, dishwasher, microwave, washer and dryer, pump, and refrigerator.
Regular Loads (> 45W)	Task light, fan, TV, home theater, printing device, desktop, and projector, etc.
Small Loads	DVD player, Set top box, laptop, monitor, shredder, cellphone charger, etc.

Table 3.2 A snapshot of database structure.

Load	Brands	Work Types	Power Supply Topology	State	Working
Space heater	Holmes	Ceramic	1.Pure Resistive	t.s	Startup
	DeLonghi	Quartz	2.Inductive adjunction		Low Taps
	Honeywell	Oil filled	3.SCR controllable	s.s	High Taps
	Lasko	Heater fan			Fan
	Pelonis				Standby

Note: t.s means transient state, and s.s means steady state.

The raw voltage and current (V/I) waveforms of all the individual loads have been collected during many different operating conditions. This includes startup, steady, standby (or other low power states), and particular operating states for some loads (e.g., printing states for printers). Each set of V/I waveforms has been sampled at 3.84 kHz for one minute. A total of 627 sets of data have been recorded.

A data preprocessing engine has been developed in MATLAB to process and analyze all the collected data, including the V/I waveform plot, V-I trajectory, Fast Fourier Transform (FFT), power factor, real power, reactive power, and apparent power. This engine provides a user-friendly interface to access the database, as well as to display the signal analysis results, as shown in Figure 3.1.

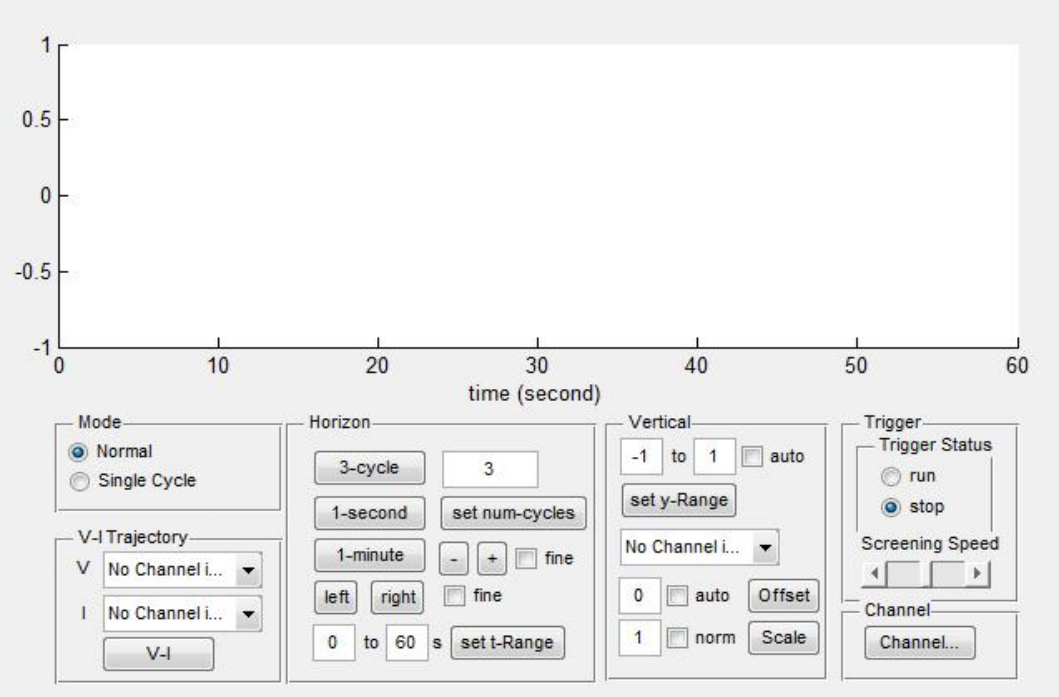

Figure 3.1 Database user interface.

3.2.2 Multi-Level Structured Taxonomy of Load Space

The number of types and models of loads in market, residential buildings, and commercial buildings is enormous. It is more practical and robust to first divide all the loads into several categories based on some prior-knowledge. Considering the fact that voltage and current waveforms are the only source of information available for signature extraction and load identification, the front-end circuit topology of the load and the electrical operation

principles play a key role as it directly determines the characteristics and shape of the current waveform. With a thorough understanding of the state-of-the-art of almost all the front-end power supply topologies and electrical operation principles, a bi-level taxonomy of current load space is proposed. The resulting bi-level structure is presented in Table 3.3.

In details, the first level, i.e. Level-I in Table 3.3 consists of 7 load categories: resistive loads (R); reactive predominant loads (X); electronic loads with a power factor correction circuit (P); electronic loads without a power factor correction circuit (NP); linear power supply using transformer to boost voltage (T); phase angle controllable loads (PAC); and complex structures (M).

The majority of resistive loads (R) are used for heating, cooking, and lighting. The representative loads include space heaters, coffeemakers, and incandescent lamps. For reactive loads, the appliances often consist of compressors, motors, or chillers. The motors commonly used for appliances are often small DC motors. The typical loads in this sub-category are fans, washers, refrigerators and shredders, etc. The next two large groups of appliances are all electronic loads, denoted as categories P and NP in Table 3.3. Since the IEC Standard 61000-3-2 limits the harmonic current level for all the loads with power above 75 Watts, it can be assumed that a power factor correction (PFC) module is needed to meet this requirement. Therefore, category P refers to electronic loads with PFC. Personal computers over 75W, projectors, LCD TVs, LED TVs (working in the “high quality mode”), Plasma TVs, home theaters and game consoles, also all belong to Category P. In contrast, Category NP refers to electronic loads that do not utilize power factor correction techniques. Small devices, such as cellphone chargers, portable DVD players, adaptors of the portable printers, scanners, fax machines and multiple function devices (MFD) using ink-jet, PC monitors, LED TVs (operating in the energy saving mode) and PCs (operating in a low

power mode) are major loads in this sub-category. Loads in Category T refer to those low power appliances that use linear DC power supplies with a small transformer at the front-end. Battery chargers, paper punchers and staplers are representative loads in this category. Devices such as light dimmers that use Thyristor phase angle voltage control are listed in the PAC category. Category M consists of appliances that often have high power consumptions, and multiple electrical systems, such as microwave ovens and laser printers.

3.2.3 Section Summary

The new taxonomy shown in Table 3.3 provides a guideline to load modeling, feature extraction, and load identification. The concept of a hierarchical load classification and identification system is illustrated in Figure 3.2.

In general, it consists of two parts. The first part is to recognize the target load as one of the seven categories based on some simpler steady state features from front-end electric circuit study comparing to the existing work. The second part is to further identify the target load as a specific load based on a combined set of transient state and finite state patterns from the study of electrical operation principle study. This hierarchical structure ensures an efficient feature selection of a smaller load set as in every level and sub-level shown in Figure 3.2.

Actually, the front-end electronic circuits of these seven categories are totally different, so as the electrical operation principles of the loads within one certain category. A summary of these topologies will be discussed in the following sessions.

Table 3.3 A list of appliance loads in two-level structure.

Load Category - Level 1	Load Category - Level 2
R: Resistive Loads	R1: Incandescent lamps (<100W)
	R2: Space heater
	R3: Bread toaster
	R4: Coffee machines - Other kitchen appliances
X: Reactive Predominant Loads	X1: Fans
	X2: Refrigerator (any with chiller)
	X3: Vending machine
	X4: Shredder
P: E-load w/ PFC	P1: PC (Desktop/Laptop) (>75W)
	P2: Projectors
	P3: Large TVs (LCD/LED) (>75 W)
	P4: Home theater/Game Consoles (70-80W)
NP: E-load w/o PFC	nP1: PC (Laptop) (<75 W)
	nP2: Charger (any with battery)
	nP3: Other small electronic devices
	nP4: FL/CFL
	nP5: Portable MFD/Printer/Scanner
	nP6: PC Monitors
T: Linear Loads	T1: Small electronics (e.g. stapler)
	T2: AA battery charger
PAC: Phase Angle Controlled Loads	PAC1: Dimmer
	PAC2: Others with Thyristor Controlled Rectifier
M: Complex Structure	M1: Microwave oven
	M2: Printer/Copier/Fax Machine/MFD

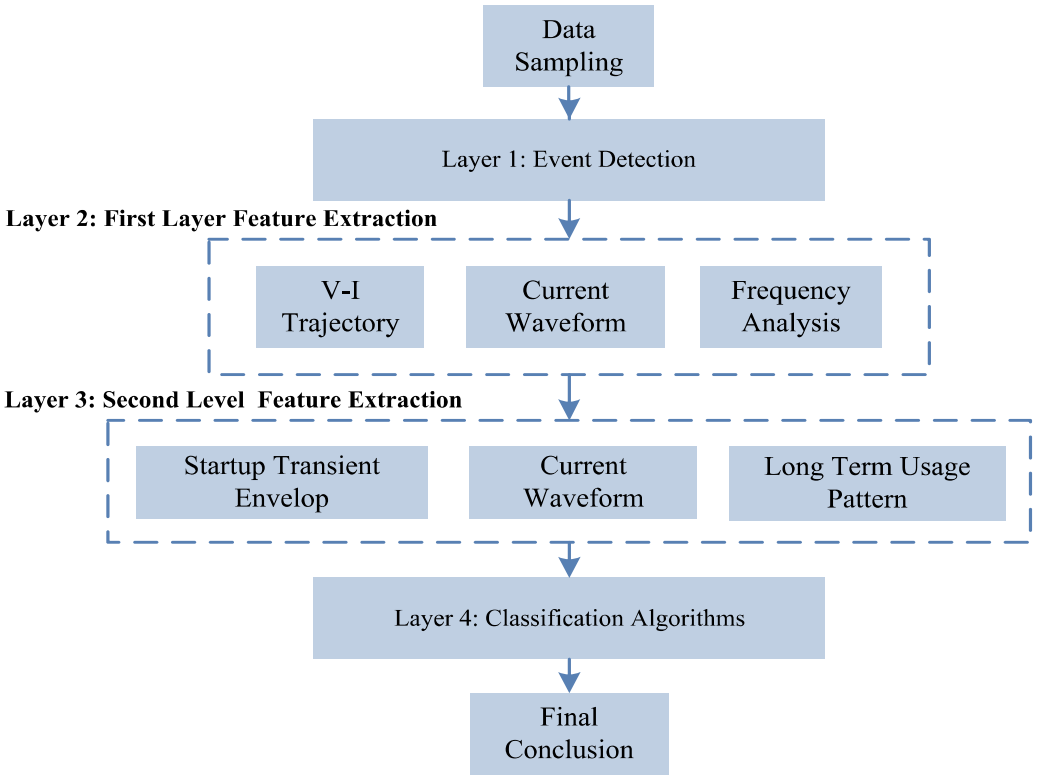

Figure 3.2 A hierarchical structure of NILM system.

3.3 Front-End Circuit Differentiation

The front-end electronic circuit of an appliance is composed of one or several of the following modules, including a front-end filter, a rectifier, a transformer, an isolated dc-dc converter, a phase angle controller (PAC), a current\voltage regulator, and/or a power factor correction module.

3.3.1 Resistive Load Category

A resistive load, as the name suggests, contains a resistance directly connected to the terminals. Therefore, there is no phase angle displacement between current and voltage waveform, and the power factor is close to unity. Figure 3.3 (a) shows a typical circuit of a heater. The normalized current and voltage waveforms are shown in Figure 3.3 (b).

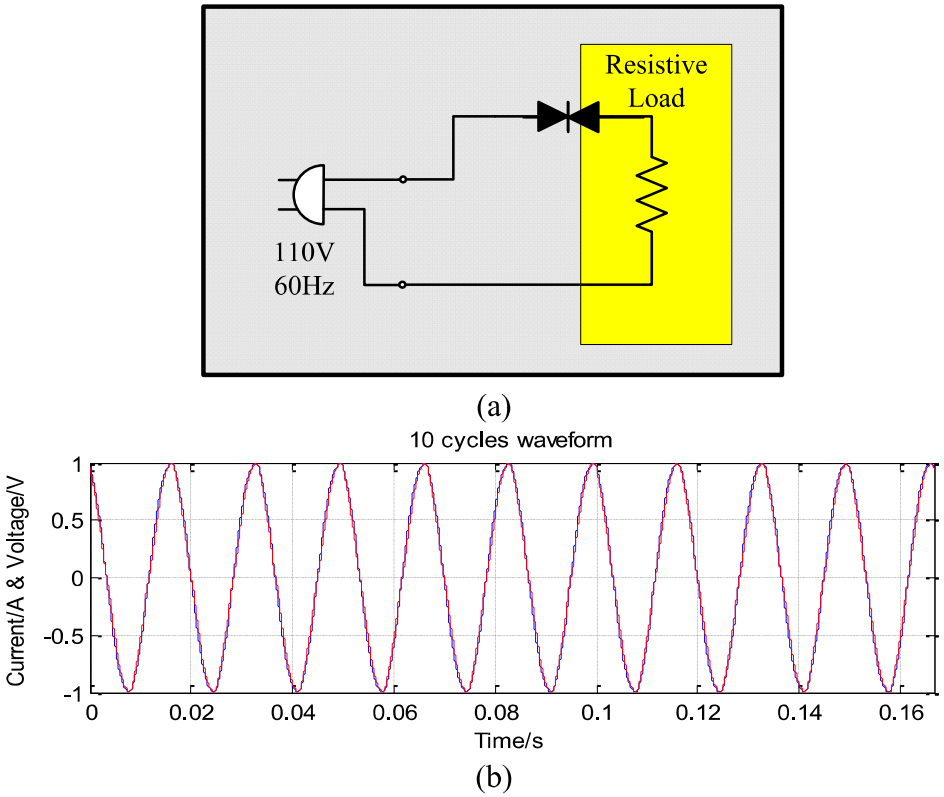

Figure 3.3 (a) The conceptual front-end circuit of pure resistive loads; (b) Normalized steady state voltage and current waveform of pure resistive loads.

3.3.2 Reactive Predominant Load Category

In this category, an inductance is connected to supply through a rectifier. Figure 3.4 (a) shows the electronic circuit for a fan driven by a DC motor. A large phase angle displacement between supply current and voltage is one of the dominant characteristics of this type of loads as shown in Figure 3.4 (b).

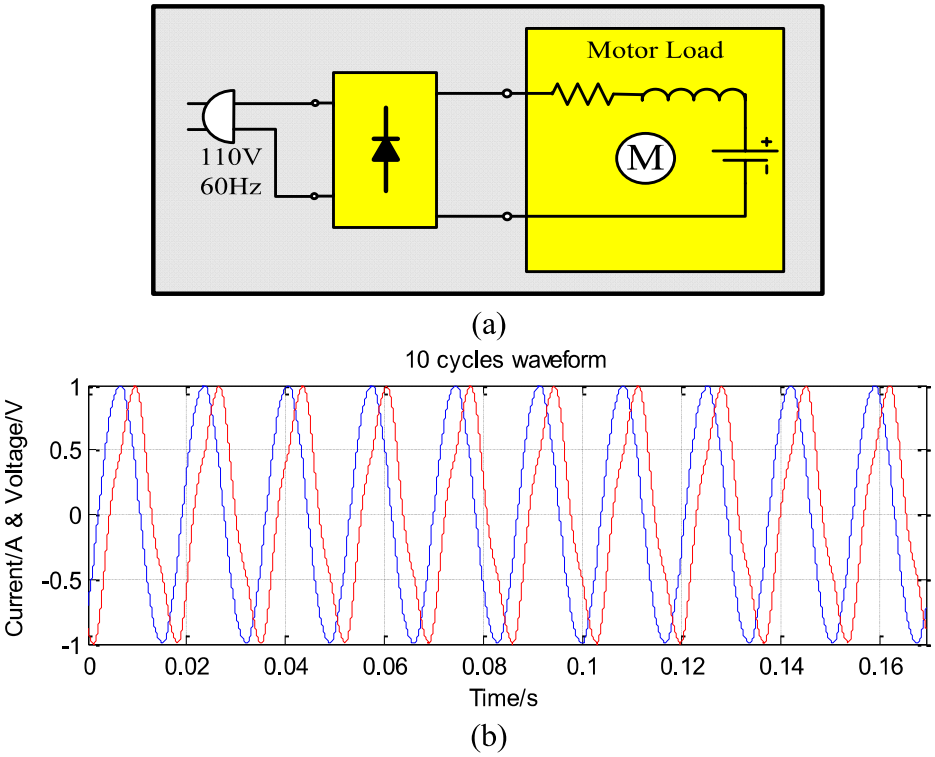

Figure 3.4 (a) The conceptual front-end circuit of inductive loads; (b) Normalized steady state voltage and current waveform of inductive loads.

3.3.3 Electronic Load without Power Factor Correction Category

An appliance in this NP-category often needs a DC power supply to power the downstream electronics. The front-end power electronic circuit typically consists of a front-end electromagnetic interference (EMI) filter, a rectifier, a voltage or current filter and a DC-DC converter, shown in Figure 3.5.

As shown in Figure 3.5 (a), a filter capacitor is utilized to supply constant DC voltage to the DC/DC converter. Because of this capacitor, the rectifier bridge conducts only when the magnitude of input voltage is greater than the magnitude of the voltage across the capacitor. Consequently, the typical utility supply current waveform to this load type appears as a periodic pulse waveform at the power frequency (i.e., 60 Hz in U.S.), as shown in Figure 3.5 (b).

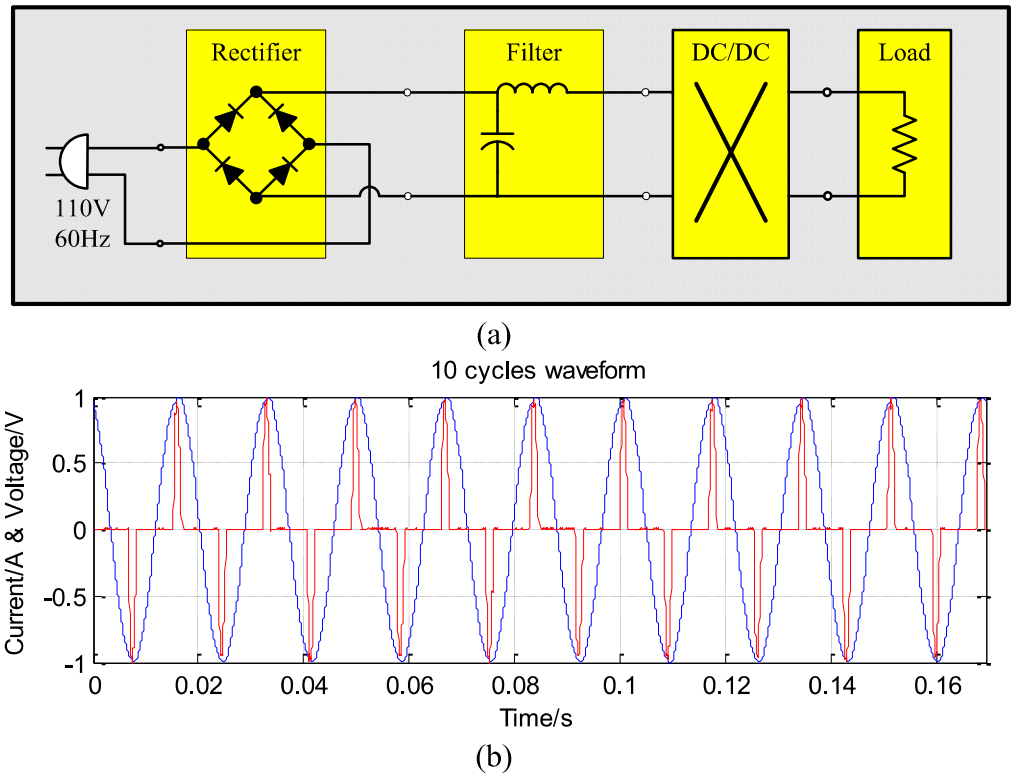

Figure 3.5 (a) The conceptual front-end circuit of ELw/oP; (b) Normalized steady state voltage and current waveform of ELw/oP.

The width of each pulse is affected by the capacitor voltage as well as the load power. The charging duration varies directly with the load power. Furthermore, the front-end EMI filter also affects the shape of the pulse. It is important to note that, the load input current (i.e., the current measured at the point of the front-end plug) is not related to the DC/DC converter, mainly because of the signal isolation caused by the capacitor filter. When a DC power supply is designed for an appliance with the power level below 75 Watts, the manufacturers often chooses a topology among three types of filter configurations and four types of DC-DC converters, as summarized in Figure 3.6.

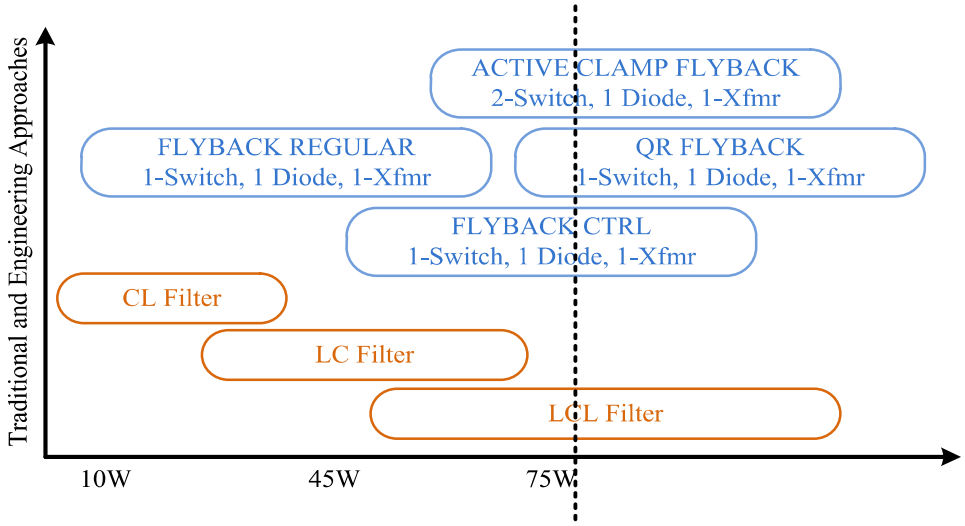

Figure 3.6 Industrial selections of switch power supply and V/I filter.

With reference to Figure 3.6, a C-L filter is usually used for portable loads such as cellphone chargers. An L-C filter is commonly selected for loads with power below about 45 W, and an L-C-L filter is used in loads with power over 45 W with a wider pulse. The representative load types that use the three types of filters are illustrated in Figure 3.7. In fact, these three types of loads have most of their characteristics in common and they have therefore been roughly recognized as one kind of load in most of the previous publications.

For loads in Category NP, there is no phase angle displacement between the power supply current and voltage waveforms; however, the current waveform contains abundant harmonics.

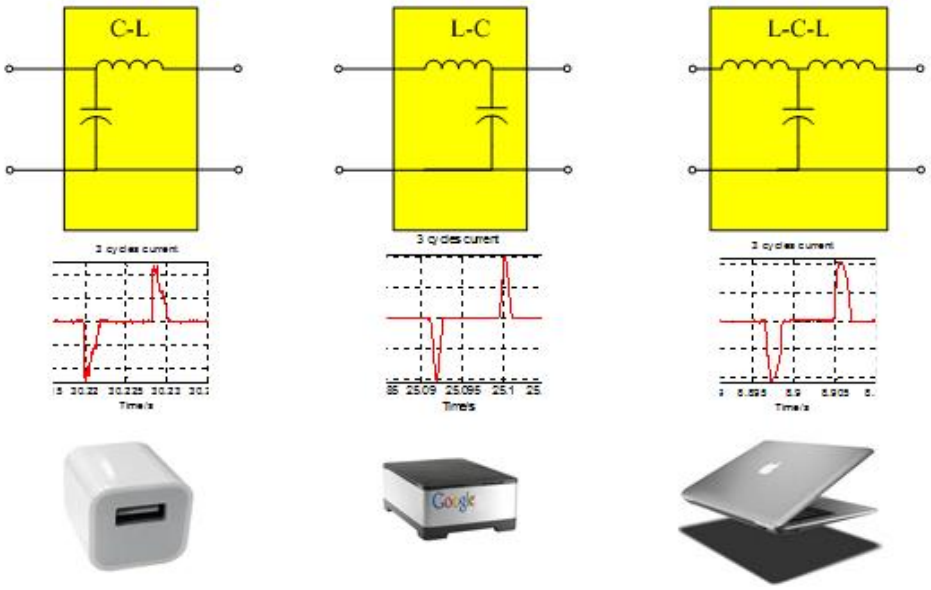

Figure 3.7 Three kinds of filters in power supply and their representative load types e.g. a cellphone charger, a set top box, and a laptop.

3.3.4 Electronics Load with Power Factor Correction Category

A DC power supply is also used in the appliances in Category P. In these cases a typical front-end electronic circuit consists of a front-end EMI filter, a rectifier, a voltage regulator, a power factor correction circuit and a DC-DC converter, shown in Figure 3.8 (a).

In this category, an L-C-L filter is typically used. As required by the IEC 61000-3-2, a front-end EMI module is always adopted, since loads that fall into this category consume more than 75 W. Unlike loads in Category NP, the input current in Category P loads appears to be sinusoidal, similar to the resistive loads. The PFC causes the rectifier to conduct for a complete cycle as shown in Figure 3.8 (b). These PFCs can further be categorized into active PFCs and passive PFCs as shown in Figure 3.9. Active PFC modules can be further classified into three structures, i.e. boost converter structures, full bridge structures and interleaved structures. For the boost type, there are three distinct control strategies which affect the signatures. These are continuous conduction mode (CCM), discontinuous

conduction mode (DCM), and critical conduction mode (CrM).

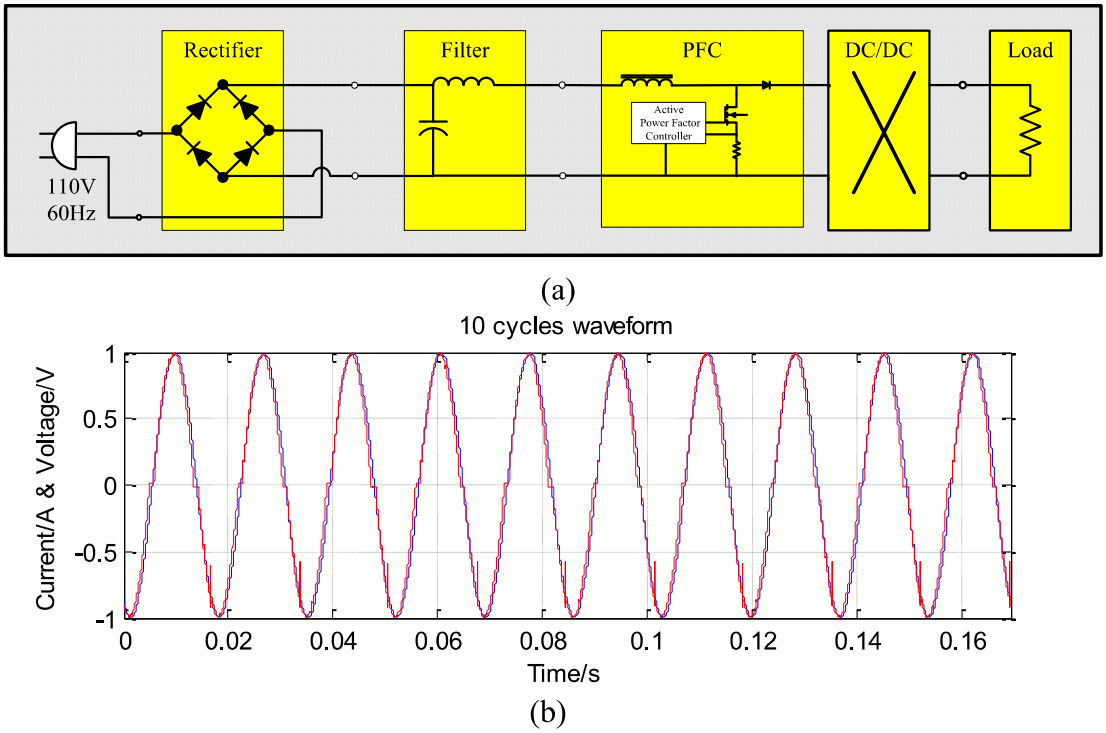

Figure 3.8 (a) The conceptual front-end circuit of P-Category; (b) Normalized steady state voltage and current waveform of ELwP.

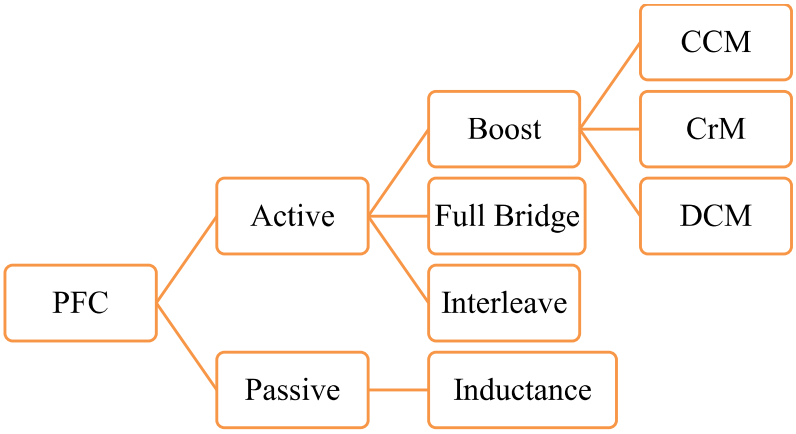

Figure 3.9 A classification of PFCs with different structures and different control strategies.

It is important to note that, for loads in Category P, there is always a short time period of discontinuous current when the voltage crosses zero. This current characteristic forms a

typical feature for the P loads, and is useful to distinguish them from a purely resistive load. For interleaved PFC structures, the PFC driver needs to verify the voltage polarity and the dead-zone at the voltage zero-cross point results in the current discontinuity. For the critical conduction mode or the discontinuous conduction mode PFC, the switching frequency is very low when current is close to zero, which causes the discontinuity.

The detailed principles of PFC converters can be found in [140]. Figure 3.10 summarizes the waveforms for different PFC topologies. Continuous Current Mode control is a current tracking strategy, thus the current waveform follows a sinusoidal reference as shown in Figure 3.10(a). DCM is a pulse width modulation (PWM) control strategy, thus a front-end high frequency filter is obligatory. The waveform after the filter is smooth as shown in Figure 3.10 (b). Passive PFCs are simply an inductor which can only increase the conduction period shown in Figure 3.10 (c). An interleaved PFC is a full bridge structure with two boost converters. Its control strategy is like the CCM control strategy, but uses a combination of two DCM PWM controls. All the information above is useful to identify those loads with the most similarity.

Appliances in the Category P often appear to be very similar to resistive loads in terms of their current waveforms. However, the existence of the current discontinuity and higher order current switching noise are the recognizable signatures for loads of this type.

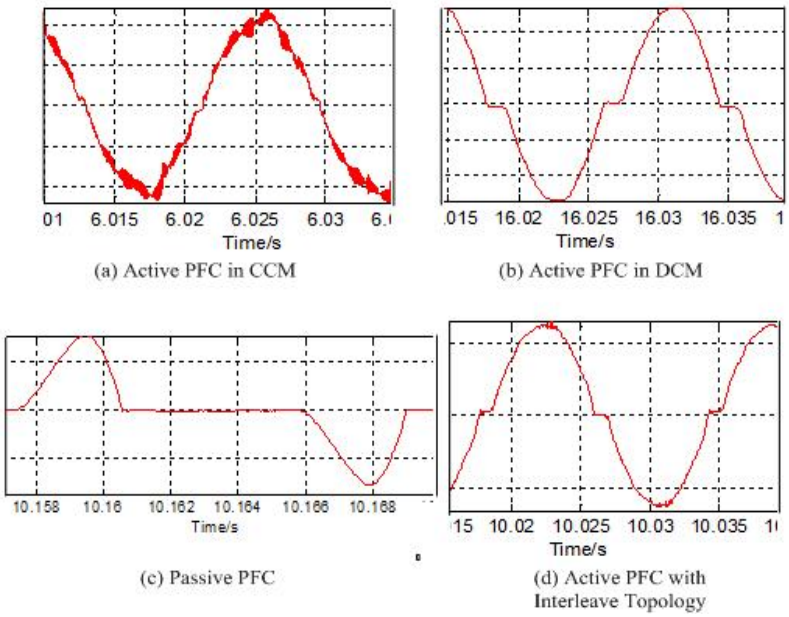

Figure 3.10 Different waveforms in terms of different PFC modules.

3.3.5 Transformer-Rectifier Power Supply Category

The transformer-rectifier DC power supply is the most traditional power supply which is still commonly used in low power devices. Figure 3.11 (a) presents a typical circuit of a transformer-rectifier DC power supply. It consists of a transformer, a rectifier, and a linear regulator. The current of this load type is highly distorted because of the transformer saturation. Figure 3.11 (b) shows a typical current waveform of a transformer-rectifier power supply. The current pulses observed at peak voltage are caused by the downstream bridge rectifier, which is similar to the electronic loads without PFC connected to the rectifier (similar to the analysis for loads of Category NP). To summarize, a large phase angle displacement exists in this category and so do the high order current harmonics.

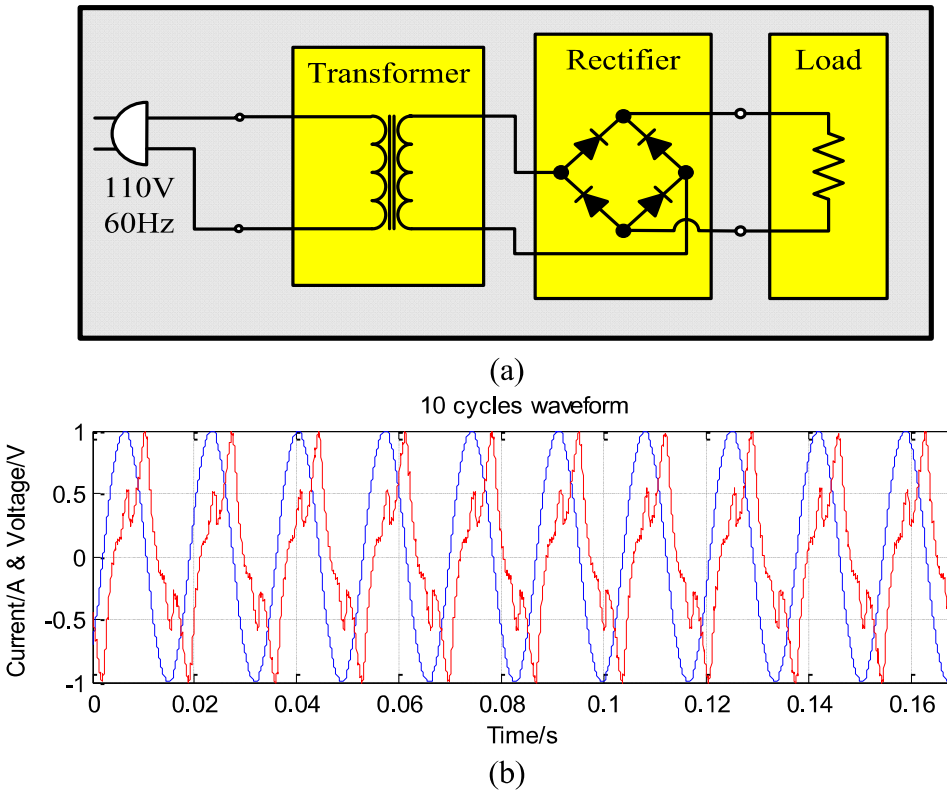

Figure 3.11 (a) The conceptual front-end circuit of linear power supply; (b) Normalized steady state voltage and current waveform of linear power supply.

3.3.6 Phase Angle Controllable Circuit Category

PAC controller is widely used for LED lightings, heaters, fans, and other appliances that require continuous voltage adjustment. Figure 3.12 (a) illustrates a typical PAC circuit. The load current can be adjusted continuously by controlling the firing angle of the thyristor. Figure 3.12 (b) shows a typical normalized current waveform of a PAC circuit.

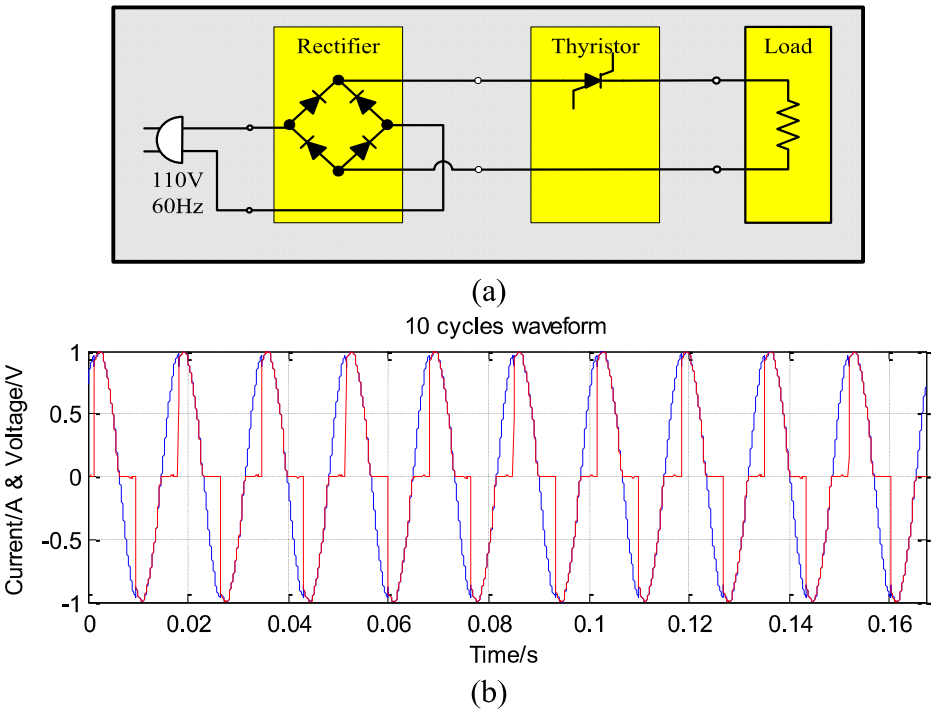

Figure 3.12 (a) The conceptual front-end circuit of PAC controllable load; (b) Normalized steady state voltage and current waveform of PAC controllable load.

3.3.7 Complex Structure Category

The appliances in Category M refer to those loads with multiple circuits supplied by independent front-end power supplies. Figure 3.13 (a) gives an example of a complex structure load, in this case a microwave oven. It is a combination of Category X and Category NP. Usually, there are two or more parallel power supplies at the load front-end. As a result, the load current appears to be composed currents from one or more of the above six categories. Figure 3.13 (b) shows a typical waveform of a microwave oven.

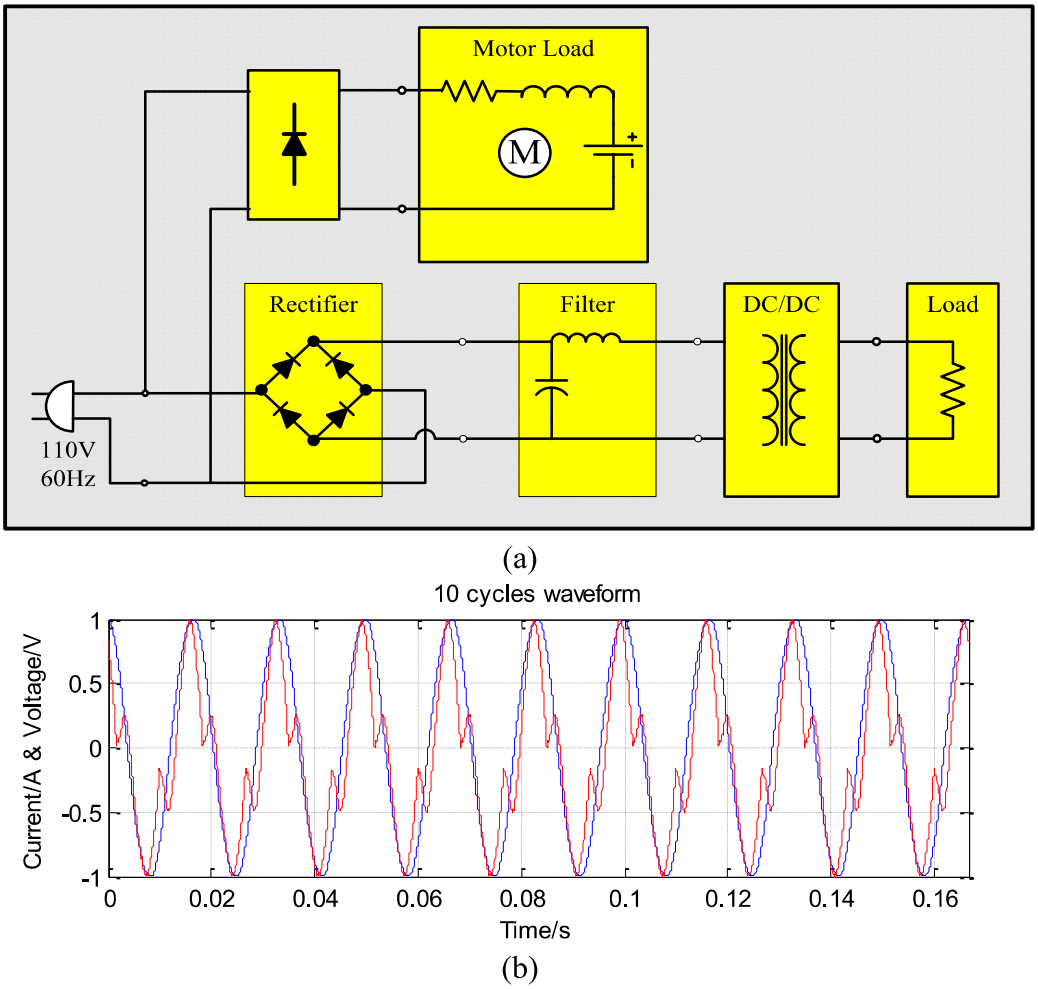

Figure 3.13 (a) The conceptual front-end circuit of complex structure load; (b) Normalized steady state voltage and current waveform of complex structure load.

Different loads in Category M will have different waveforms since they are composed of different category structure. This diversity can be beneficial for the second level classification. At the same time, it increases the difficulty in extracting some common features in the first level classification. Besides, it is possible that the current waveform of loads in Category M is similar to the other six categories since some category's circuit structure may dominate the front-end topology. Some more sophisticated steady feature extraction methods are needed.

3.3.8 Session Summary

The steady-state features that are commonly used for NILM can be classified into three groups, i.e., time-domain features, frequency-domain features, and V-I trajectory graphical features. Typically, the dimension of these three feature spaces in literatures is on a scale of 10 to 15 to ensure a satisfied result [98, 106, and 141]. There is no guideline to drive an optimized feature selection. For example, the most commonly used frequency-domain features include the first 10 to 15 harmonics and the phase angle displacements between voltage and the 3rd and 5th order current harmonics. Even though all the above features are utilized, it is still difficult to distinguish and identify loads with the granularity as defined in Level II (depicted in Table 3.3). Therefore, a multilevel classification structure is used to drive the feature set selection. The proposed structure divides a complex problem into several simple problems. Moreover, it drives a more generalized solution, and is easy to be extended because the development of the structure is supported by a complete power supply market study.

When the NILM problem is divided into a multilevel classification problem, the feature space can be analyzed in two steps as given in Session 3.2.3. If only the Level-I categories are considered in the first step, all the loads present very distinct characteristics from one category to another. A set of three features in frequency domain, i.e., normalized 5th order current harmonic component, fundamental phase angle displacement and the total RMS high frequency content, has proved, as shown in Table 3.4. It is much simpler than the original feature space without sacrificing identification performance in this level.

Table 3.4 Features from frequency analysis.

Category [n]	$5^{th}/1^{st}$ [%]	High Frequency [0/1]	Phase Angle [°]
1	0	0	0
2	0	0	[45,90]
3	[60,100]	1	[0,10]
4	[0,10]	0	[0,10]
5	[10,60]	0	[45,90]
6	[10,60]	1	[10,35]
7	[10,60]	1	x

A self-organizing map (SOM) based solution has been proposed to use the extracted feature in the author's collaborated work [142, 143]. The reported classification results are able to reach a 95% successful rate.

For the second level of classification, the problem becomes more complicated for the following reason. First of all, using steady state features alone cannot completely distinguish the loads in Level II. Secondly, every Level II category needs to have its own individual set of features. Therefore, the feature selection for each category has its own focus due to the physical characteristics of the devices within that category. This process can result in an optimized and simple feature selection for the entire load space. The following paragraph considers the NP category (DC converter without PFC) as an example to prove the point.

In previous research, the corresponding identification performance and effectiveness for loads with similar electronic front-ends (i.e., the Level-II sub-categories/loads in the same Level-I category in Table 3.3, e.g., NP-category loads) have often been overlooked. It has been recognized that most of the steady state features currently used cannot further drive a meaningful load identification solution with Level-II granularity no matter how sophisticated the algorithms are. Considering the NP-category, the main circuit structure of all the NP loads are almost the same with only limited differences caused by the component

selection when the DC/DC converters and voltage/current regulators are designed. Even though the topologies of voltage or current regulators are different from one load to another, relatively small changes have been observed in those features that are commonly adopted in the literature. This is because the features were not selected to address the important subtle differences.

Taking the three types of filter topologies utilized in NP-category loads as an example, there are small but explicit differences between the three current waveforms as a result of a circuit discrepancy, as shown in Figure 3.7. These small differences are difficult to distinguish using FFT analysis or V-I features. However, several additional time-domain features, e.g., the slope rate of a current waveform and the monotonicity of a half-cycle current waveform are useful to distinguish between the above variations. Combining these two new features with the first three frequency-domain ones, results in a feature vector based on a multilevel structure that is simpler and more efficient.

While only the NP-category was used as an example, the transient information, such as startup or special working states, are the major potential features which can be utilized in all of Level II.

3.4 Electrical Operation Study for In-category Classification

3.4.1 Remaining Problems for In-category Classification

Most of the steady state features extracted from the electric-circuit study cannot further drive a meaningful load identification solution with Level-II granularity no matter how sophisticated the algorithms are. The transient waveform studies based on the electrical operation principles are expected.

Table 3.5 defines parts of the remaining load identification challenges after Level-I identification. It is worth mentioning that there are still some other loads to be studied.

Table 3.5 Remaining in-category load identification problem.

Level 1	Level 2	Challenges
Resistive Loads	Coffee Maker	Same steady state waveform and power level.
	Toaster	
E-load w/o PFC	Monitor	Same kinds of front-end topology and power level.
	Laptop	
	Set-top Box	Same steady state waveforms.
	Scanner	
	Printer	Different printers have different steady state waveforms.
E-load w/ PFC	LCD/LED TV	Different TVs have different steady state waveforms.

Based on Table 3.5, three kinds of electric loads are discussed in this section, i.e. resistive loads, loads without PFC front-end module and loads with PFC front-end module.

3.4.2 Coffeemaker

For a traditional coffee maker, its basic structure includes a heater, water tubes, a water reservoir, a shower head, a switch and some temperature sensors with fuses. When the switch is turned on, the resistive heating element starts heating the aluminum tube, and eventually the water around the tube boils. The power consumption of a coffee maker mainly comes from the heating element which actually is a coiled wire, and the control strategy is rather simple, a bang-bang control. A temperature sensor is pre-set slightly higher than the boiling point in the coffee maker. It will detect and cut off the current when the coil is getting too hot, and turn it back on when the temperature of the coil is low enough, illustrated by the red part illustrated in Figure 3.14. However, when the coffee maker is in 'keep warm' mode, a lower pre-set temperature is applied. In this case the current waveform is shown like the blue part toward the end in Figure 3.14.

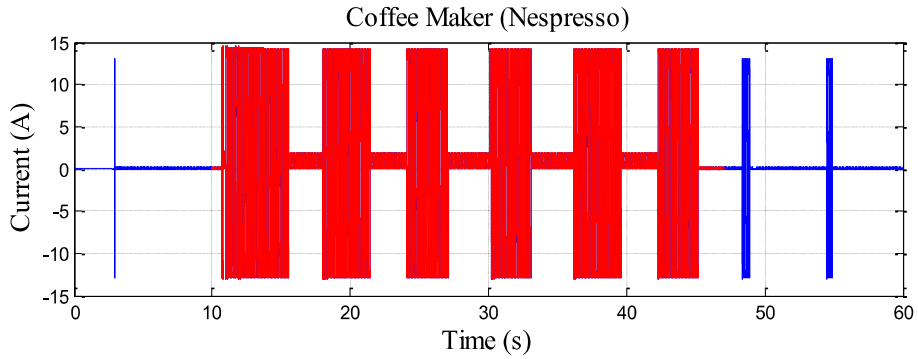

Figure 3.14 The working current of a typical coffee maker.

3.4.3 Laptop

The structure of a laptop mainboard is composed of two parts, South Bridge and North Bridge, as shown in Figure 3.15. When the laptop is plugged into a power outlet, the mainboard is reset and some parts connected to the South Bridge in the mainboard are initialized, waiting for a start-up signal. When the laptop is turned on, the North Bridge as well as the CPU will be reset with the screen lighting up. Because the power consumption of a laptop is mainly drawn by these components, there is a spike in the current waveform at the startup moment. The first 20s to 40s after the laptop is turned on, is the time for a BIOS automatic system check and loading the operating system. Because of the activation of computer components such as hard disc, audio card and network card, the amplitude of the current has a rising trend. When the operating system starting procedure is completed, the laptop displays the system desktop and remains on no-load status. For energy conservation, the frequency of the CPU will decrease automatically and bring a drop of current value. The rise and drop procedure can be observed in Figure 3.16. Because most of the devices connected to the laptop are capacitor-like components, the current waveform will show spikes whenever these devices are triggered on, like the audio card or the keyboard. The red part in Figure 3.16 shows these unstable features.

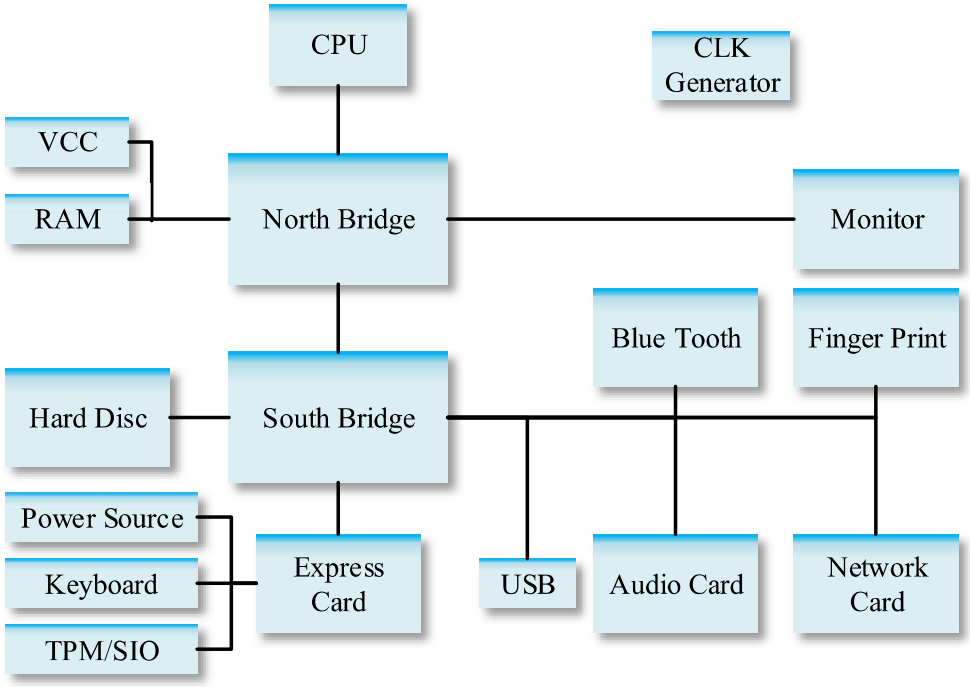

Figure 3.15 The structure of a typical laptop.

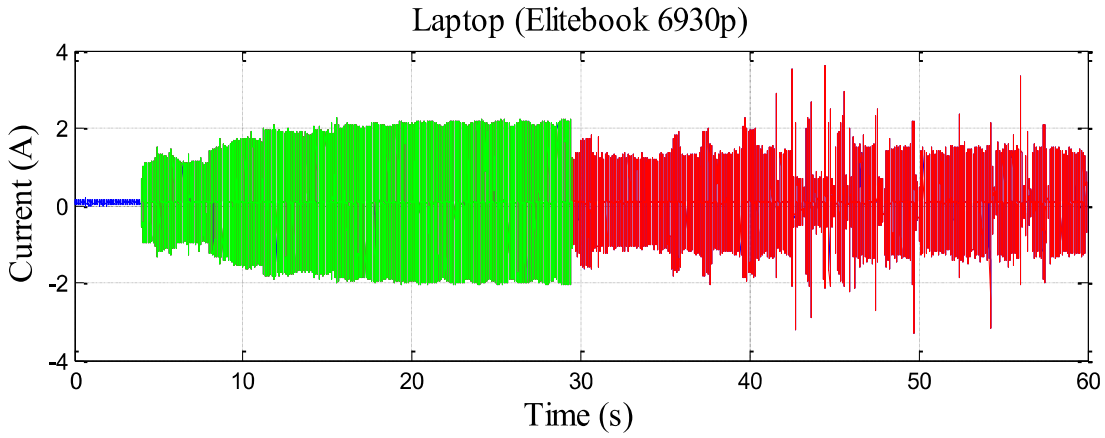

Figure 3.16 The start-up current of a typical laptop.

3.4.4 Monitor

There are two kinds of monitors on the market, i.e. LCD monitors and LED monitors. However they have similar start-up characteristics. Therefore, only LED monitors are

discussed here. An LED monitor consists of a control board, a matrix display driver, LED arrays and a power supply module.

The start-up current of monitor is shown in Figure 3.17. Firstly, there is a small jump-up in the current for the initialization of the power supplier and the control board. Then the current magnitude reaches a higher level by two or three step-ups instantly as the cold cathode fluorescent lamp (CCFL) light source or the LED array is powered on. It is decided by the power supply structure and it is shown as the green part in Figure 3.17. At this time, the electrode in LCD monitor or the lens in LED monitor would consume power to control the light and display certain image.

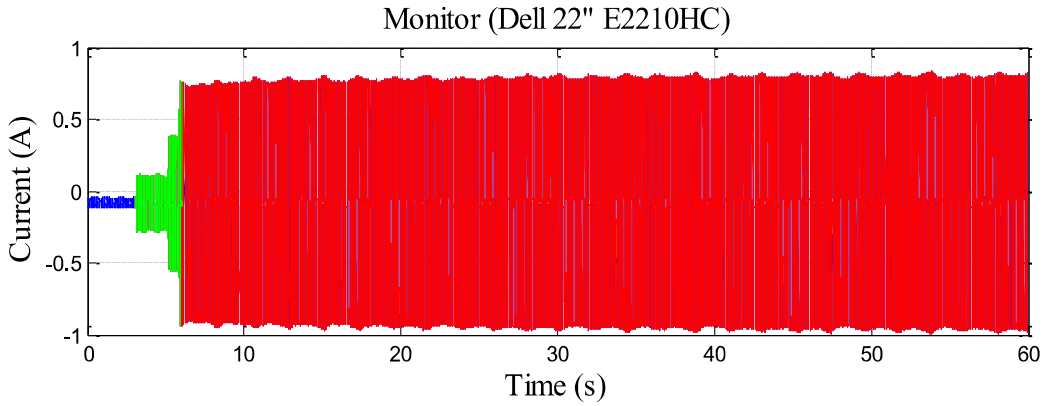

Figure 3.17 The start-up current of a typical monitor.

3.4.5 Scanner

A typical scanner consists of an original manuscript platform, an optical imaging unit, a photoelectric conversion unit and a mechanical transmission unit. The current of a scanner is mainly from the optical imaging unit, the control circuit in the photoelectric conversion unit and the stepper motor for the scan head.

Originally, only the control circuit and some steady power-consuming parts are turned

on. As a result, current magnitude is very small. Later on, the mainboard and connection circuit of the scanner begin to work, and the light is on to lighten the original file. At the same time, the current magnitude reaches a high value. Next the reflected light is received by the CCD array. A stepping motor drives the light tube and the light scans the file until the scanning is completed. During this session, Part B in Figure 3.18, the stepping motor has a reverse stage to send the light tube back to its original position so that the current has a fall and a rise continuously.

The scanner keeps processing the signal and connecting to other devices such as a PC after the motor is turned off. The current magnitude decreases to a relatively lower and steady level.

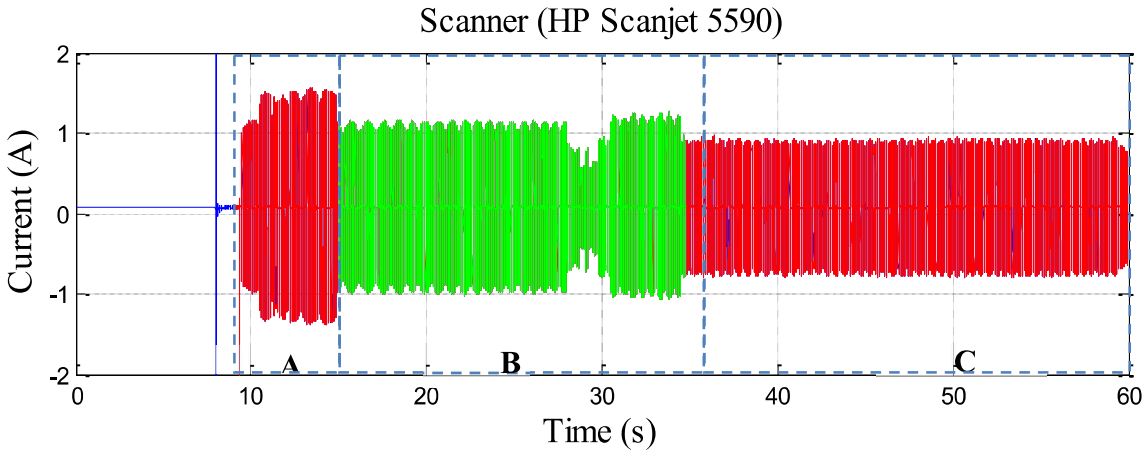

Figure 3.18 The start-up current of a typical scanner.

3.4.6 Set-top Box

The typical structure of a STB consists of a CPU, a mainboard, a modem, a power supply and many I/O ports. Because a STB does not have a stand-by mode, its power consumption is independent of the TV working status. Once plugged-in, the STB begins to work and maintains a stable current magnitude as in Figure 3.19.

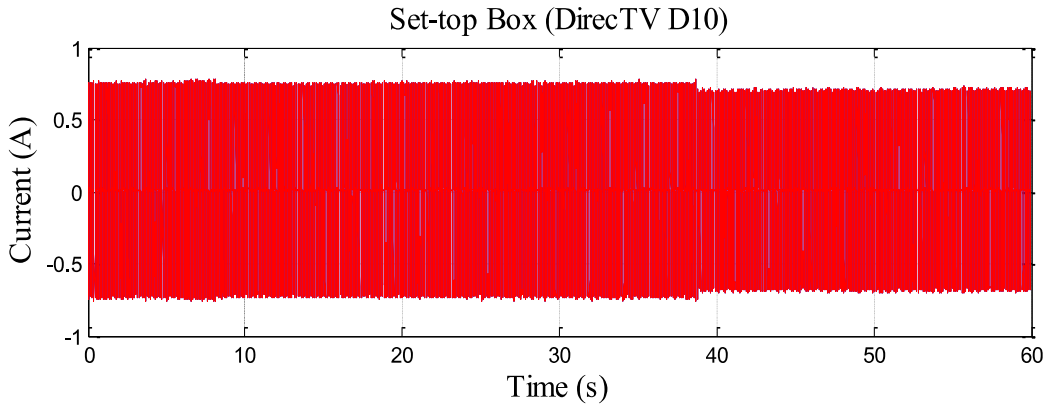

Figure 3.19 The start-up current of a typical set-top Box.

3.4.7 Printer

There are two kinds of printers on the market, i.e. inkjet printers and laser printers. Only a laser printer is considered here because it is more widely used. The current waveform of a laser printer is mainly from the rollers, the control board, the drum, the laser assembly and the fuser. The fuser, which is made of a pair of rollers, is heated to a high temperature when it is working. The largest power consumption part of the printer comes from the heating components.

Some laser printers start preheating at the beginning and maintain a high temperature waiting for the printing work, thus it presents a mid-level magnitude of current as the blue part in Figure 3.20. When printing, the power of the heating components reaches the highest level and the print assembly as well as the roller begins to work. The current shows strong periodicity because the movement of the laser assembly is periodic. The power during the interval between each cycle is mainly for the fuser heating. The cycle is related to the printing and paper passing speed, ranging from five seconds to ten seconds for an office or personal printer.

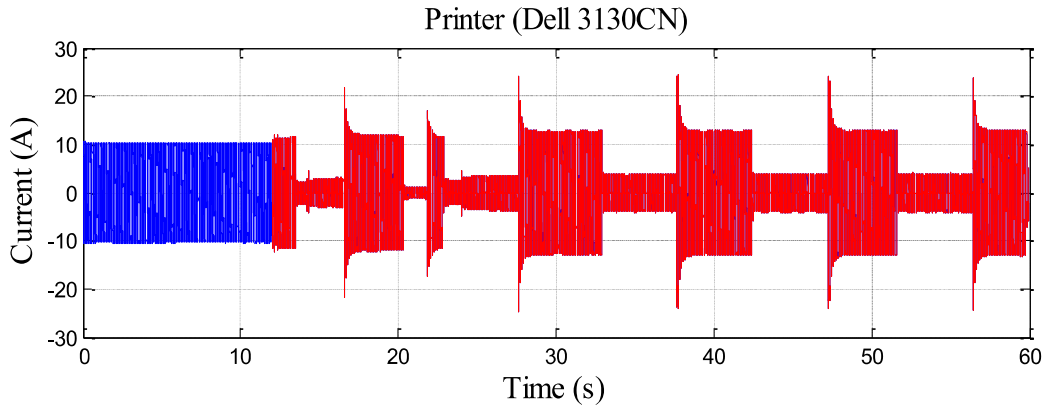

Figure 3.20 The working current of a typical printer.

3.4.8 LCD/LED TV

The power consumption of a television comes from two major parts. One is the control circuit, including the main board and supplier, and the other one is the backlight source, which is the dominating consumer of the energy.

Originally, the current has a small value, which means the power supplier is working and the machine is at standby mode. When a turn-on signal is acquired, the mainboard begins to work and the whole system starts warming-up. Similar to a monitor, a step-like rising edge occurs first in the current waveforms as shown in Figure 3.21. The step is caused by LED matrices. What is different from the monitor lies in the drop-down-period of the current after the TV reaches the steady state. Usually the current will return to steady state soon. Actually, this is because of the brand show-time on the screen. During this time the control system will accomplish video and audio settings as well as the signal processing. The startup time and duration of this interval is different from one brand and model to another. Furthermore, when the backlight source in self-regulation mode is applied, the LCD/LED luminance is adjusted to match the environment. Thus the power consumption for some advanced TVs may increase in dark surrounding conditions and decrease in bright

conditions.

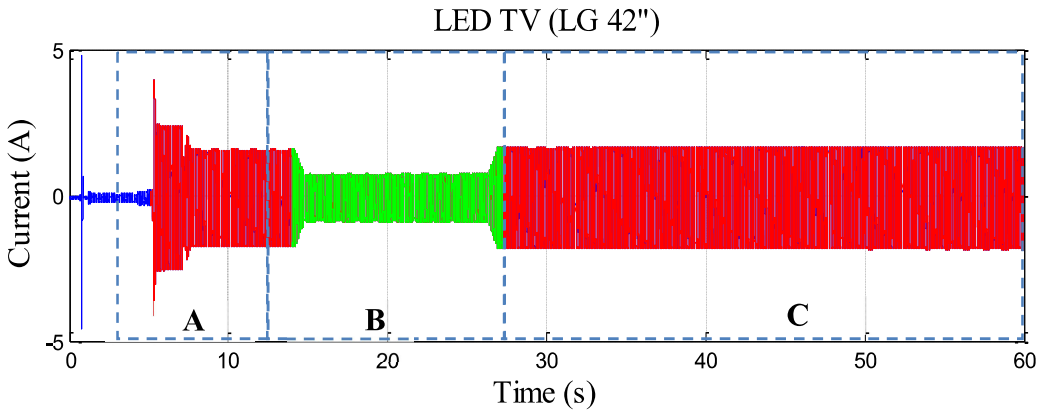

Figure 3.21 The start-up current of LCD/LED TV.

3.5 Finite State Machine Model based on Electrical Operation Study

The transient or long-term feature analysis is commonly used for modeling wavelet and finite state machines in NILM [104, 109]. Similar to the steady state feature space, there is no guideline either to drive an optimized and reliable transient feature selection. Therefore the problem of the poor repeatability of transient events always happens to the existing algorithms, which results in the lack of robustness and reliability. The electrical operation study in this work provides a solid support to the finite state machine algorithms proposed in the authors' collaborated work [144]. A FSM modeling containing four elements is presented, i.e. steady state, semi-steady state, spikes, and oscillation. Several example candidate features are listed here, like time duration of each pattern, a history vector (the power level at each state, the number of self-loops), the number of states for a certain length of observations, the percentage of time (similar to duty cycles) of the FSM staying at semi-steady states and steady states for a certain length of observations. A detailed introduction of

the algorithms can be also found at [144].

The FSM model of the loads studied in this paper is provided in Figure 3.22, Figure 3.23, Figure 3.24, Figure 3.25, and Figure 3.26. The challenges listed in Table 3.5 are solved by the FSM mode as discussed in [144]. Moreover the new FSM model is more reliable because of the good repeatability.

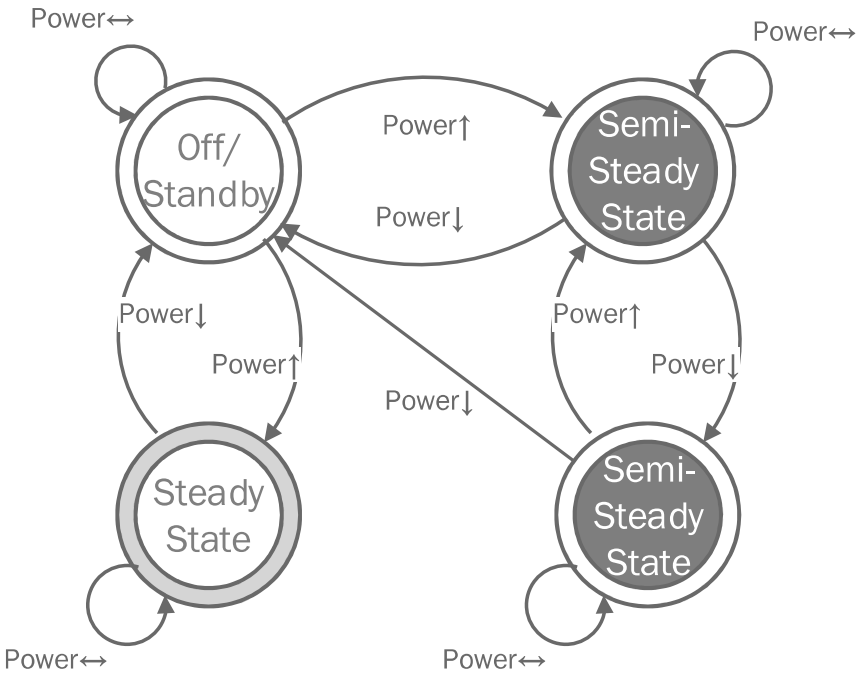

Figure 3.22 The finite state machine model of a coffee maker.

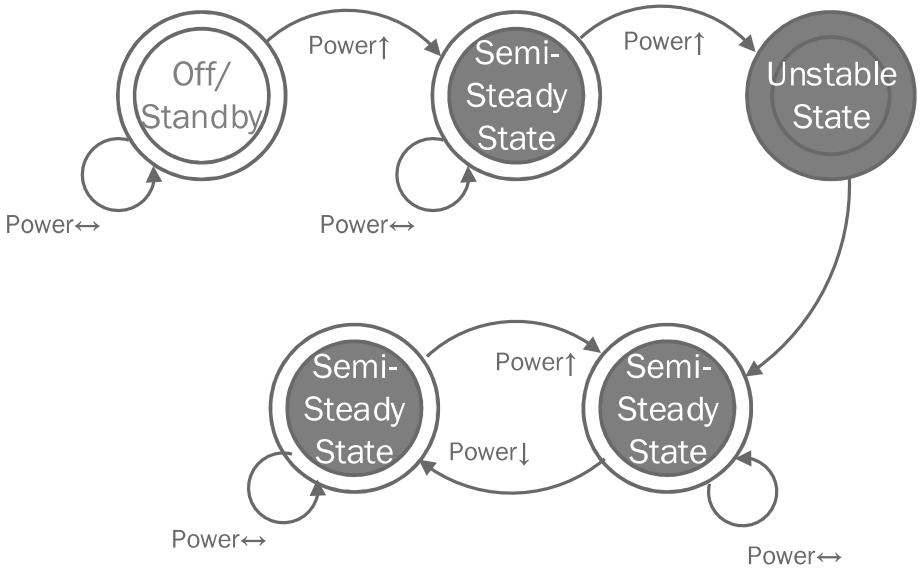

Figure 3.23 The finite state machine model of a laptop.

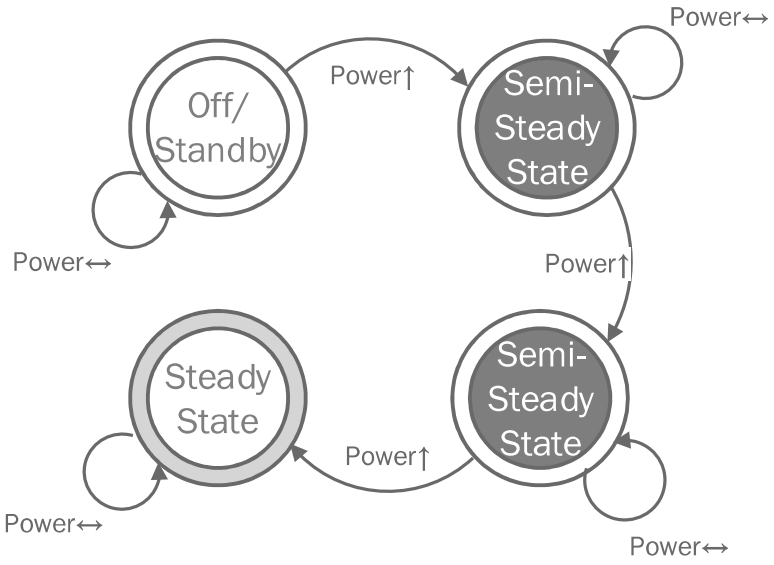

Figure 3.24 The finite state machine model of a monitor.

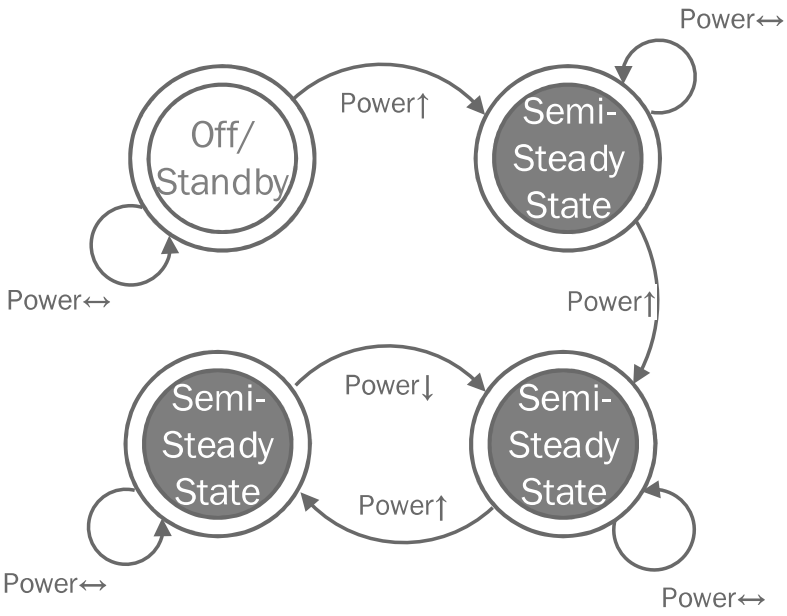

Figure 3.25 The finite state machine model of a scanner.

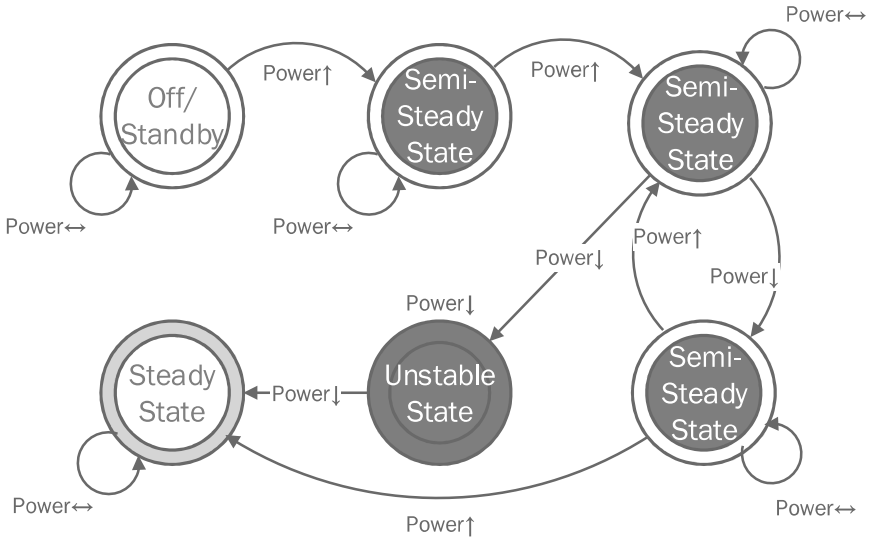

Figure 3.26 The finite state machine model of a scanner.

Through the in-depth study of the electrical operating principles, a more generalized and efficient finite state machine algorithm can be realized. The FSM modeling procedure is

driven by an understanding of the relationship between different transient state current waveforms and their corresponding electrical operations. Ref. [144] has proved that this established relation is very helpful to optimize the feature space and to define a reliable FSM. The next stage of the NILM study will consider a self-adaptive and self-debugging mechanism.

3.6 Chapter Summary

A comprehensive study on the electric schemes and operation principles of the major loads in the market is proposed in this chapter. This fundamental study is able to enhance the efficiency and quality of the features, therefore greatly contributes to the algorithm development. The features proposed in this chapter have been applied in the author's other work collaborated with the other Ph.D. They are proved valid and useful for NILM identification. However, as mentioned before, since the load space and consumer electronics technology updates very quickly, the knowledge database has to be updated time by time. Actually, a self-adaptive and self-debugging algorithm is expected. And the next chapter will discusses an online learning algorithm based on the feature study did in this chapter.

CHAPTER 4 ONLINE LOAD IDENTIFICATION FOR RESIDENTIAL ENERGY AUDITING

4.1 Chapter Overview

Even though many new model-driven features have been extracted above, there is still no promise that such a feature set can be valid to identify all the loads in the market. As a result, when the input sample is a load of a model that is not covered in the training set, incorrect identification frequently occurs. Besides, with the development of consumer electronic industry, new types, brands and models of appliances are emerging at a fast speed, which further aggravates the problem. This chapter proposes an adaptive nonintrusive load identification model to address this problem. The proposed model is not dedicated to identify all the loads in one time, but it will grasp knowledge from samples that are not identified in the real application, and gradually form a new learning procedure so as to identify more and more new samples correctly. The random forest algorithm is introduced here to realize the objective and a case study is carried out to verify the effectiveness of the model.

In detail, when an input sample doesn't match any existing loads in the database, it will be assigned an 'unknown' label. To gain the knowledge from the unknown samples, online clustering algorithm will be applied first to find new load classes or new load variants. If a new class or new variant is generated, it will be manually assigned a class label, which can either be one of the existing class labels if it's a variant of a known load class, or a new class label if it's a completely new load class. After acquiring the new knowledge, the classification model will be updated as well.

4.2 Data Preparation

The load space used in this chapter is established based on the load study in Chapter 3, which almost covers all the appliances with high difficulty to be classified as mentioned in the author's collaborated work [145]. Actually, the load space is very complex. On one hand, given the same type of load, they may not have same patterns because of the different operating principles, such as the laser printer and the inkjet printer under the printer family. On the other hand, even for one load, it may have various patterns because of the different modes, such as the heating and the defrosting mode of a microwave. However, there is no need for an online learning algorithm to know the entire load space at first due to its adaptive nature. Therefore the load space used for an online learning algorithm should be carefully defined.

From the perspective of an online learning algorithm, there are three optional states for each load.

State I: The loads that have been studied and whose operation principles and power supply structures are relative stable and will not change frequently. The representative load is like the monitors, shown in Figure 4.1.

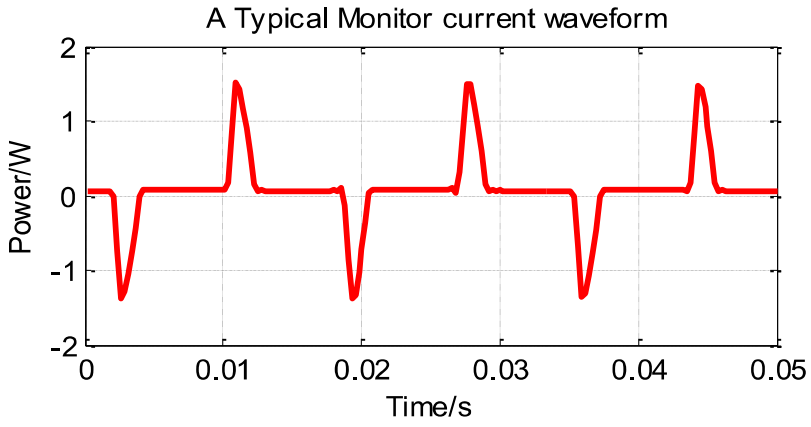

Figure 4.1 A typical monitor current waveform.

State II: The loads that usually have various operation principles or power supply structures such as LED TVs vs. LCD TVs, or power factor correction equipped PCs vs. normal PCs, shown in Figure 4.2. Therefore, only one or several of these variants have been studied.

State III: The loads are totally new, therefore their structure and operation requirements have not been defined by industry standards yet. These loads usually cannot be studied at the initial stage. The examples are new LED bulbs or Xbox Player, shown in Figure 4.3.

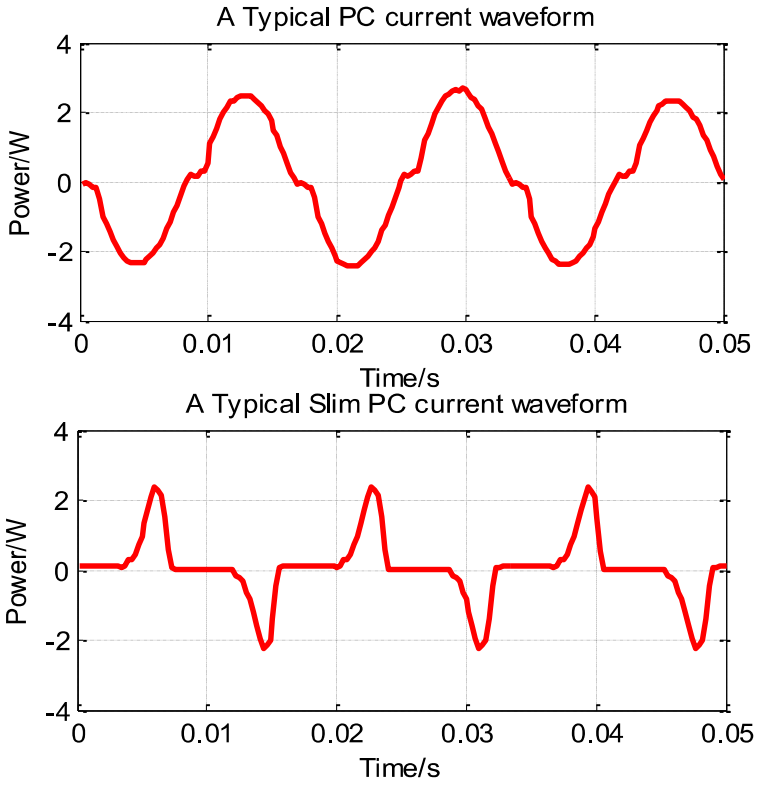

Figure 4.2 Two typical PC current waveforms.

The two major targets of an online learning algorithm can be summarized as follow. The algorithm should be capable to detect the load if it is a variant of an existing load or a new load (State II or State III), and then convert it to State I. Moreover, the algorithm should be able to successfully identified the State I load. Given such a structure, to know the state

of each type of load at the initial stage turns out not to be very important any more. Actually, the loads can be located in any state at first. However, given the research purpose, a load space to be studied should be able to clearly represent the challenges of the two targets. An empirical load space is generated in this paper, shown in Table 4.1. This load space represents the characteristics of the loads very well by considering both the similarity and the variety of each load at the same time.

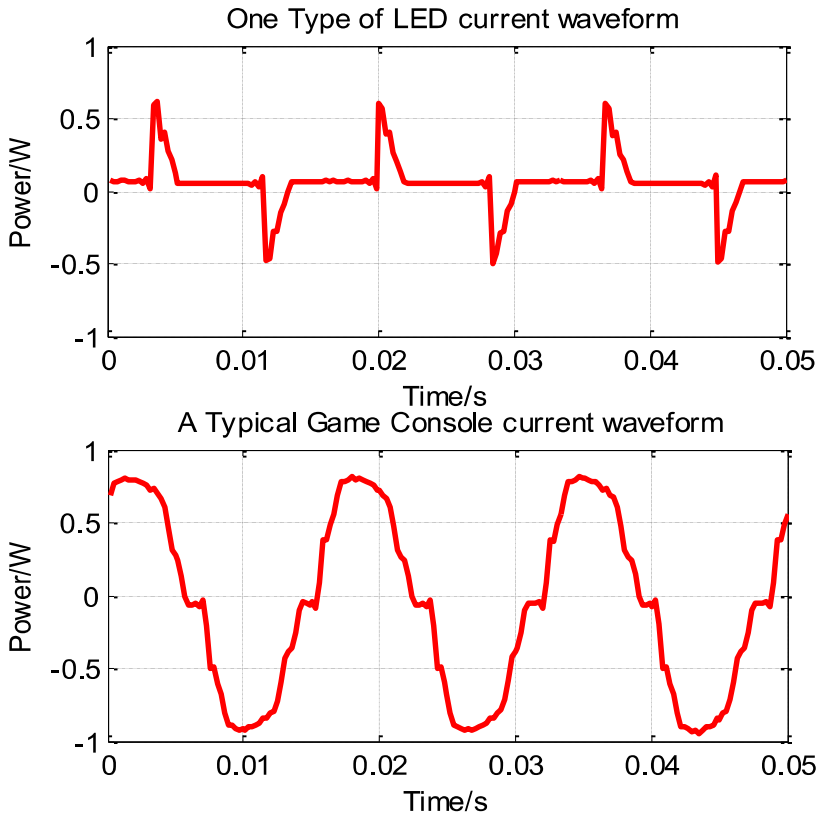

Figure 4.3 The current waveforms of a LED bulb and a game console.

In detail, the voltage and current are measured at 3.84 kHz. According to the study of [70], most plug-in household appliances can achieve steady state within one minute. Therefore a total of two minutes of V/I data will be collected for each sample in this work, during the first minute, transient features will be collected and steady features will be

collected in the second minute. To manage such a large amount of data, several new units, *cycles*, *clips*, *vectors, observations* and *samples*, are introduced to present the data, shown in Table 4.2.

Table 4.1 Load space definition.

S.T.	Load
I	DVD, STB, Fan, Heater, Florescent Light, Monitor, Projector, Microwave, Scanner.
II	TV, Desktop, Laptop, Printer.
III	LED Light, Xbox.

Table 4.2 The definition of unit.

Unit	Definition
Cycle	One single sinusoidal waveform, there are 60 cycles per second in U.S.
Clip	Ten cycles of waveform.
Vector	The feature vector to be put into the algorithms, generated by one clip and one transient waveform
Observation	Composing of 10 vectors, used for unknown detection test.
Sample	One two-minute's measurement for a single load

Given the definition above, the term *Unknown* is defined as follow. Once a new load is plugged in the smart outlet, a sample will be generated. The transient features are extracted from the first minute waveform and the steady features are extracted from the second minute. Usually the entire first minute waveform is needed to determine the transient features while only one clip of steady state waveform is enough to determine the steady features. Therefore, randomly picking 10 clips in steady state waveform and combining them with the transient features collected in the first minute will generate an observation. This observation will be tested into the detectors. If over 80% of those vectors in one oberservation are not

recognized by the well-trained unknown detector, then the appliance being tested will be considered as *Unknown*.

4.3 Introduction of the Algorithm and Theory

The overall structure of the system is shown in Figure 4.4. Once a load is plugged into the outlets and turned on, a two-minute measurement will be triggered on. The data generation module will automatically generate the validation test samples as mentioned above for the unknown detection and the load identification.

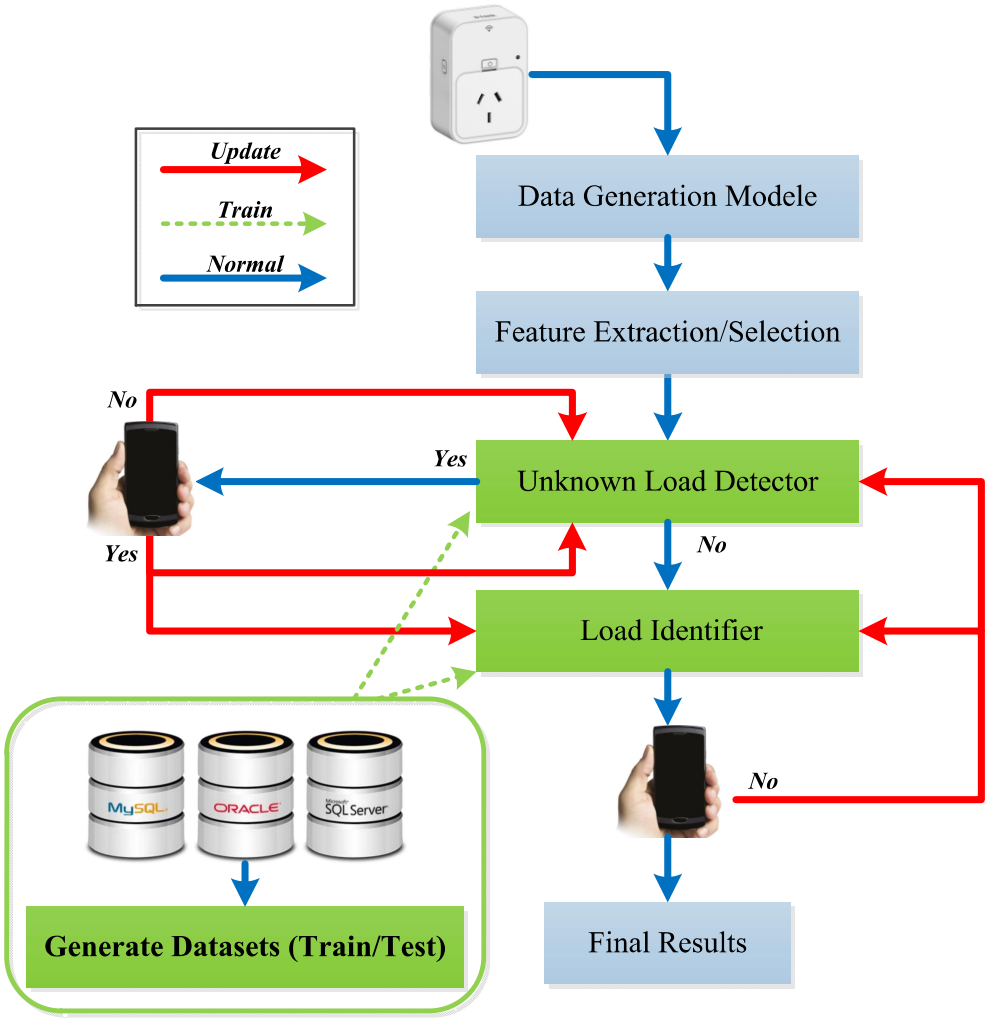

Figure 4.4 The flowchart of the proposed self-learning NILM system.

Moreover, the feature extraction module will generate the corresponding feature sets for the detection and the identification. Next, these feature sets for each test samples will be put into the unknown detector. If it is recognized as a new load, the results will be first sent to the customer. Once it is confirmed as an unknown load by the customer, it will be automatically skip the detection and identification module. The final results will be provided by the customer directly. An update signal will also be sent to the detection and the identification module. However if it is confirmed as a wrong detection, the data will be used to re-train the unknown load detection module again. If the load is recognized as an existing load, it will be sent to the load identifier, and the identified results will be delivered to the customer again. Usually, if it is right, no action is required and the final results will be presented. However, if it is wrong, an update signal will be sent to the detection and the identification module, a self-learning process is triggered again.

In such a system, the detector and identifier have to be good at online learning and easily updating. The random forest algorithm proposed in [146] shows great characteristics on the online learning procedure and therefore is a good candidate for the identifier. Besides, the general linear regression (GLR) algorithm is introduced as the unknown detector because of its good characteristics on online updating. The idea is to model each type of load in the load space as a binary classifier. Empirically, the extracted features will exert great influences on the GLR performance, since a good feature set will greatly reduce the detection efforts and guarantee the good results. Besides, GLR is a binary classifier and will have to balance the trade-off between the recall and the precision [147]. It is also highly dependent on feature set selected for each single GLR detector. Therefore, a feature selection is required for the proposed algorithm. In detail, the feature selection module has to process the capability not only to study the relationship between the features within the

feature set, but also to model the relationship between the input features and the output variables. It is very hard for those conventional feature selection solutions like principle component analysis (PCA) and independent component analysis (ICA) because they usually use a simplification of dependence like the covariance to study the relation of two random variables, which is not suitable for the complex relationship between the input and output variables. Consequently, none of them can select a compact and informative subset, which is the most important goal in this paper for the feature selection. A new feature selection method based on the Copula theory is introduced in this chapter [148].

4.3.1 Feature Selection

Many features have been studied during the past ten years. This chapter will put all these features in the candidate pool during the feature selection stage, as shown in Table 4.3.

Table 4.3 Summary of the input features.

State	Symbol	Description
Steady State	*P&Q*	Active and reactive power [20]
	PC	Peak current [101]
	AC	Average current [110]
	CF	Crest factor [143]
	F	1^{st} to 15^{th} order harmonic components of current waveform [143]
	VI	voltage-current (V-I) trajectory [106]
	θ	Phase angle differences of V-I [143]
	O	Other features like slope, ramp rate, area, etc. [143]
Transient State	*W*	Wavelets of current waveforms [104]
	IA	Instantaneous admittance [149]
	IP	Instantaneous power [107, 150]
	EI	Eigenvalues of current waveforms [141]
	EN	Envelope of the current waveforms[144]
	FSM	Finite state machine of current waveforms [109]

If assuming the waveforms are denoted by

$$V(t) = \Sigma_{p=1}^{\infty} V_p \sin(p\omega_0 t + \delta_p) \tag{4.1}$$

$$I(t) = \Sigma_{p=1}^{\infty} \mathrm{I}_p \sin(p\omega_0 t + \theta_p) \tag{4.2}$$

The mathematical expressions of these features are listed below.

1) Real power P and reactive power Q.

2) Displacement power factor

$$dpf = \cos(\delta_1 - \theta_1) \tag{4.3}$$

3) The total harmonic distortion (THD) in the current

$$THD = \frac{\sqrt{\sum_{p=2}^{\infty} I_p^2}}{I_1} \tag{4.4}$$

4) Power factor

$$pf = \frac{\cos(\delta_1 - \theta_1)}{\sqrt{1 + THD^2}} \tag{4.5}$$

5) Crest factor or peak-to-average ratio (PAR):

$$cf = \frac{|\, I_{peak} \,|}{I_{RMS}} \tag{4.6}$$

6) Eigenvalues: for dynamic loads, their waveforms could vary from cycle to cycle. Eigenvalues are introduced to capture the dynamics. In brief, firstly rearrange the waveform series into a matrix with each row representing one cycle, and then apply singular value decomposition (SVD) to this matrix, which will decompose the matrix to the product of 2 unitary matrixes and a diagonal matrix.

The eigenvalues would be the values in the diagonal matrix.

7) Up to 25th harmonics (amplitude and phase) of the current.

Copula theory is a powerful tool to describe the dependence between random variables [151, 152]. Two main advantages of the Copula are summarized as follows. One is the possibility to build a variety of dependence structures based on the existing parametric or non-parametric models of the marginal distributions. Therefore, it can provide a more accurate mathematical expression of the relationship between the input features and the output variables. Another advantage is the relative mathematical simplicity of copula theory in describing the features without calculating the joint-CDF like these conventional methods.

In detail, assuming the marginal cumulative distribution functions of a random vector $(X_1, X_2, \dots, X_d)$, are continuous functions, according to Sklar's Theorem [148], the joint CDF of this vector can be written as,

$$H(x_1, \dots, x_d) = C(u_1, \dots, u_d). \tag{4.7}$$

where function C is defined as the copula of $(X_1, X_2, \dots, X_d)$. The theorem also states that, given *H*, the copula C is unique.

The flowchart of the proposed feature selection algorithm is shown in Figure 4.5. In detail, there are five major steps in the algorithm. The algorithm estimates two copulas, C_1, the copula of X_{d+1} with the features $(X_1, X_2, \dots, X_d)$ and C_2, the copula of $(X_1, X_2, \dots, X_d, X_{d+1})$ with Y.

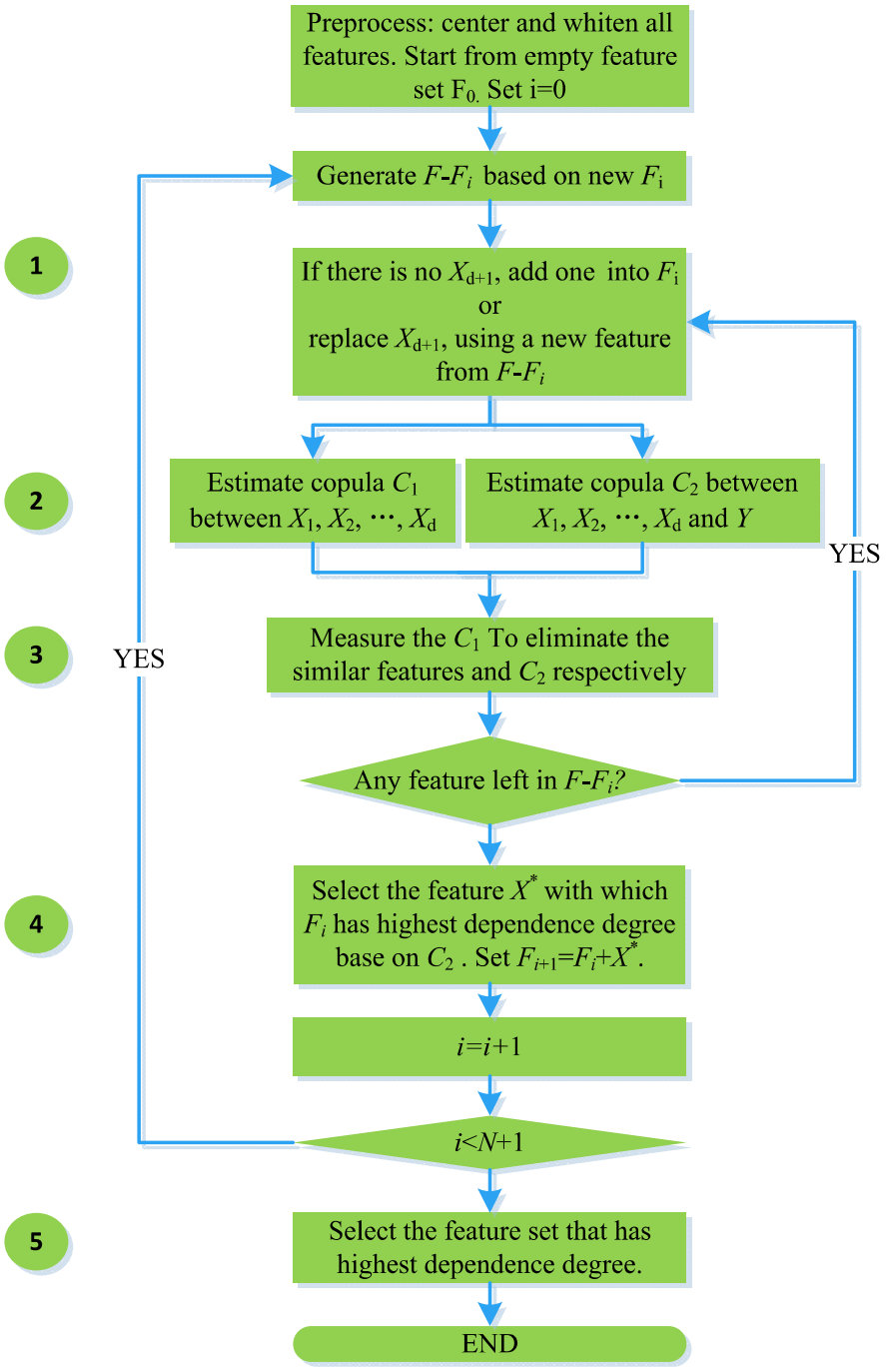

Figure 4.5 The flowchart of the proposed feature selection algorithm.

Firstly, each feature in the original feature set will be first sent to a temporary set F_i. Then, the estimations of copula C_1 and copula C_2 are calculated. In this paper, since no any prior-knowledge is provided from the data set, a non-parametric estimation based on the

empirical copula is applied. [148]

After the estimation of the copula, the next step is to measure the dependence degree. The similarity function between the new input X_{d+1} and each X_i in F_i is calculated, so as the function between $(X_1, \dots, X_{d+1})$ and Y. In the first loop, if the new added feature has a high dependence rate with the other exiting features, this feature will be firstly removed from the feature sets. After the searching procedure, a group of C_2 is generated, the highest dependence degree of the calculated C_2 will be selected, with the X_{d+1} added in the feature set.

Finally, the size of F_i keeps increasing, and for each increase, it will have a new C_2. The algorithm will select the highest C_2. The feature sets that have low dependence degree will be discarded. The input order will affect the results. A searching algorithm can be added to solve this problem.

4.3.2 Unknown Pattern Recognition

The unknown detection model is based on the Generalized Linear Regression (GLR) model [153]. A generalized linear regression model G_i is constructed for each type of known load i, for $i \in \mathcal{L} = \{1, \dots, N\}$. We denote the collection of the GLRs by $\mathcal{G}$. For an input sample $x = (x_1, \dots, x_k) \in \Omega$, where Ω is the k-dimensional sample space, the model G_i outputs a value y_i based on the following equation,

$$y_i = f\left(\sum_{j=1}^{k} \beta_j^i x_j\right) \tag{4.7}$$

where f is the logistic function mapping $\mathbb{R}$ to inverval $[0,1]$ defined by

$$f(t) = \frac{e^t}{1 + e^t} \tag{4.8}$$

In the above equations, $\{\beta_j^i : 1 \leq j \leq k\}$ is the parameter for model G_i. The output of each model y_i lies between 0 and 1 and represents the probability of the input x being generated from load i. Thus, the closer to 1 y_i is, the more likely the input is generated from load i. After the outputs $\{y_i, i = 1, \dots, N\}$ of all GLR models are collected, an unknown index, $U(x) = \max_{1 \leq i \leq N} y_i$ is calculated based on the maximum value of the y_i, and it means the probability of the input x being generated by the most probable load. If $U(x)$ is less than a pre-specified threshold S, i.e. $U(x) < S$, it means that x is not likely generated by all the known loads $i \in \mathcal{L}$, and the detector declares 'positive', which means x is declared as an unknown sample; on the other hand, if $U(x) \geq S$, the detector declares 'negative', which means *x* is declared as known.

There is a classical tradeoff between this type of binary classifications, the trade-off between false-negative and false-positive. Under our setting, false-negative means that an unknown input is declared as a known load and false-positive means that a known input is declared as an unknown load. Generally it is hard to reduce the probability of both false-negative and false-positive, because if the probability of false-negative goes down, the probability of false-positive will generally go up, and the same is true for the other way around. The key in balancing this tradeoff is to match the probability of false-negative and false-positive with the practical needs. This means, if in practice false-negative is more tolerable than false-positive, then the detector should be tuned to reduce the probability of false-positive, even though this will increase the probability of false-negative. In reality, it is hard to define the practical needs, and the practical needs can be constantly changing. This poses the need of an adaptive unknown detector, an unknown detector that can tune itself so

that the tradeoff can adapt to the changing practical needs.

Before formally introducing the self-adaptive rules of the model, it is good to discuss a few observations motivating the adaptive model. There are several factors affecting the false-positive false-negative tradeoff. The first is the threshold S. The larger S is, the detector is more inclined to declare positive, and thus it is more likely to result in false-positive and less likely to result in false-negative. The second factor is the sample space of the GLR models $\mathcal{G}$. If a sample of a known load i comes to the GLR model G_i, but the sample lies in an area of the sample space that is not captured by G_i, the GLR model G_i will possibly give a low output (G_i does not know load i can generate samples lying in this area) and the detector result is likely to be false-positive.

In light of the above two factors, the update rules of the unknown detection model are designed as follows. There are three types of updates. The first type corresponds to the first factor described above. It works by tuning the model's threshold parameter S based on the feedback from the customer decision.

$$\tilde{S} = S \pm \Delta S \tag{4.9}$$

where ΔS is the step size, and $\pm$ depends on the customer's preference between false-negative and false-positive.

The second type of update corresponds to the second factor. It updates a GLR model for a known load, say G_i, in such a way that, a subset of the sample space that is previously not captured by G_i is now incorporated into G_i. This is can be done by the following online update rule of GLR models. Suppose a $\tilde{x}$ is a new sample generated by load i, then the parameter β^i is shifted along the negative gradient direction of the log likelihood function generated by the new data $\tilde{x}$.

$$\tilde{\beta}^i = \beta^i - \lambda \nabla_\beta l(\beta^i, \tilde{x}) \tag{4.10}$$

Where

$$l(\beta^i, \tilde{x}) = \ln f(\sum_{j=1}^{k} \beta_j^i \tilde{x}_j) \tag{4.11}$$

and therefore

$$\nabla_\beta l(\beta^i, \tilde{x}) = \frac{f'(\sum_{j=1}^{k} \beta_j^i \tilde{x}_j)}{f(\sum_{j=1}^{k} \beta_j^i \tilde{x}_j)} \tilde{x} \tag{4.12}$$

In the above equations, λ is a step size parameter. The larger λ is, the update rule is more inclined to use the information from the new sample $\tilde{x}$ compared to the old samples.

The third type of update is to construct a new GLR model from a collection of unknown samples that have been verified to belong to a new class of load. This can be done by the GLR training algorithm, e.g. reweighted least square algorithm. Once this is done, new samples from this new class of load will no longer be classified as unknown because the new load information has been captured by the detector.

Figure 4.6 summarizes all the components of the unknown detector model.

To validate the model, a straightforward way is to compute the accurate rate. Given a collection of input samples $x^1 \ldots x^m$ and there associate outputs, $y^1 \ldots y^m$, where $y^i = 1$ means x^i is generated by a known load $i \in \mathcal{L}$ and $y^i = 0$ means x^i is generated by an unknown load $i \notin \mathcal{L}$. Let $\hat{y}^i$ be the detector output for x^i. Then the accuracy is defined as

$$Acc = \frac{\sum_{i=1}^{m} 1\{y^i = \hat{y}^i\}}{m} \tag{4.13}$$

where $1\{\}$ is the indicator function. And due to the adaptive nature of this model, we can also calculate the accuracy over time, to validate whether the update mechanisms are effective in improving the detector accuracy.

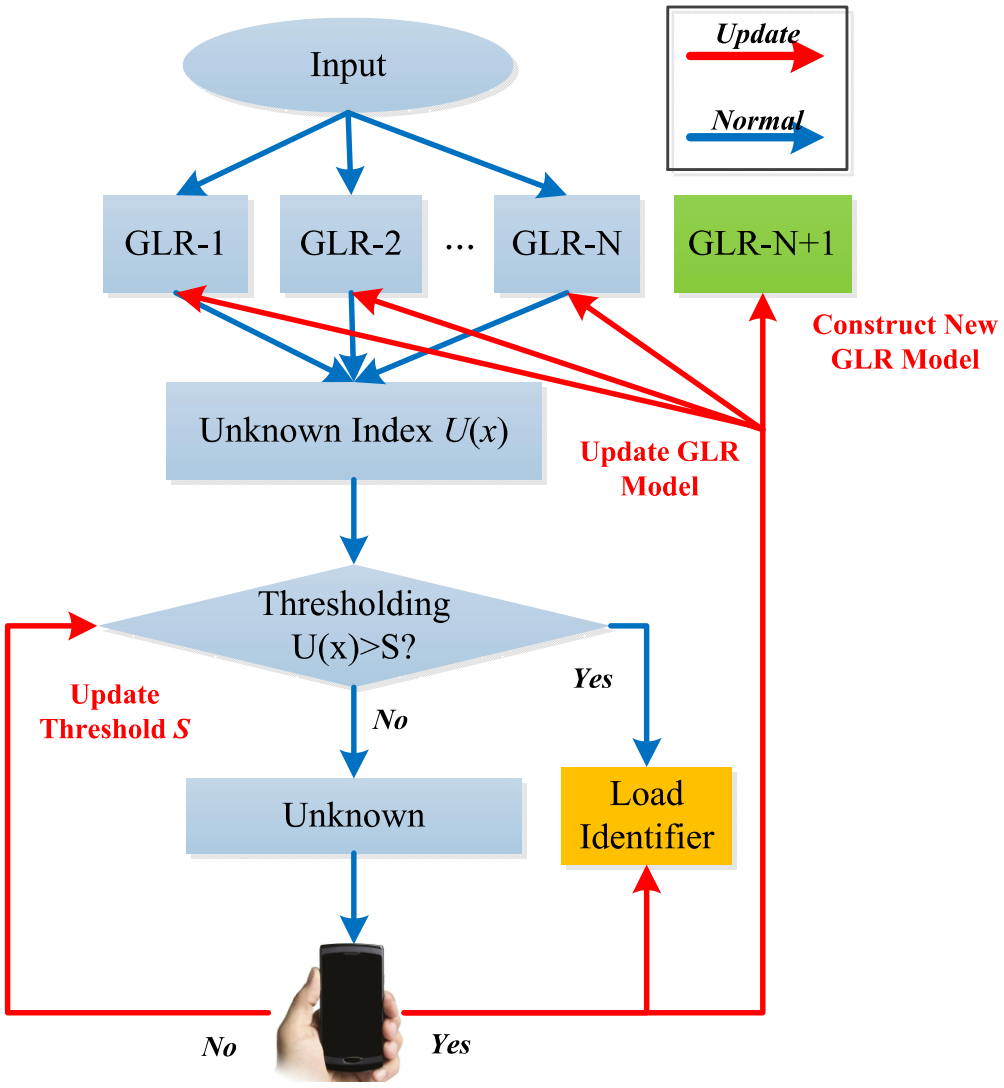

Figure 4.6 The flowchart of the proposed unknown model detection algorithm.

4.3.3 Random Forest Algorithms

The predecessor of random forest (RF) as well as classification and regression tree (CART), was invented in 1984 by L. Breiman [154]. Breiman later introduced another essential technique for RF called “bagging” in 1996 [155]. The emergence of RF was also influenced by the work of Y. Amit [156], and T. K. Ho [157] who introduced some ideas relating to RF such as the decision randomization and the random subspace selection. The

formal introduction of RF was made by L. Breiman in 2001 [158], which formed the basis of the modern practice of RF.

RF is an ensemble learning method for classification (and regression). It is based on two techniques, the classification and regression tree algorithm as well as the bagging mechanism. The classification and regression tree algorithm is a tree-structured model that maps the observations about an item to the conclusions on the item's class. A simple illustration of the classification and regression tree can be found in Figure 4.7. In Figure 4.7, the classification and regression tree growing procedure can be described as iteratively splitting each node into two sub-nodes by finding a best split variable along with a best split value till reaching minimum node size. The advantage of the classification and regression tree algorithm is that it can be fitted to the data well, however the accuracy of classification and regression tree method is low. In other words, this method has a low bias but suffers from a high variance.

To solve this problem, the classification and regression tree method is extended by introducing a bagging mechanism, which is called random forest. The introduction of the bagging mechanism will reduce the variance of the classification and regression tree method while keeping the bias low. What's more, random forest adopts a trick called randomized node optimization to further reduce the variance of the classification and regression trees. All above modifications avoids the disadvantages of the classification and regression tree and proves to achieve a good performance.

The Breiman's Algorithm of random forest is presented below. In brief, the procedure is to construct a set of classification and regression trees fitted to the bootstrap sampled datasets. Note in step 1-b-i and 1-b-ii, instead of searching for the best split variable among all p variables, random forest limits the candidate best split variables to m randomly chosen

variables. This is the randomized node optimization mentioned above as a trick to reduce the variance of the classification and regression trees.

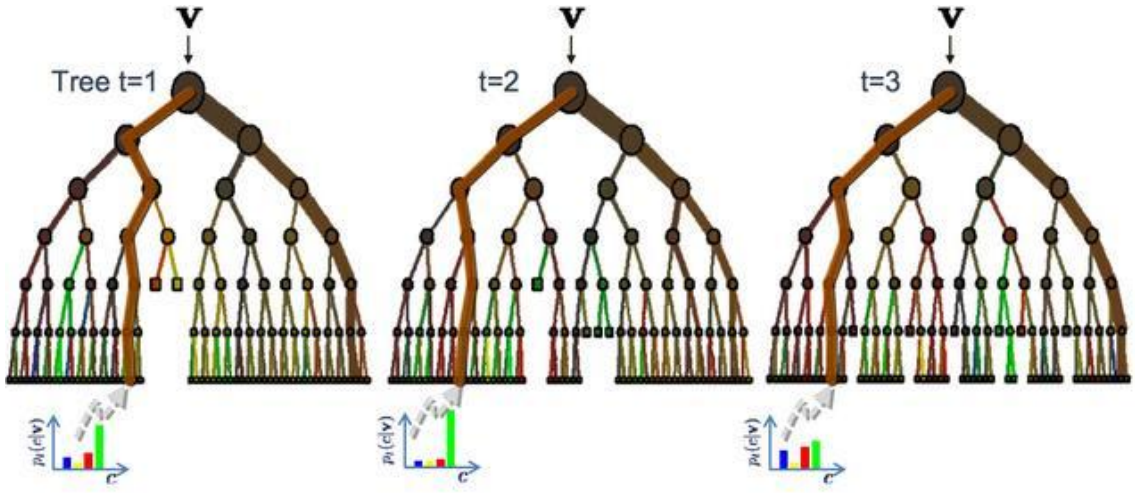

Figure 4.7 A simple illustration of CART.

In addition to the low bias and the low variance, random forest has several other desirable features. Firstly, RF can generate an out-of-bag error in its growing procedure, while other models generally require multiple training procedures like cross validation. Secondly, RF is robust against irrelevant features and outliers in the training data and finally, RF is structured as a tree, which makes it easy to be expanded to fit more data by growing more 'branches'.

All these features enable random forest to be a good online learning algorithm and a nice adaptive machine learning model [159].

Next, the online update procedure will be fully discussed in details. The algorithm combines the ideas of the online bagging and the extremely randomized forests, and further proposes an on-line decision tree growing procedure.

Growing Stage:

Input: Training Data: N p-dimension samples along with their class labels.

Require Parameter B: Number of trees.

Require Parameter m: Number of candidate split variables at each split;

Require Parameter n_{min}: Minimum node size.

For b = 1 to B:

(a) Draw a bootstrap sample Z^* of size N from the training data.

(b) Grow a random-forest tree T_b to the bootstrapped data, by recursively repeating the following steps for each terminal node of the tree, until the minimum node size n_{min} is reached

i. Select m variables at random from the p variables

ii. Pick the best variable/split-point among the m

iii. Split the node into two daughter nodes

Output the ensemble of trees $\{T_b\}_1^B$

To make a prediction at a new point *x*:

Let $\hat{C}_b(x)$ be the class prediction of the b_{th} random-forest tree. Then $\hat{C}_{\text{rf}}^B(x) = majority\ vote\{\hat{C}_b(x)\}_1^B$

For the bagging part, the sequential arrival of the data is modeled by a Poisson distribution, in which each tree is updated on each sample k times, where k is a random number generated by Poisson (λ). During the growing of a randomized tree, each decision node randomly creates N random tests S and picks the best according to *Gini* index. The *Gini* index is defined in (4.14)

$$L(R) = \sum_{i=1}^{K} p_i(1-p_i) \tag{4.14}$$

where R denotes the point set and K denotes the number of classes and P_i denotes the label density of class i in the points set. The reason of using *Gini* index is because it can measure the homogeneity of a dataset, and the smaller it is, the more homogeneous the point

set is.

Meanwhile, corresponding statistics of the split made with each test in S are collected: for a random test in S, P_{jls} and P_{jrs} corresponding to the statistics of samples falling into left and right partitions are collected. The test with the highest gain is chosen as the main decision test of that node. Unlike off-line, the statistics are gathered over time, therefore, the decision on when to split depends on if there have been enough samples in a node to have robust statistics and if the splits are good enough for the classification purpose.

Two hyper-parameters are introduced in [159], i.e. the minimum number of samples a node has to see before the splitting α, and the minimum gain a split has to achieve β. After a split occurs, the P_{jls} and P_{jrs} are propagated to the subsequent newly generated left and right leaf nodes, respectively. The entire on-line random forest can be seen in the pseudo-code below.

An illustration of the update of a tree based on the pseudo-code is shown in Figure 4.8.

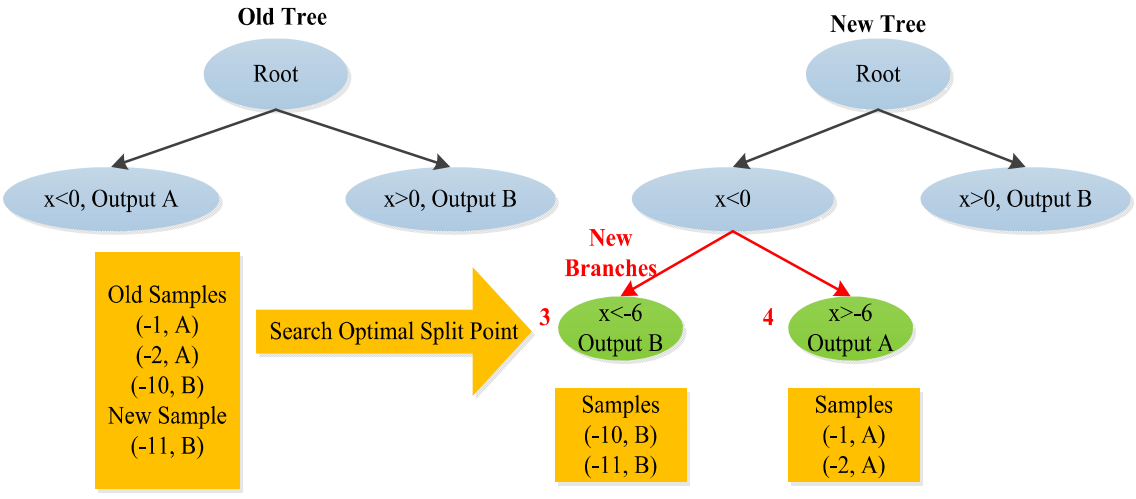

Figure 4.8 An illustration of the update of a tree.

Require: Sequential training example $< x, y >$
Require: The size of the forest: $\boldsymbol{T}$
Require: The minimum number of samples: α
Require: The minimum gain: β
// For all trees
for t from 1 to T do
    $k \leftarrow$ Poisson(λ)
    // Update k times
        for u from 1 to k do
            j = findLeaf(x).
            UpdateNode(j; $< x, y >$).
            if $|\mathcal{R}_j| > \alpha$ and $\exists s \in \mathcal{S}: \Delta L(\mathcal{R}_j, s) > \beta$ then
                Find the best test: $s_j = \arg\max_{s \in \mathcal{S}} \Delta L(\mathcal{R}_j, s)$
                CreateLeftChild($\mathbf{p}_{jls}$)
                CreateRightChild($\mathbf{p}_{jrs}$)
                UpdateGiniIndex.
            end if
        end for
end for
Output the forest $\boldsymbol{F}$.

4.4 Case Study and Simulation Results

4.4.1 Case List

The case studies are designed for unknown load detection and online learning respectively. A case study on GLR and Gaussian Mixture Model [146] and a case study on the random forest and the SOM [143] are prepared respectively.

4.4.2 Unknown Load Detection

The training sets are generated as the following rules, a total of five samples are used

for each type of load, for each samples, 500 clips are selected randomly combining with the transient features to act as the input vectors. Therefore, a total of 2500 input vectors are generated for each type of load in the training stage. However, the samples in State II will only represent one type of variant, such as only LCD TV will be used for TV training. No samples will be generated for loads in State III in the training stage.

As for the test sets, two samples are used for each type of load, and 500 vectors are generated per sample in the same way as the training set. However, every 10 vectors yield one observation for the test procedure. Therefore, a total of 100 observations for each type of load are generated in the testing stage. Actually such a modification is a way to reduce the influences of the "recall" of the detection method [147]. Moreover, two samples in State II will be a variant corresponding to load type selected in the training stage, such as LED TV for TV. The samples in State III will only consider one variant first, such as one single type of LED bulb.

In addition, the unbalance of the training set also needs to be considered when preparing for the GLR. The unknown detection model is a combination of many GLR models, therefore for each GLR, if no modification is implemented, the number of true case vectors will be 2500 while the number of false cases will be N times 2500, where N is the total number of load types. This will result in a useless of the detection model when N is too large. In this paper, the false vectors used for training is also randomly selected from the training sets of the rest of N-1 load types. The size will be 10000, four times of the size of true case vectors.

The global classification rate is used for the evaluation because the misclassification cost is different. The recall rate of the unknown detection cannot be too high, because it will result in a great inconvenience for the customers. The evaluation equation is shown in (4.15).

$$GCR = \frac{(TruePositive + TrueNegative)}{Total\ Number} \times 100\%$$

$$TP = \frac{TruePositive}{Total\ Positive} \times 100\% \tag{4.15}$$

$$TN = \frac{TrueNegative}{Total\ Negative} \times 100\%$$

In (4.15), the *TotalNumber* denotes the total number of tests put in the test stage. The feature selection results and the global classification rate (GCR) for each well-trained initial GLR is shown in Table 4.4.

To sum up, the loads such as STB and DVD player have very similar characteristics therefore very easy to be misclassified for each single GLR, however can be both detected as an known load.

The comparison results between GLR and Gaussian Mixture Model (GMM) [160] are shown in Table 4.5. The input samples of GMM are same as GLR, however, the input vectors for each sample composes of the entire feature set instead of a selected one.

The true positive (TP) is used to compare the results, since all the unknown loads will be added to the database and converted to the known loads after the first test. No new loads will exist in the coming test. However, the training sample for the new added loads are limited at first, it can also be seen from the TP3 of Table 4.5, which is lower than TP1. As the test sets are run times by times. The results of GLR are getting better and better. GMM is getting better first and then stops improving anymore because the GMM can only update the threshold and easily vibrates at a certain area. Besides, the global classification rate of GMM is also lower than the one of GLR. It is because the features used for GMM exert great influences on the final results. An obvious example feature is the power of loads, which is not a great feature for TVs and LED bulbs because there are many different power levels for

such loads.

Table 4.4 Summary of the selected input features.

State	Load	Feature Selected	GCR
I	DVD	*P, CF, F3, F5, F7, F11*	**76%**
	STB	*P, CF, F3, F5, F7, F11*	**84%**
	Fan	*CF, PC, VI, θ, O*	88%
	Heater	*CF, PC, VI, θ, O*	94%
	Florescent	*PQ, CF, F3, F5, F7, θ, VI, EI*	92%
	Monitor	*P, CF, F3, F5, F7, F11, O, FSM, EI*	82%
	Projector	*P, CF, EN, EI, FSM*	80%
	Microwave	*IA, IP, EI, W2, W4*	90%
	Scanner	*PQ, PC, AC, CF, EN, FSM*	78%
II	TV	*CF, EN, θ, F3, O, FSM, EI*	88%
	Desktop	*CF, EN, VI, θ, F3, F15, W2, W4, O, FSM*	74%
	Laptop	*CF, EN, VI, θ, F3, F15, W4, O, FSM*	72%
	Printer	*PQ, CF, EN, EI, θ, O, FSM*	78%
III	LED	*P, CF, F3, F7, VI, θ , O*	N/A
	Xbox	*CF, EN, θ, F3, O, FSM, EI*	N/A

Table 4.5 Results of the unknown detection model.

ALG/%	GCR	TN1	TP1	TP3	TP5	TP10	TP20
GMM	80.9	81.1	**80.8**	**78.5**	82.7	84.5	83.3
GLR	86.8	89.3	**85.9**	**82.4**	84.6	86.1	90.9

4.4.3 Load Identification

The training samples used for SOM is the entire load sets in Table 4.4, including the new added State II and State III loads. The training samples for random forest will be the same as the one used in the Case I, nevertheless all the features in Table 4.3 will be employed instead of the selected ones in Table 4.4. The test samples are also same as Case I

and will be run several times randomly. Because there is no need to bundle ten vectors as one test, therefore a total of 200 vectors for each type of load are selected. The performance evaluation method used here is based on (4.16). The comparison results are shown in Table 4.6.

$$SuccessRate = \frac{NumberofIdentified}{TotalNumber} \tag{4.16}$$

Based on the results, the performance of the random forest based method increases with the online training. The identification performance of RF on most of existing load is better than the one of SOM, and so as to the new added load after 5 times' online training. It is because RF randomly selects several of features for each tree instead of taking all the features at one time, while will run many times. This will weaken the influences of the unrelated features to some extent. However, RF still fails to provide a solid solution for the very similar loads like DVD and STB with the existing feature pools. Based on the study of [161], it will need more external information based on the behavior to solve such problems. It will happen to the heater if the coffee maker is added in the training set, since they are both pure resistive loads, and therefore it is impossible to identify them if no other usage information like "working duration" is added.

Almost all the existing method uses the absolute successful identification rate of each load as the major metric to evaluate the algorithm. However, it is highly dependent on the load space used, like mentioned above, if a coffee maker is added, the successful rate of heater will change. The most valuable information from Table 4.6 is the trend of successful rate as the online learning continues. This proves the validity of the online learning algorithm.

Table 4.6 Summary of the results.

State	Load	R1	R2	R5	R10	R20	SOM
I	DVD	72%	74%	80%	82%	80%	76%
	STB	84%	86%	82%	82%	86%	72%
	Fan	88%	90%	92%	92%	96%	90%
	Heater	94%	94%	98%	98%	98%	88%
	Florescent	92%	88%	94%	96%	96%	90%
	Monitor	82%	80%	88%	90%	94%	92%
	Projector	80%	82%	86%	90%	92%	94%
	Microwave	90%	90%	92%	92%	96%	94%
	Scanner	78%	80%	88%	88%	90%	86%
II	TV	88%	90%	94%	94%	98%	78%
	TV-LED	N/A	82%	88%	94%	96%	
	Desktop	82%	82%	86%	88%	94%	76%
	D-Slim	N/A	88%	88%	90%	92%	
	Laptop	72%	72%	76%	80%	84%	84%
	L-Game	N/A	70%	76%	84%	88%	
	Printer	78%	70%	78%	82%	88%	80%
	P-Laser	N/A	92%	92%	94%	94%	
III	LED	N/A	76%	78%	80%	84%	62%
	Xbox	N/A	80%	84%	88%	88%	74%

4.5 Chapter Summary

This chapter proposes a new perspective for the nonintrusive load identification problem. Instead of introducing more features, the report presents an adaptive solution consisting of an unknown recognition module and an online identification module. The adaptive solution proves to be able to recognize those easily misclassified loads as unknown loads and correctly identify these loads after gaining the knowledge from them.

Given the fact that the variety of home appliances is growing at a very fast speed, and

no robust feature sets have been extracted to correctly classify all varieties of loads, this adaptive model might present a practical and effective solution.

CHAPTER 5 SMART METER DATA ANALYSIS BASED ON LOAD DISAGGREGATION

5.1 Chapter Overview

Apart from incorporating the current NILM algorithm with an adaptive learning to handle with the unlimitedly large load sets in the market, most of the researchers today begin to come up with some more specific applications of NILM with an acceptable load space and the practical computation effort. Load disaggregation based on the data measured in the main service entrance metering point for the demand response service is one of the options.

As discussed in Chapter 2, HMM is one of current popular solution for load disaggregation work, which outperforms most other existing solutions. However, when applying HMM into smart meter data analysis, three critical issues in HMM-based NILM systems remain unsolved. In short, firstly, almost all existing NILM systems are designed only for signal sampled at 1Hz or higher frequencies except several preliminary studies on a 15-minute resolution data while with an average 50% accuracy such as [81, 162, 163]. However, most residential buildings' smart meters can only measure power at the frequency of 1 per 15 minutes. Secondly, most HMMs need supervised learning which makes the ground test for existing solutions very difficult. Finally, the number of simultaneous events also increase greatly because of a 15-minute duration is adopted comparing with the 1-second duration.

This chapter presents a solution to the above three problems. Firstly, an unsupervised learning algorithm that can learn automatically without individual load waveforms or any other *priori* knowledge is proposed. The proposed algorithm estimates the number of loads

and their parameters from the aggregated signal. Admittedly, it is impossible to *identify* each disaggregated load with zero input on individual load information. Therefore the name of each disaggregated load in the final results will be presented as a symbol of APP_x.

Furthermore, to overcome the challenge of low sampling frequency, the HMM model is modified by introducing the usage behavior features like usage duration and time stamp. Moreover, the working power of each appliance is modeled by normal distribution, which will be used to modify the emission matrix of HMM model.

Finally, to overcome the overlap problem, inspired by [83, 123], an iterative learning framework is established. We don't expect our algorithm to successfully disaggregate all the loads at one time. But if we can identify several of them, we will remove these loads from the raw curve and then continue to learn new patterns.

In addition, this paper does not expect to provide a solution that can disaggregate all the loads at home, which is almost impossible for the 15-minute resolution smart meter data.

5.2 Hidden Markov Model

The Hidden Markov Model (HMM) is to study a sequence of unobservable states following the Markov process. Therefore, the distribution of t^{th} state $S(t)$ given the $(t\text{-}1)^{th}$ state $S(t\text{-}1)$ is independent of previous states. The dependency of $S(t)$ on $S(t\text{-}1)$ is characterized by a state transition matrix $\boldsymbol{A}$, Different from the standard Markov process, there is another observable output sequence which are decided by the distribution of unobservable states. The HMM assumes that the current output only depends on the current state, which is associated with an emission function $\boldsymbol{B}$. To find the most possible sequence order of the unobservable states, two important procedures, decoding and learning, are implemented in the HMM. The detailed algorithm can be found in [83]. This paper only presents the equations that will be revised for the purpose of NILM.

5.2.1 Decoding

Decoding is one of the most important problems associated with HMM. It aims to determine the most likely underlying hidden state sequence given a series of outputs. It is a maximum-likelihood problem which is usually realized by Viterbi algorithm. In order to produce meaningful decoding results, Viterbi Algorithm requires all underlying loads being modeled by the HMMs. The Viterbi algorithm consists of a forward procedure and a backward procedure.

In the forward procedure, the forward probabilities $V_{t,k}$ can be calculated by,

$$V_{1,k} = p(Y_1 \mid \mathrm{S}(1) = k)\pi_k \tag{5.1}$$

$$V_{\mathrm{t},k} = p(Y_t \mid \mathrm{S}(t) = k) \max_{x \in S}(a_{x,k} V_{t-1,x}) \tag{5.2}$$

where π_k denotes the initial probability of state k, S denotes the set of all states, $a_{x,k}$ denotes the transition probability from state x to k and $V_{t,k}$ denotes the probability of the most probable state sequence responsible for the first t observations that has k as its final state.

In the backward procedure, the most probable final state is determined first and then the algorithm will trace back previously computed forward probabilities to find the most probable state sequence. Denoting the x selected in (5.2) by $Ptr(k, t)$, the backward procedure is formulated in (5.3) and (5.4).

$$x_T = \arg\max_{x \in S}(V_{T,x}) \tag{5.3}$$

$$x_{t-1} = \mathrm{Ptr}(x_t, t) \tag{5.4}$$

5.2.2 Learning

Learning aims at estimating the HMM parameters, including the transition matrix, the emission function parameters and the initial state probabilities under an certain output

sequence. Usually, it is intractable to find the global maximum for such a problem, however a local maximum can be derived efficiently using the famous Baum-Welch algorithm which is a maximum-likelihood approach. Baum-Welch algorithm requires prior distribution of parameters θ and consists of a forward procedure, a backward procedure and an update procedure. In the forward procedure and the backward procedure, the forward probability, which is the probability of being at state k and seeing current and previous outputs, can be calculated as (5.5); and the backward probability which is the probability of seeing future outputs conditioned on currently being at state k, can be calculated as (5.6).

$$F_{t,k} = P(Y_1 = y_1, ..., Y_t = y_t, X_t = k \mid \theta) \tag{5.5}$$

$$B_{t,k} = P(Y_{t+1} = y_{t+1}, ..., Y_T = y_T \mid X_t = k, \theta) \tag{5.6}$$

Furthermore, (5.7) and (5.8) shows the *posterior* distributions of states and state transitions respectively, which can be calculated based on (5.5) and (5.6),

$$\gamma_{t,k} = P(\mathrm{X}_t = k \mid Y, \theta) \tag{5.7}$$

$$\xi_{t,i,j} = P(X_t = i, X_{t+1} = j \mid Y, \theta) \tag{5.8}$$

Finally, the parameters θ can be updated based on (5.7) and (5.8), and was resent to (5.5) until it converges.

5.2.3 The HMM for NILM

In order to better model loads, in this paper an extension of the HMM called Factorial HMM (FHMM) is adopted [83]. As illustrated in Fig. 1, the FHMM consists of a set of parallel HMMs that share a common output.

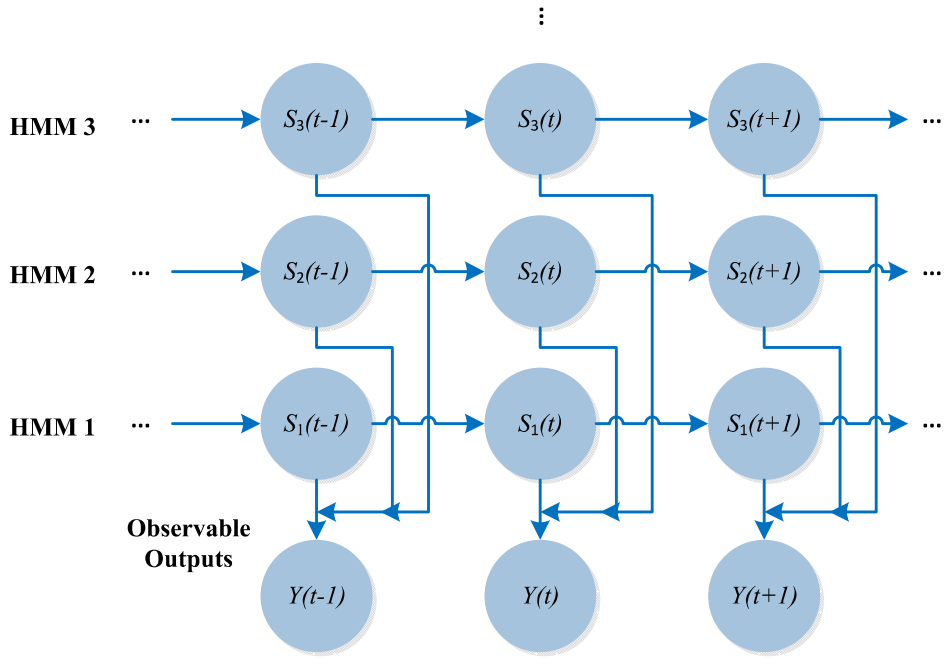

Figure 5.1 Architecture of factorial-HMM.

As shown in Figure 5.1, each HMM in FHMM represents a load and the shared output represents the first order difference of the aggregated power signal. The output is thus the sum of first order power differences of individual loads, which are modeled by state-dependent Gaussian distributions and are characterized by means and variances attached to individual states of the loads. Therefore, the shared output is also Gaussian distributed, whose mean and variance are the sum of means and variances that are associated with the current states of the HMMs. A detailed explanation will be given in next section.

As stated above, since HMMs are required to model the first order power differences, states in the HMMs represent change of mode. As illustrated in Figure 5.2, states in the HMM are not 'mode' of loads ('on' and 'off'), instead the change of 'mode' ('off-off', 'off-on', 'on-on', 'on-off') [83].

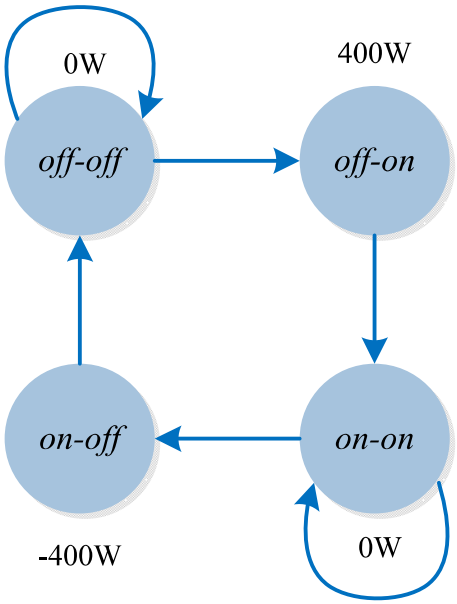

Figure 5.2 A typical state transition diagram of HMM aiming at modeling first-order power difference of loads.

Further, the user behavior of loads is introduced in the proposed model, characterized by a 96-dimensional (corresponding to the daily 96 smart metering point) turn-on time distribution vector associated with each HMM. To summarize, all the parameters in the proposed FHMM model is listed in Table 5.1.

Table 5.1 Parameters in the factorial-HMM model.

S.T.	**Load**
$\pi_i(0)$	Initial state probability distribution vector for load i.
A_i	State transition matrix for load i.
B_i	An N-by-2 matrix, where N denotes the number of states in load i. First column of the matrix denotes the means associated with the states of load i, and the second column denotes the variances.
C_i	A 96-demensional vector, denoting turn-on time distribution of load i.

5.3 Proposed Disaggregation Algorithm

The unsupervised learning algorithm consists of several sequentially connected modules as illustrated in Figure 5.3. First, aggregated signals are preprocessed. Second, the preprocessed signals are broken up into event snippets where an event snippet is defined as a signal segment that starts with a large rising edge and ends with returning to initial power level. Third, event snippets are mapped to feature vectors. Forth, event snippets are clustered based on their associated feature vectors. The feature vector and the clustering algorithm are designed so that the snippets within each cluster are generated by one common load. At last, an HMM is constructed for each cluster and all the HMMs constitute the FHMM.

5.3.1 Preprocessing

Modeling aggregated power signal with an HMM suggests that aggregated power should be piecewise constant due to the finite state nature of the HMM. However, affected by brown loads along with noise signal, the aggregated signal exhibits itself as finite number of power levels combined with small disturbances. These undesirable fluctuations might have a bad influence on the disaggregation accuracy of the signal. The brown load here is referred to the frequently used small power loads. Usually it is the base energy consumption of a residential house, shown in Figure 5.4.

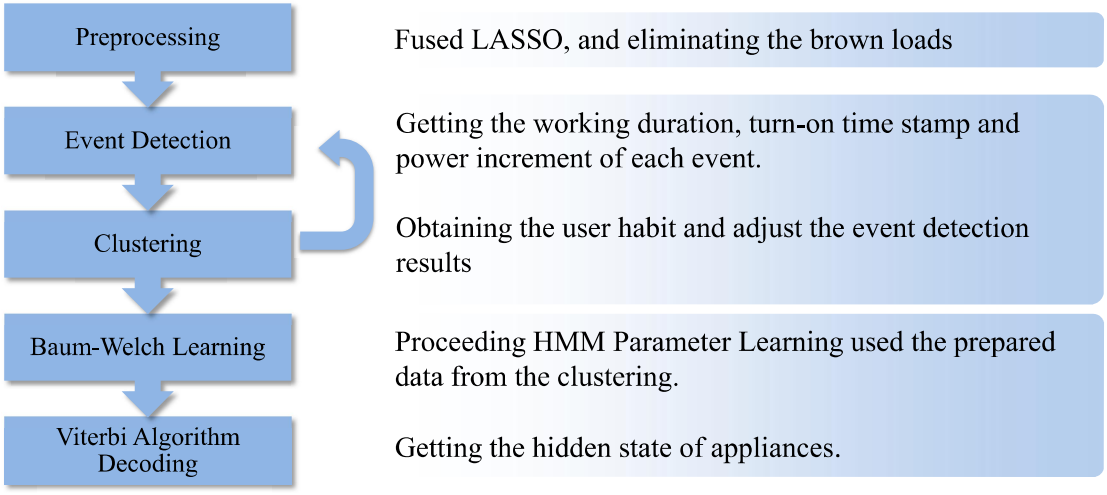

Figure 5.3 The unsupervised learning method.

To mitigate the influence of noise, a preprocessing algorithm, 'Fused Lasso' [164], is implemented to make the signal piecewise constant. Denoting the raw signal by $y = (y_1, \ldots, y_n)$, the algorithm reconstructs the signal through an optimization procedure shown in (5.9)

$$\hat{\beta} = \arg\min_{\beta \in R^n} \frac{1}{2} \sum_{i=1}^{n} (y_i - \beta_i)^2 + \lambda \sum_{i=1}^{n-1} | \beta_{i+1} - \beta_i | \qquad (5.9)$$

where β is the reconstructed signal and λ the penalty factor. The algorithm uses β to estimate the raw signal, minimizing the squared error while penalizing on the first order difference of β. Instead of taking the squared form or forms of higher order, the penalty term in (9) adopts the first order form (absolute value) because in quadratic optimization problems with first order penalty terms like (9), with the growth of penalty factor λ, the penalty terms decrease and what's more, they vanish, which is a favorable feature because it makes the reconstructed signal β piecewise constant. As illustrated in Figure 5.4, with the preprocessing algorithm, the raw power signal (above) is converted to the piecewise style (below), accommodating further process by the remaining parts in the framework.

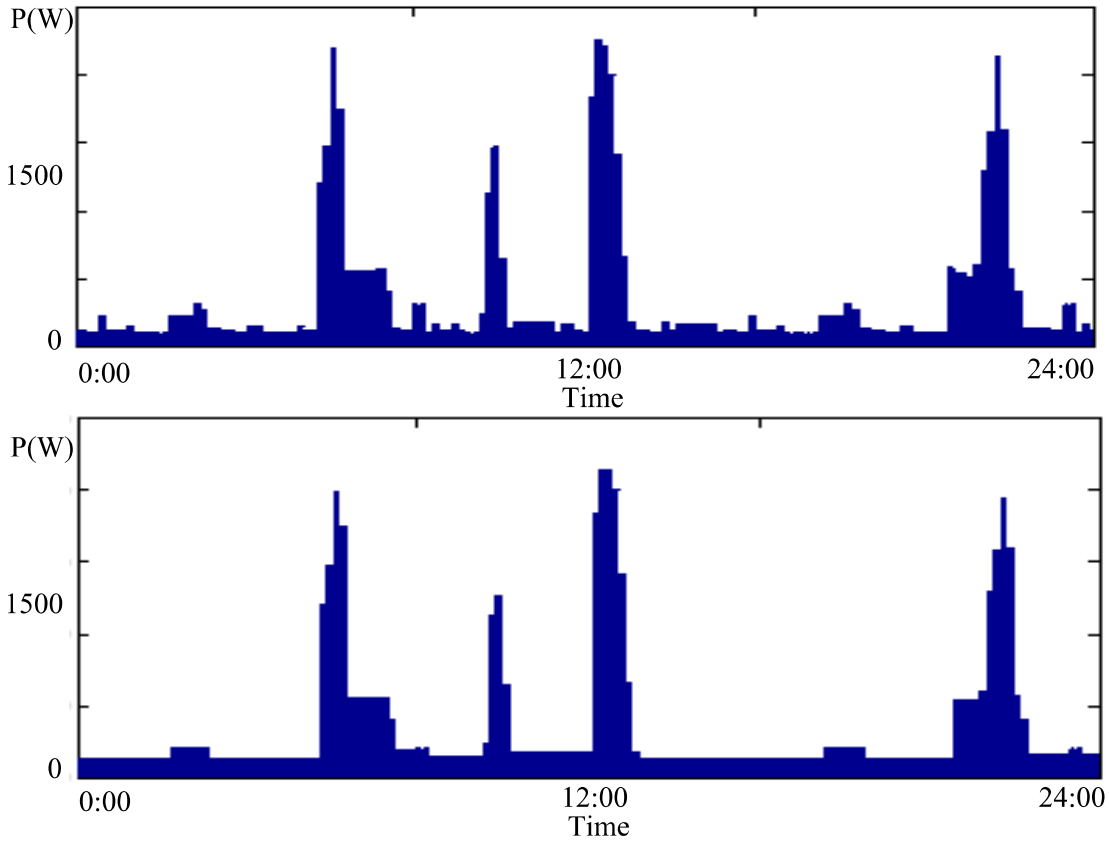

Figure 5.4 An illustration of the 'Fused Lasso' preprocessing algorithm.

Next, to eliminate the influences of the brown loads, different from the tradition threshold selection method [165], a self-adjusted threshold is applied for different houses. Firstly, the statistical analysis of eleven houses' three month smart meter data is given. The frequency distribution histogram of the power change of a single house is shown in Figure 5.5. In the histograms, it can be found that most power changes are lower than 200W. Furthermore, the number of the events whose powers are larger than 300W is much smaller. Given that the number of brown loads is much larger than that of the major loads, while the power of rising edges of brown loads are much smaller than those of major loads, the

threshold could be the inflexion of the frequency distribution histogram In Figure 5.5, it is 200W.

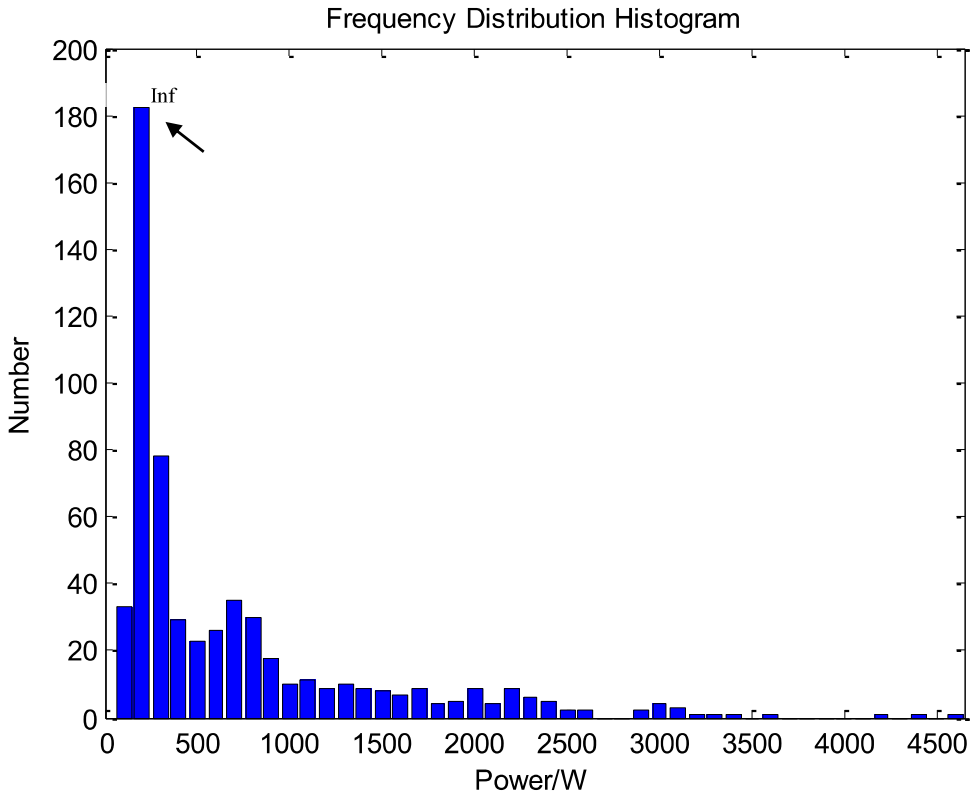

Figure 5.5 Frequency Distribution Histogram.

Moreover, to eliminate the brown loads, the cubic spline interpolation is applied the points whose power change is below the threshold, as shown in Figure 5.6.

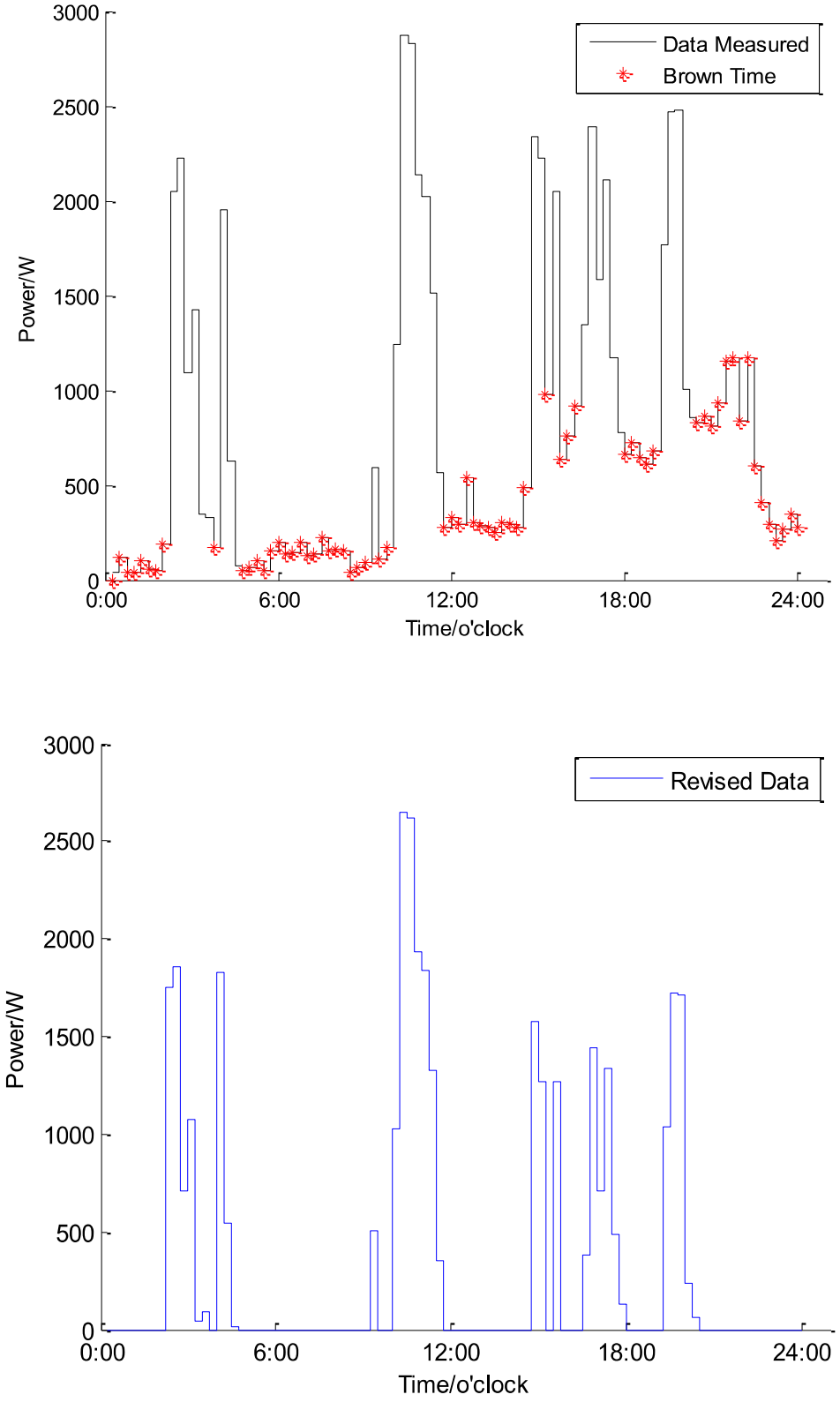

Figure 5.6 Brown load elimination.

5.3.2 Event Detection

Event detection module aims to break the aggregated signal up into individual snippets that start with a large power rise and end by returning to the initial power level. The event detecting algorithm is illustrated in Figure 5.7. In details, the event detection process is shown in Figure 5.8. The bottom figure shows the typical power match process. The above figure shows a typical event.

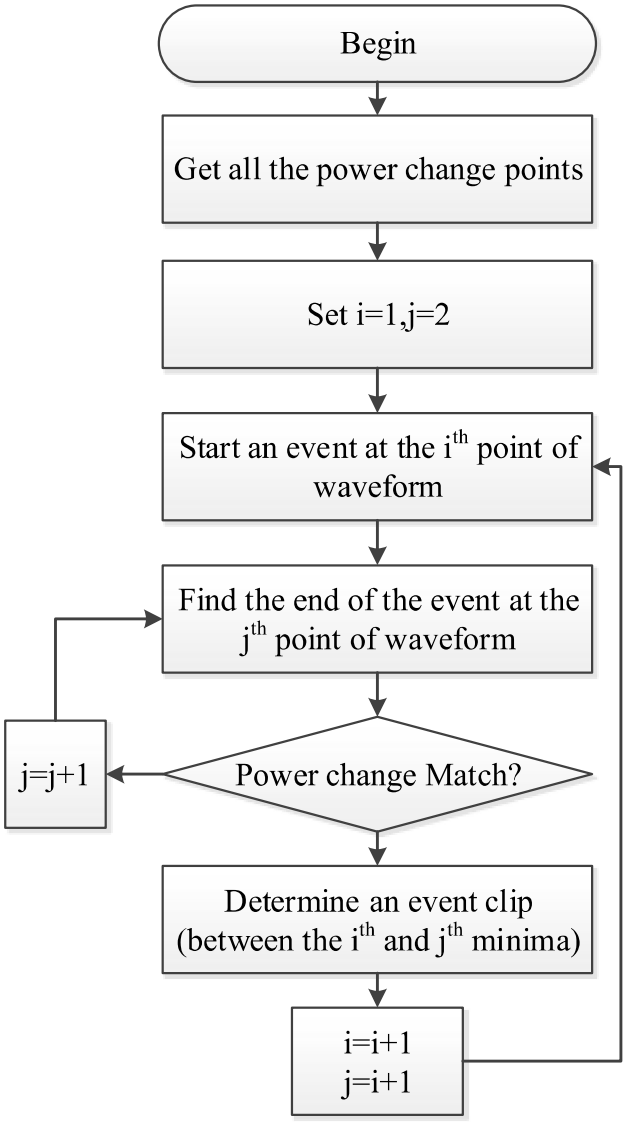

Figure 5.7 Flowchart of the event detecting module.

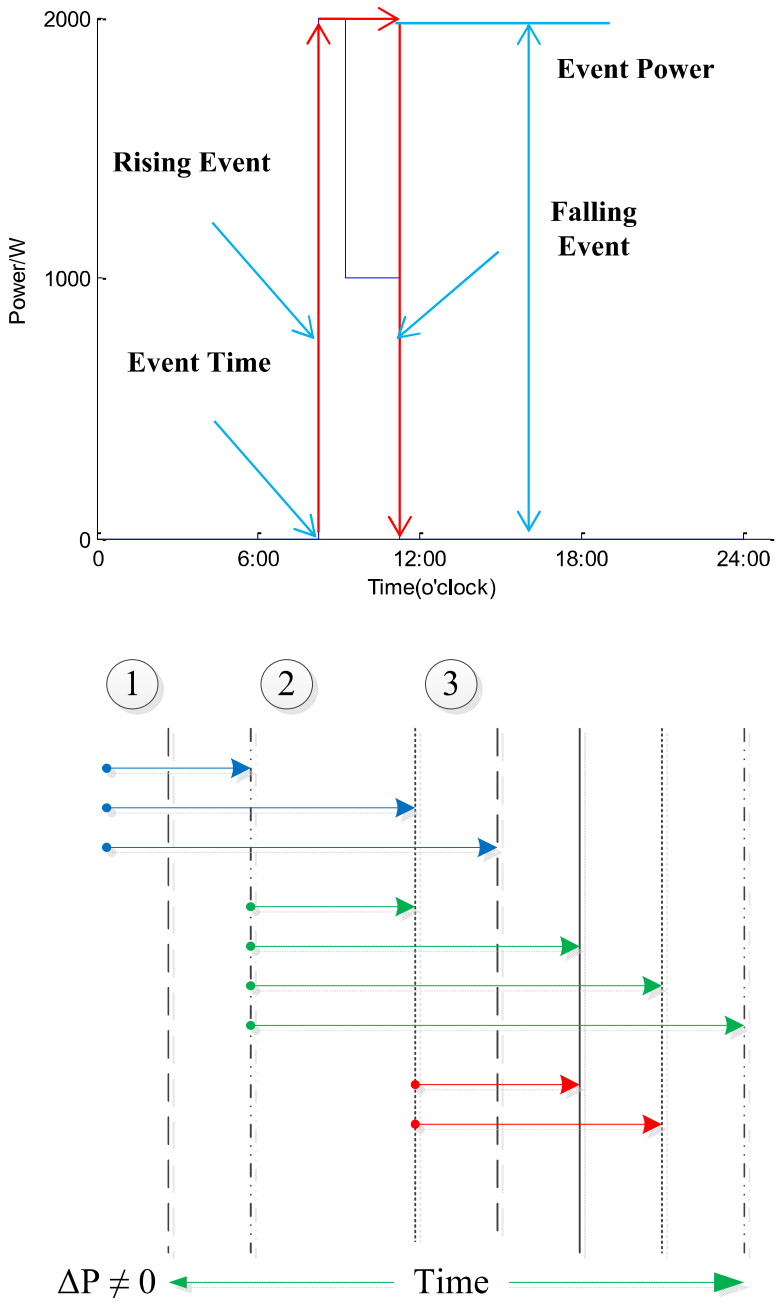

Figure 5.8 Demo of the event detecting process.

5.3.3 Feature Extraction

A map from event snippets to feature vectors needs to be designed, such that feature vectors associated with the same load are close to each other while feature vectors

associated with different loads are far from each other. Since the only way to characterize a load is its operating powers, the feature vector should reflect the operating powers of the load. Since a load might have multiple operating states, we make an assumption that the operating states of the load are ordered by a predefined way and only change of sequential load state is allowed. To obtain the feature vector from a snippet, firstly we find the operating powers that occur in the snippet and order them by the time of occurrence. Then, the first order difference of the powers is calculate, as shown in (5.10), so as the length of time for which the operating powers in the snippet last, shown in (5.11). Equation (5.11) will later be used in HMM parameter estimation.

$$P = \{P_1, P_2, ..., P_k\} \tag{5.10}$$

$$T = \{T_1, T_2, ..., T_k\} \tag{5.11}$$

5.3.4 Clustering

K-means algorithm is applied to the feature vectors generated in the previous step. K-means requires a proper distance measure. Other than the popular Euclidean distance, we adopt a different difference measure as shown in (5.12).

$$d(x, y) = \sqrt[p]{\frac{\sum_{i=1}^{n} | \mathrm{x}_i - \mathrm{y}_i |^p}{n}} \tag{5.12}$$

In (5.12), $x = (x_1, x_2, ..., x_n)$ and $y = (y_1, y_2, ..., y_n)$ are two vectors and $d(x, y)$ is their distance measure. p is a parameter. The higher p is, the more the distance measure tends to the maximum of $|x_i - y_i|$ ($i = 1, .., n$). When comparing the operating powers extracted from two snippets, a large difference between one of the operating powers will greatly discredit the judgment that the two snippets are generated from the same load. Under this

consideration, other than two (the Euclidean distance), a larger p is preferred.

After clustering, clusters that are too disperse or too small will be filtered out to make sure the rest clusters only contain event snippets that are generated from a common load.

5.3.5 Parameters Estimation

Baum-Welch Algorithm will be used for the HMM parameters estimation, which usually include the transmission matrix $\boldsymbol{A}$, emission matrix $\boldsymbol{B}$.

The clustering procedure actually contributes to the parameters estimation a lot by providing three important features extracted from (5.9) and (5.10). The power distribution of each cluster $\boldsymbol{P}$ is used to update the $\boldsymbol{B}$ matrix, which contains the mean and variance of each cluster to promise the fault tolerance capability of the algorithm. The start-time $\boldsymbol{T}$ is used to generate the adjustment matrix $\boldsymbol{C}$, which plays as a multiplier for transmission matrix $\boldsymbol{A}$ to generate the new $\boldsymbol{A}^*$, shown as (5.13). In details, the component c_{jt} in matrix $\boldsymbol{C}$ is a number located between 0 and 1, which is decided based on the probability that if certain state j will be turned on at time t. The probability is calculated based on (5.11).

$$\boldsymbol{A}^*(t) = \{a^*_{ij,t}\}: a^*_{ij,t} = a_{ij}c_{jt},\ C(j \times t)\text{: } c_{jt}\text{, the coefficient of state j works at time } t \quad (5.13)$$

After obtaining HMMs from the snippets, parameters of the HMMs will be averaged to constitute a HMM representing the load underlying the cluster. Since Baum-Welch Algorithm does not guarantee a global optimum, finding close-to-optimum initial parameters is crucial to assure high performance of the Baum-Welch Algorithm. The average on-duration of each cluster calculated by utilizing the P in (5.10) and the T in (5.11) associated with the snippet is used to update the initial states. Based on the P and T, the state transition diagram with predefined initial parameters is shown in Figure 5.9.

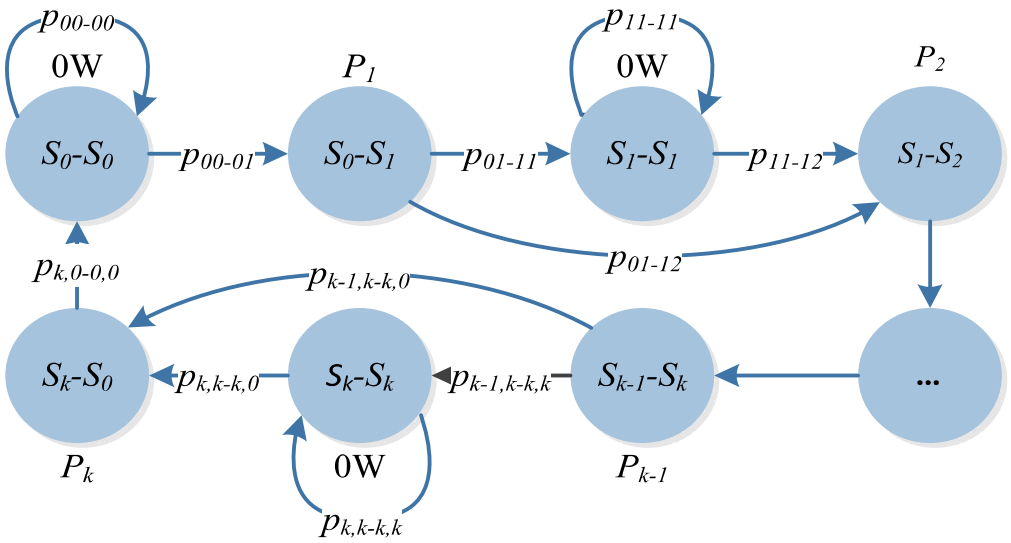

Figure 5.9 State transition diagram of HMM with predefined initial parameters.

In Figure 5.9, $\{S_0, \ldots, S_k\}$ is the load operating modes. S_0 denotes the off state while $S_1, \ldots, S_k$ denote a series of different on states. The states of the HMM is the change of load states. According to the assumption made in Session 1.2.3, only change of two sequential load states is permitted. Thus, the HMM state can only take the form S_i to S_{i+1} (except for the last state S_k to S_0. Table 5.2 summarizes the values we set to the initial HMM parameters.

Table 5.2 Initial parameters for Baum-Welch algorithm.

Parameter	**Value**
$p_{0,0;0,0}$	0.8
$p_{0,0;0,1}$	1- $p_{0,0;0,0}$
$p_{i\text{-}1,i;i,i}$	min(T_i-1, 1)
$p_{i\text{-}1,i;i,i+1}$	1- $p_{i\text{-}1,i;i,i}$
$p_{i,i;i,i}$	max(1/(T_i – 1), 1)
$p_{i,i;i,i+1}$	1- $p_{i,i;i,i}$
$B_{i\text{-}1,i}$	P_i
$B_{i,i}$	0

5.3.6 Robust Decoding and Iterative Learning Framework

In [124], a robust Viterbi algorithm is proposed that allows the existence of unmodelled loads. It can disaggregate power of modeled loads from the aggregated power signal while leaving power of unmodelled loads in the residual signal. The idea behind the robust Viterbi algorithm is quite simple. It adds a pre-filter to (5.2) as shown in (5.14) and (5.15).

$$V_{\mathrm{t},k} = p(Y_t \mid \mathrm{S}(t) = k) \max_{x \in S}(a_{x,k} V_{t-1,x}), \text{ if } t \in S \tag{5.14}$$

$$V_{\mathrm{t},k} = \max_{x \in S}(a_{x,k} V_{t-1,x}), \text{ if } t \notin S \tag{5.15}$$

Compared with (5.2), (5.14) and (5.15) filter out the emission probability $p(Y_t|\mathrm{S}(t) = k)$ when t is not in set S. S defines the set of observations that can be explained by modeled loads. It is determined by the comparison between the Y_t and the power values that can be generated by the FHMM. Adding the pre-filter prevents unmodelled observations from intervening the decoding result and thus makes the decoding algorithm robust against unmodelled loads.

We extend the robust decoding algorithm to an iterative learning framework. It learns one load in each iteration. Figure 5.10 shows the flow chart of the framework. The framework can be divided into 4 steps, as shown below.

1) *Step 0*: Set the aggregated signal as Y^0. Set $k = 0$; Set $\mathrm{FHMM}^0 = \{\}$;
2) *Step 1*: Apply the unsupervised learning algorithm to Y_k. If the learning algorithm generates more than one load, keep the one that is most likely to be correctly recognized as Load^k and discard the others. Denote the HMM associated with Load^k by HMM^k and set $\mathrm{FHMM}^{k+1} = \{\mathrm{FHMM}^k, \mathrm{HMM}^k\}$. If the learning algorithm learns nothing, terminate the algorithm and return FHMM^k.
3) *Step 2*: Use the robust decoding algorithm to disaggregate the power consumption of

Load^k from Y_k. Set the residual signal as Y_{k+1}.

4) *Step 3*: Set $k = k + 1$. Return to step 1.

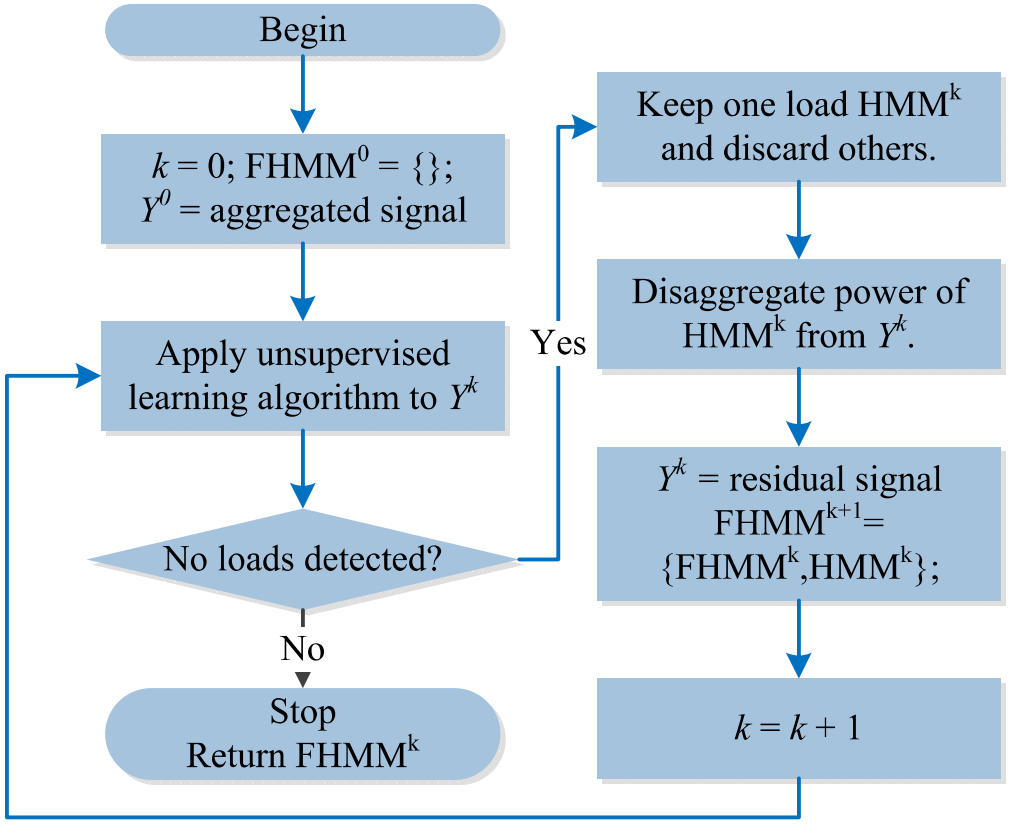

Figure 5.10 The iterative learning framework.

The iterative learning framework has the following advantages. First, removing one waveform in each iteration simplifies learning for remaining loads. Second, removing one waveform in each iteration recovers load waveforms that overlap with other waveforms in previous iterations.

5.4 Case Study and Validation

It is acknowledged that only large and repeatedly used loads can finally be utilized in

demand responsive or energy efficiency rebate programs, which are our targets in this paper. Correspondingly, loads with small power consumptions are called the brown loads. This paper focuses on the former. Specifically, this paper studies air conditioners (APP1), bathroom GFAs (APP2) and stoves (APP3), washers and dryers (APP4), the most common major loads in residential buildings.

5.4.1 Data Analysis

The data used in this paper come from a real project supported by American Public Power Association, working with Marietta Power. The real smart meter data of five residential homes are used. The Centron Type 2S meter of Itron [166] provides 15-minute resolution data including average energy, minimum power, and peak power. A common daily power profile is illustrated in Figure 5.11.

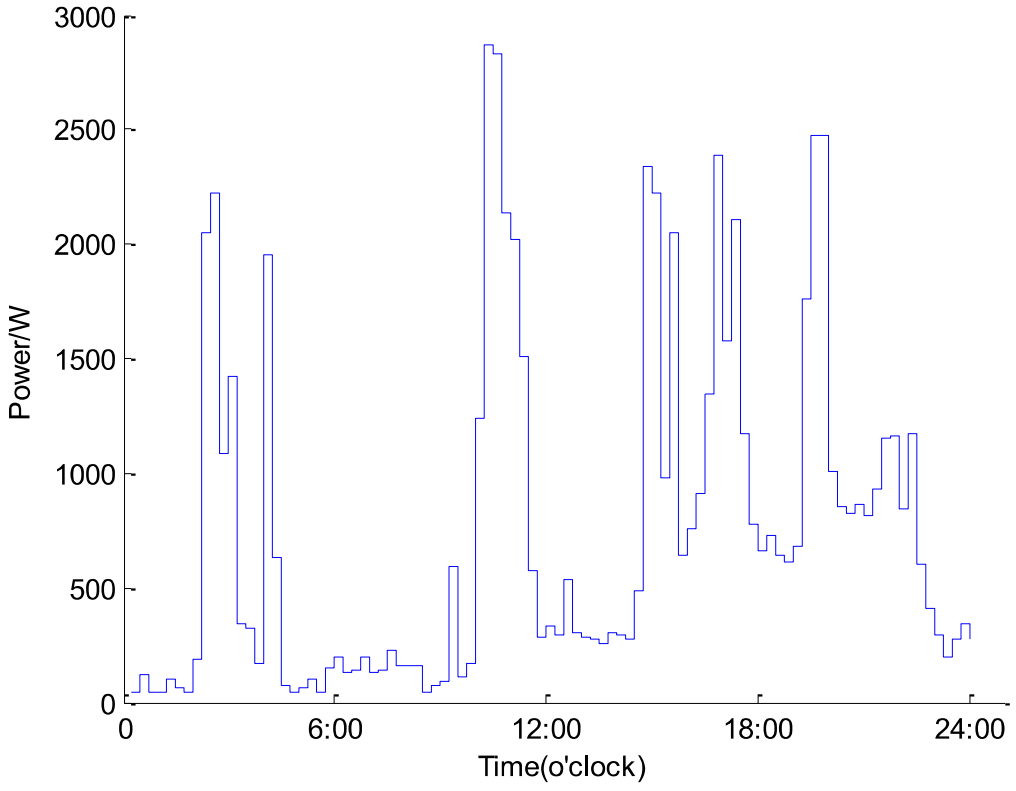

Figure 5.11 Generation of 1 per 15 minutes data.

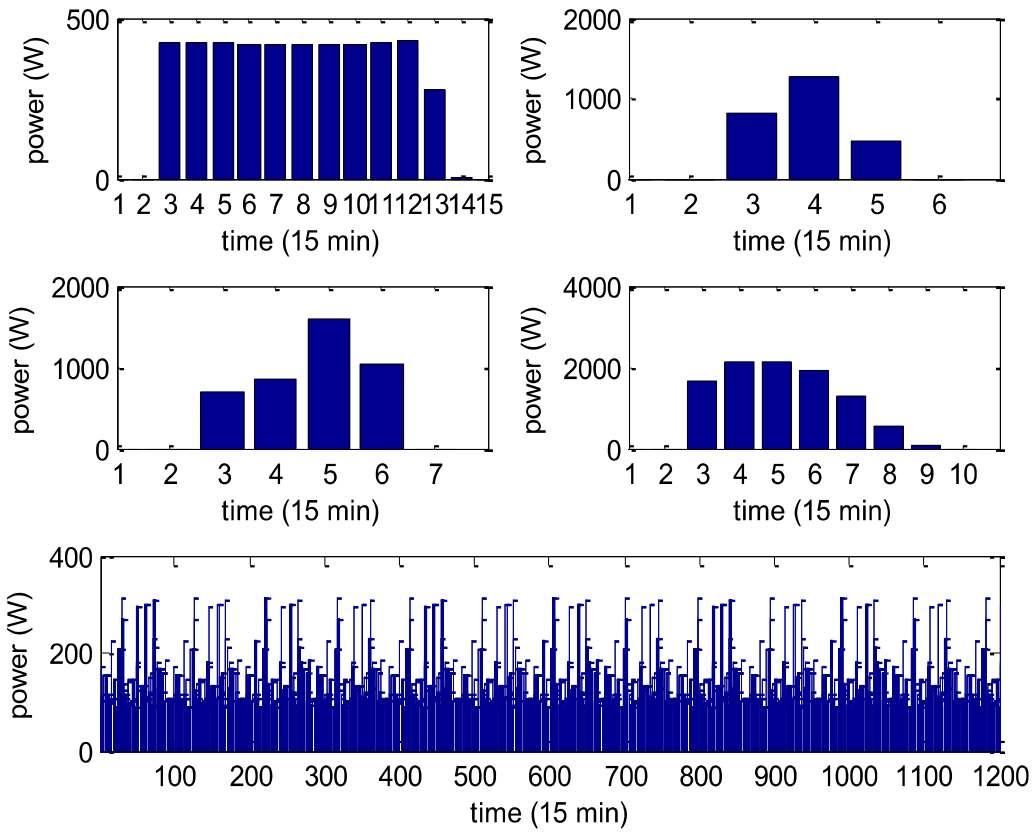

Figure 5.12 Individual load waveforms in the aggregated signal. From top to bottom, left to right: APP1, APP2, APP3, APP4 and brown loads.

Figure 5.11 shows parts of the power signal to be disaggregated in this case study. It is contains four major loads along with other low power loads. Their individual waveforms are shown in Figure 5.12. From Figure 5.11 and Figure 5.12 it is apparent that:

a) All loads have more than 2 operating states.

b) All snippets of APP1 overlap with snippets of other loads.

The length of the aggregated signal applied in this paper is 30 days. We divide it into two parts. The first 20 days of the signal will be used for training as well as validating and the rest 10 days will be used for test. This number is also based on the current DR baseline

load calculation standards in most of utilities or ISOs [167].

5.4.2 Performance Metrics

Regarding to the disaggregation problem, an overall disaggregation accuracy of the loads is adopted by most of the researchers [83]. However, an individual way is applied in this paper which is required to present the contribution of the iterative logic design. The performance metrics used here for disaggregation error is $(x_i - \widehat{x_i})/\, x_i$ per t duration where x_i is the number of the measured signal for load *i,* $\widehat{x_i}$ is the number of the signal from the disaggregated load *i.*

5.4.3 Demonstration of Learning and Behavior Features

Two iterations are run for the training data. In the first iteration the unsupervised learning algorithm detects 3 loads: APP2, APP3, APP4. The disaggregation results for the first iteration is shown in Figure 5.13. Because of the remove of waveform of APP2, APP3 and APP4, the waveform of APP1, which in the raw signal overlapped with waveform of APP4 and thus was not unidentifiable, is now recovered and identifiable.

Based on the residual signal we run the second iteration and detect APP1, and the disaggregation result is shown in Figure 5.14.

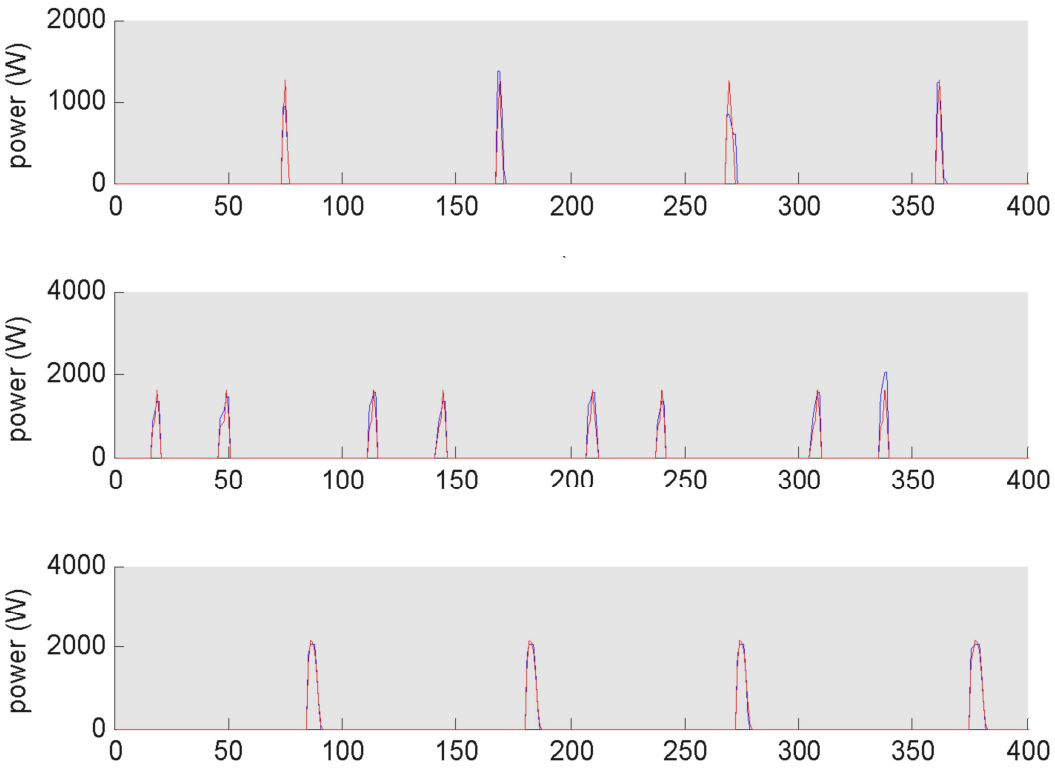

Figure 5.13 Disaggregated power signal in the first iteration. Blue line denotes the disaggregated power signal; red line denotes true measured circuit-level power signal.

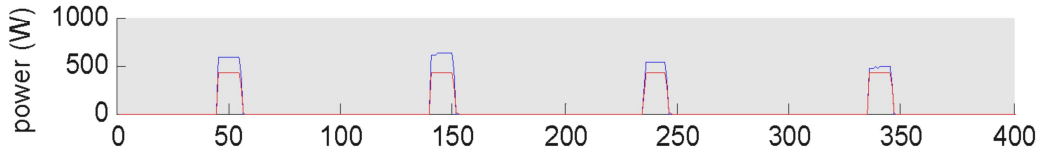

Figure 5.14 Disaggregated power signal in the second iteration.

From the figure give above, it is easily found that the algorithm successfully disaggregated the most of the loads in the first step except the air conditioner. It is because the air-conditioner is overlapped with lots of other appliances. However, in the second step, the data of the other loads will be removed from the aggregated signal. Consequently, the air

conditioner is successfully disaggregated. The total power consumption estimation error of the air-conditioner is high because the working power of air-conditioner is a continuous value. The disaggregation rate for the demo period (4 days) is almost 100%. When the system is used to the 10 days test data, the disaggregation results are shown in Table 5.3. The unrecognized energy present the 8% of the total energy measured (The disaggregation method could not obtain the name of the loads)

Table 5.3 Disaggregation results.

S.T.	Load	Estimated Peak Power	Decoding Accuracy
AC	APP1	532W	94%
GFI	APP2	1146W	95%
Stove	APP3	1912W	88%
Washer/Dryer	APP4	2100W	96%

Given the proposed solution, all the four loads are disaggregated after two iterations, and the average unrecognized events present the 8% of the total events measured. Moreover, because the power difference of the tested data is large enough, few crossing identification mistake exists. The dominant reason of event missing lies in the “event detection procedure”. In detail, if some events happen not in the routine time that are learned in the event detection procedure, it usually will be overlooked because the proposed algorithm focuses on the habitual events only. In addition, because we use 15 minute resolution data, the computing time for the four load case is less than 0.01s on a Dell PC with 64GB RAM, and Intel i7 CPU with 3.84 GHz. Since our targets are demand responsive loads, the scalability should not be a problem for such an application.

To verify the contribution of behavior features, a new load (APP5) similar to APP3, but used in different time period are manually added in the raw data to generate an artificial load

profile. As shown in Figure 5.15. In the first artificial dataset, the possible routine time range for APP5 is not overlapped with APP3, in the second artificial dataset, the 80% percent of the routine time period of APP5 is overlapped with APP3. Table 5.4 summarizes the results. Given the results, if the usage habit is different, i.e. used at different times or with different durations, we can still successfully identify the loads with similar power consumption. But if two loads have same power consumptions and usually are used at same time period, then it is impossible to differentiate if only active power is used for the proposed algorithm.

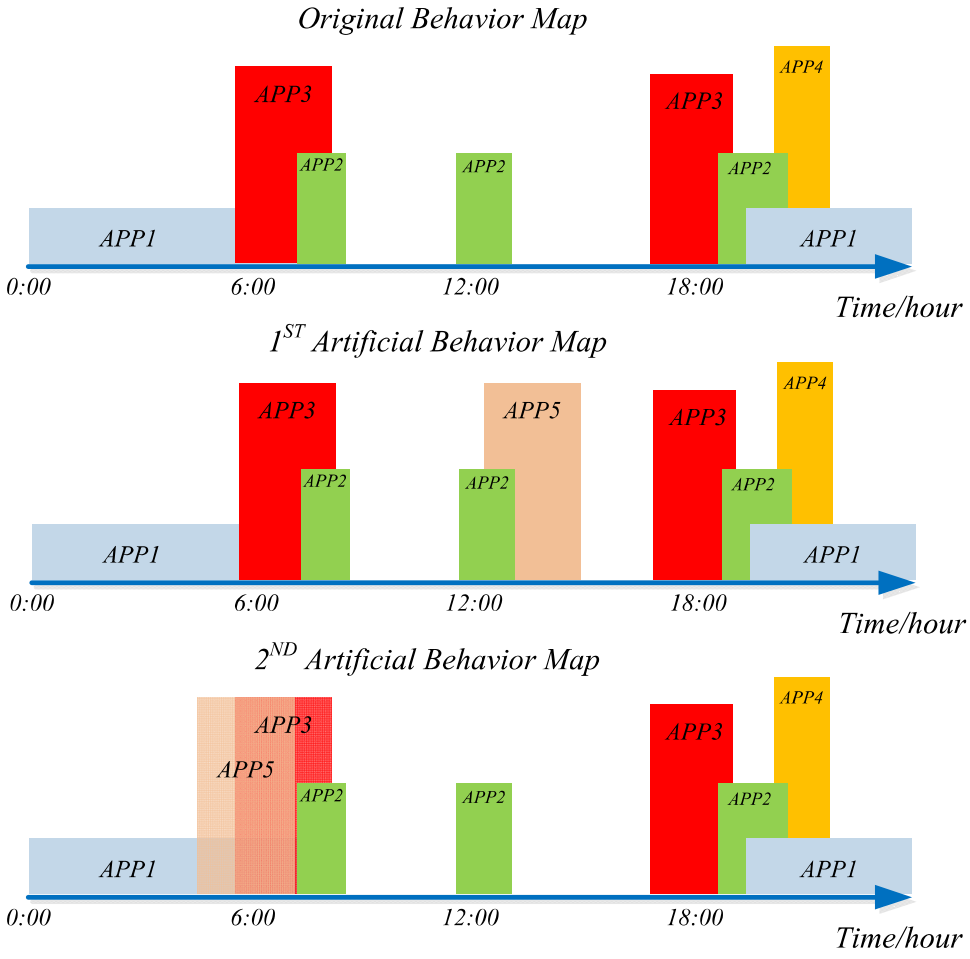

Figure 5.15 Artificial case profile.

Table 5.4 Disaggregation results of similar loads.

S.T.	Load	1st Artificial	2nd Artificial
AC	APP1	94%	90%
GFI	APP2	95%	95%
Stove	APP3	82%	90%
Washer/Dryer	APP4	96%	94%
Pseudo-Stove	APP5	88%	22%

5.5 Chapter Summary

The contributions of this chapter can be summarized as following two aspects.

1) The specific design for DR. We added an unsupervised clustering process before HMM, therefore eliminate the random behaviors and small loads, only remain the habitual usage behavior and integrate these behavior features in the HMM model training.
2) The iterative idea. It is greatly helpful to solve the overlap problems.

However, plenty of challenges need to be solved. First, this chapter assumes that the load only change its operating modes in a sequential manner, while there always exist some loads with more complicated state transition patterns. In addition, this model is based on an assumption that users' habits don't change much. And the features of on-duration and starting time may be disturbed by the brown loads or newly-introduced appliances. Future work should be focused on these problems.

CHAPTER 6 APPLYING NILM INTO FAULT DETECTION OF AIR CONDITIONER SYSTEM IN BUILDINGS

6.1 Chapter Overview

The faults of HVAC include hard fault, soft fault as well as imperfect operational situations [168]. Some types of fault detection can make a big difference in the efficiency of a building. With a proper detection system, the imperfect operation can be figured out and energy can be greatly saved by adjusting the HVAC to the perfect state. Besides, a good fault detection method can also reduce the probability of false detection. However, most of the methods of the fault detection now are either not reliable enough or expensive.

Recently, an electrical measurement solution is proposed in [92] as studied in Chapter 2. This method measures the currents and the voltages at the terminals of the electromechanical device, and then identifies faulty mechanical behavior on the basis of these observations. Such a solution is much easier to install, less expensive and more convenient than conventional mechanical sensor based solutions. Besides, with the help of non-intrusive load monitoring (NILM) technique, it can further reduce the number of sensors needed to identify the operation of loads and monitor the whole system timely. However, these methods still bear with many drawbacks listed in Chapter One. This chapter will continue the idea in [92], further investigate some more robust solutions for different types of faults. Two major faults will be considered in this chapter which are airflow blockage faults and refrigerant leakage faults respectively.

6.2 Overview of the Proposed Solution and Introduction of Electrical Machinery

Any mechanical change happened to the HVAC system will result in the changes of the

sensing data. It is the fundamental assumption for the fault detection of HVAC no matter whether it is a mechanical measurement based method or an electrical measurement based method. Nevertheless searching the bijective parameters for each type of fault is the main challenge. The first electrical measurement based solution in [92] actually bears such problems by using working power as the major monitoring parameter. The working power may be influenced by too many external environmental factors, therefore it is very hard to be matched contain type of fault accurately. Figure 6.1 defines the problem of the proposed electrical based fault detection method intuitively. It is to find a bijective function Y to represent the measurement data with the mechanical change of the system, such as airflow rate and temperature. Figure 6.2 further provides the theory fundamentals of the proposed solution, which are based on the electrical machinery, signal processing, data science, and mechanics. In detail, fluid mechanics will be used for the airflow rate modeling and thermodynamics will be used for the thermal modeling of compressors.

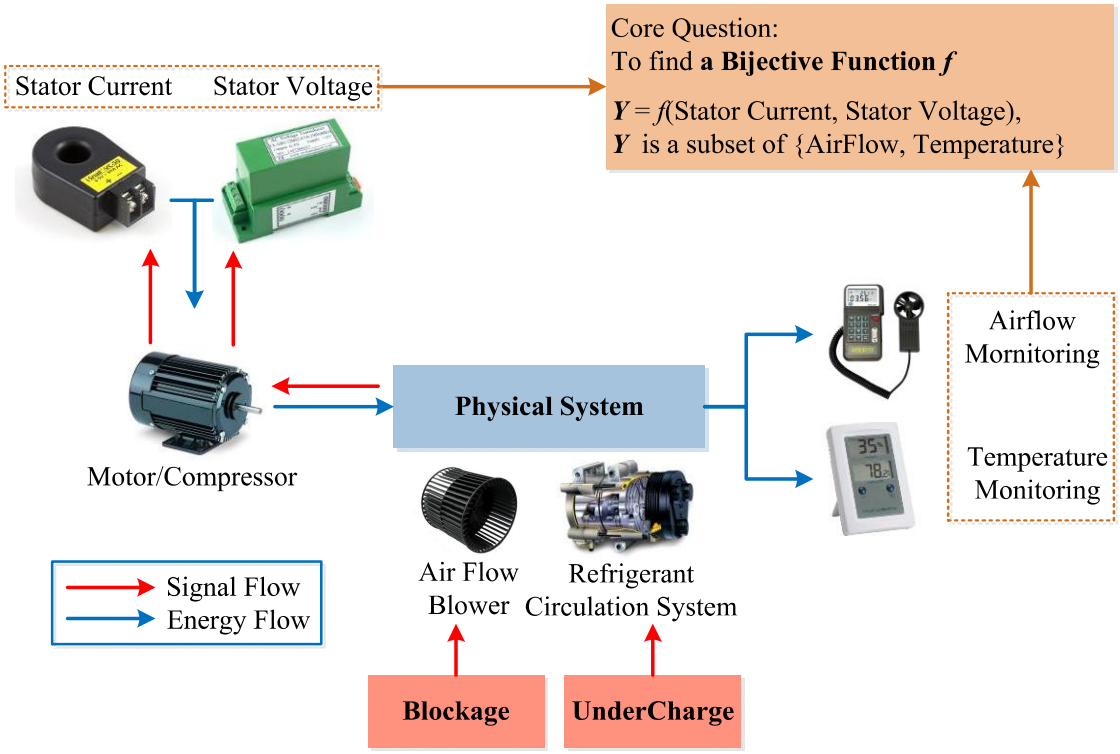

Figure 6.1 Architecture of electrical measurement based fault detection of HVAC.

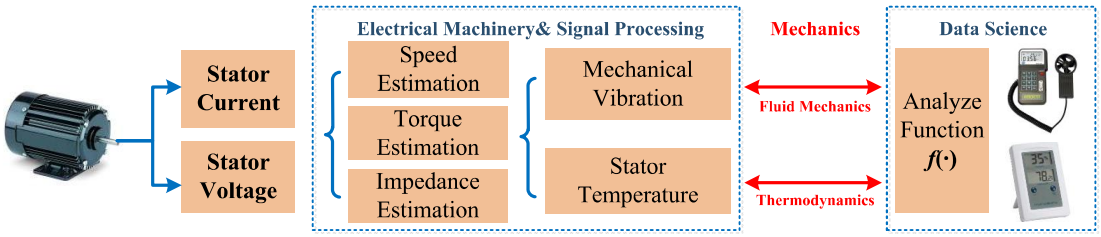

Figure 6.2 Theory fundamentals of the proposed solution.

6.2.1 Speed Estimation Algorithms

A well-known and widely applied speed estimation method is to detect the relevant harmonics in stator current spectrum [169]. As explained in [169], the stator current is influenced by the induced voltage which is produced via the varying air-gap flux. And the flux is determined by the product of the air-gap mutual magnetic flux (MMF) and the

permeance. The sources of the permeance and MMF variation are briefly introduced in the Figure 6.3. In general, the permeance variation is usually caused by the uneven air-gap due to the surface of the slots. Thus, some current harmonics will repeatedly show up as the rotor runs. And these harmonics contain the important speed information. The detailed mechanical and physical principles are fully explained in [170].

In summary, the interaction between the air gap MMF and the permeance produce a set of harmonics in the current spectrum as shown in (6.1).

$$f_h = [(kZ + n_d)\frac{1-s}{P} \pm v]f_s \tag{6.1}$$

where f_h denotes all the possible harmonic frequencies, $n_d = 0 \ or \ 1$ indicates the harmonics either with or without eccentricity, s is the rotor slip, v demonstrates the order of the interacted MMF harmonics, k is the order of varying permeance, Z is the number of slots and f_s is the fundamental MMF frequency which is 60 Hz in this experiment.

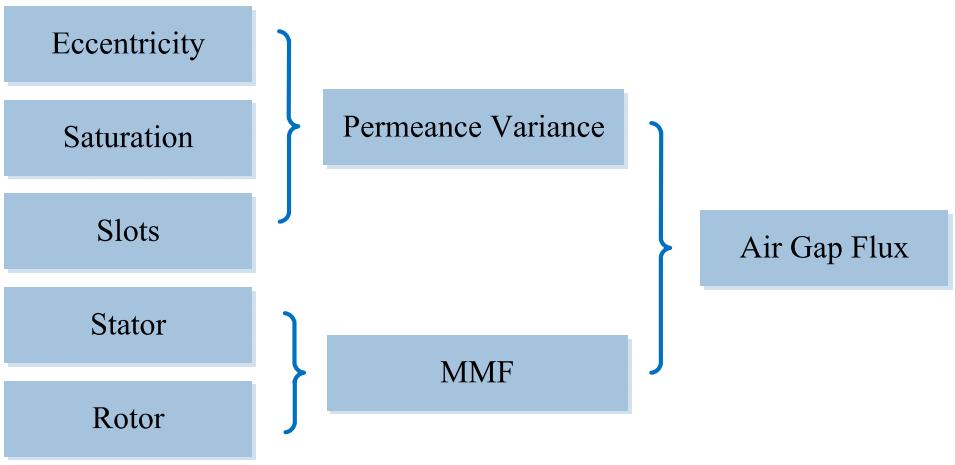

Figure 6.3 Sources of current harmonics [170].

Although most of the harmonics expressed in (6.1) seem to contain motor speed

information, not all the harmonics are easy to be detected, as explained in [169]. The condition of $k = 0$ and $n_d = 1$ is considered here, which is solely influenced by the eccentricity, and therefore usually called eccentricity harmonics f_e. It is given by,

$$f_e = [\pm \frac{1-s}{P} + 1] f_s \tag{6.2}$$

6.2.2 Torque Estimation Model

Usually there are two major methods to estimate the motor torque, i.e. static model and dynamic model. Both the methods have their own advantages and disadvantages, which will be used in different situations. In the aspect of airflow blockage detection, the blockage usually will not affect the transient process of the induction machine. Therefore the static torque estimation model can be used here, which needs less inputs and lower measuring requirements than the dynamic model. Admittedly, the accuracy of the static model is lower than the dynamic model, and lots of motor constants need to be provided in advance. A detailed introduction of the static model and dynamic model is provided below.

6.2.2.1 Static Torque Estimation Model

In the static model, the mechanical power is converted from the electrical power via stator coils, air gap, and rotor coils because of the electromagnetic effects. Within this process, the energy transmission efficiency under the full-load condition varies from 85% to 97%. In detail, the energy loss can be broken down roughly as Table 6.1 [171]:

Table 6.1 Composition of the energy losses of a motor.

Loss Name	Percentage in Total Loss
Stator losses	25% – 40%
Rotor losses	15% – 25%
Iron or core losses	15% – 25%
Friction and windage losses	5% – 15%
Stray load losses	10% – 20%.

Usually, the friction and stray losses only account for a minority of the total loss comparing with the other three losses and they are relatively constant. The iron or core losses, as one of the three major losses, are proportional to the square of flux, which are determined by the magnitude and frequency of the supply voltage. If ignoring the voltage drop due to the stator resistance, the iron or core loss will remain constant as long as the supply voltage is constant. The stator losses and rotor losses are relative complex. The losses change under different working scenarios. Typically, they are expressed by (6.3).

$$P_{loss} = C + P_{sloss} + P_{rloss} = C + 3I_s^2 R_s + 3I_r^2 R_r \tag{6.3}$$

where R_r is the rotor resistance, R_s is the stator resistance, I_r is the rotor current, I_s is the stator current, $\boldsymbol{C}$ is the sum of the constant power losses including iron losses, friction and stray load losses, P_{loss} is the total loss of the motor, and P_{sloss} as well as P_{rloss} is the stator losses and rotor losses respectively.

To estimate the torque, electromagnetic power is utilized, which is the sum of rotor losses and mechanical power, shown in (6.4).

$$P_{em} = P_m + P_{rloss} = P_0 - C - 3I_s^2 R_s \tag{6.4}$$

where, P_{em} is the electromagnetic power, P_0 is the total input electrical power, and P_m is

the output mechanical power.

Then the torque is deduced from the electromagnetic power as (6.5).

$$\tau = \frac{nP_{em}}{\omega_s} = \frac{n(P_0 - C - 3I_s^2 R_s)}{\omega_s} = C_1 - \frac{3nI_s^2 R_s}{\omega_s} \tag{6.5}$$

where, ω_s is the synchronous speed and n is the number of pole pairs.

6.2.2.2 Dynamic Torque Estimation Model

Dynamic torque estimation has been widely used in direct torque control in industry today [172]. Many different papers contribute to this area to guarantee a sufficient accuracy of the estimation [173-176]. In this chapter, only the fundamental stator voltage model is introduced because the motor in HVAC system seldom run at a low speed [177].

In detail, the electromagnetic torque produced by the machine can be written in terms of the stator current and flux as (6.6).

$$\tau = n(\psi_{\alpha s} i_{\beta s} - \psi_{\beta s} i_{\alpha s}) \tag{6.6}$$

where, n is the number of the pole pairs in the machine, $\psi_{\alpha s}$ and $\psi_{\beta s}$ are the stator flux components in the stationary reference frame, and $i_{\alpha s}$ and $i_{\beta s}$ are the stator current components in the stationary reference frame.

According to (6.6), the calculation of the torque requires the stator flux, which can be obtained based on the voltage integral model, shown in (6.7).

$$\begin{aligned} \psi_{\alpha s} &= \int (u_{\alpha s} - i_{\alpha s} R_s) dt \\ \psi_{\beta s} &= \int (u_{\beta s} - i_{\beta s} R_s) dt \end{aligned} \tag{6.7}$$

where $u_{\alpha s}$ and $u_{\beta s}$ are the stator voltage components in the stationary reference frame, and R_s is the stator resistance which needs to be measured in the static model.

The dynamic torque estimation model can be summarized as Figure 6.4.

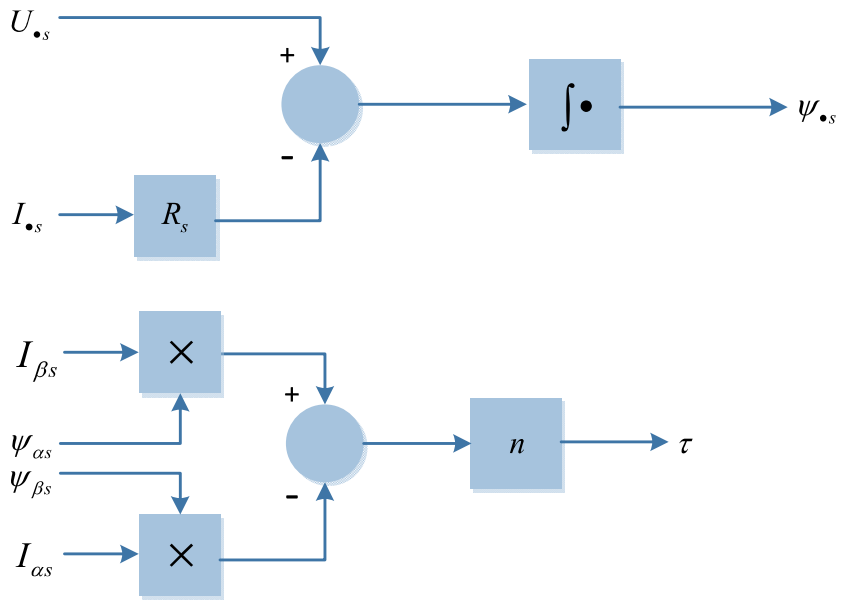

Figure 6.4 Dynamic torque estimation model.

6.2.3 Impedance Estimation Algorithms

The static equivalent circuit of an induction machine is shown in Figure 6.5.

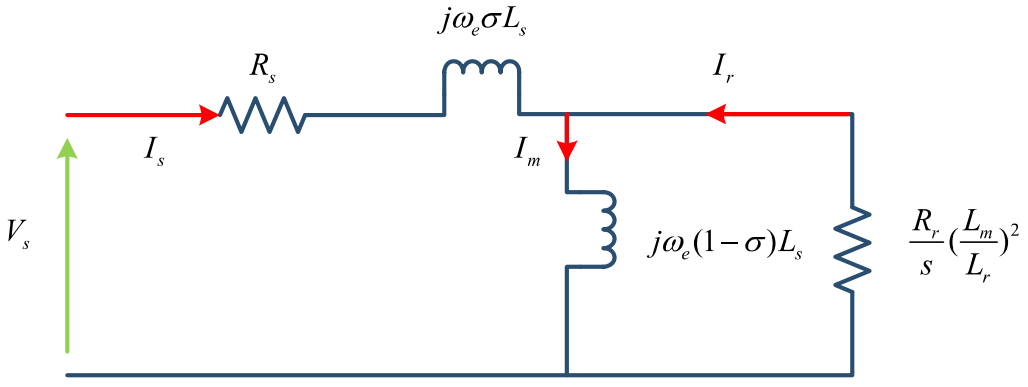

Figure 6.5 The steady-state equivalent circuit of an induction machine.

R_s is the stator resistance, R_r is the rotor resistance referred to the stator side, L_{1s}, L_{1r}

and L_m are the stator leakage, rotor leakage and magnetizing inductance, respectively; the stator self-inductance L_s, is the sum of L_{1s} and L_m, the rotor self-inductance L_r, is the sum of $L_{1r}$and L_m, the leakage factor σ is defined as $\sigma = 1 - {L_m}^2/\mathrm{LsLr}$, and ω_e [rad/s] is the angular speed corresponding to the power supply frequency.

Usually, the impedance estimation includes four parameters, the resistance R_s or R_r and the inductance L_s as well as σ.

In detail, the equivalent circuit can be formulated as (6.8) and (6.9):

$$\vec{V}_s = (R_s + j\omega_e L_s)\vec{I}_s + j\omega_e(1-\sigma)L_s\vec{I}_r \tag{6.8}$$

$$0 = j\omega_e(1-\sigma)Ls\vec{I}_s + [r_2 + j\omega_e(1-\sigma)L_s]\vec{I}_r \tag{6.9}$$

The elaborate derivation can be found in [185], r_2 is the equivalent resistance of the rotor and usually very small comparing to the stator resistance. It will be ignored in the estimation process. Then (6.8) and (6.9) can be changed to (6.10).

$$[\omega_e I_s V_{sy} \quad -\omega_e{}^2 I_s{}^2]\begin{bmatrix}(1+\sigma)L_s \\ \sigma L_s\end{bmatrix} = V_s{}^2 + I_s{}^2 R_s{}^2 - 2R_s I_s V_{sx} \tag{6.10}$$

where V_{sx} and V_{sy} are the projection of V_s on x-axis and y-axis, and the same for I_{sx} and I_{sy}. (6.9) can be converted to a scalar equation, shown in (6.11).

$$UP = Y \text{, namely} \begin{bmatrix}u_1 \\ u_2 \\ \cdots \\ u_n\end{bmatrix} p = [y_1, y_2, ..., y_n] \tag{6.11}$$

where $\mathrm{u}_i = [\omega_e I_s V_{sy} \ -\omega_e{}^2 I_s{}^2]$, $\mathrm{y}_i = [V_s{}^2 + I_s{}^2 R_s{}^2 - 2R_s I_s V_{sx}]$, $P = [\begin{matrix}(1+\sigma)L_s \\ \sigma L_s\end{matrix}]$.

To estimate the parameters of the motor, the least square algorithm is applied to the measured (V_s, I_s) pairs.

6.3 Airflow Fault Detection of the Air Handling Unit

Air handler unit (AHU) is considered as the main part of the HVAC system. According to the Federation of European Heating, Ventilation and Air-conditioning Associations, AHUs can be applied in many different conditions such as office buildings, cleanrooms, swimming pools, etc. Before 1970, the requirements for AHUs were basically humidity and temperature adjustment. Other requirements such as low acoustic noise were added and explained in the literature [178]. Because of these new requirements, today's AHUs consume large amount of energy that account for almost 44% of the energy used by the whole HVAC industry [22]. The structure of a typical AHU is illustrated in Figure 6.6.

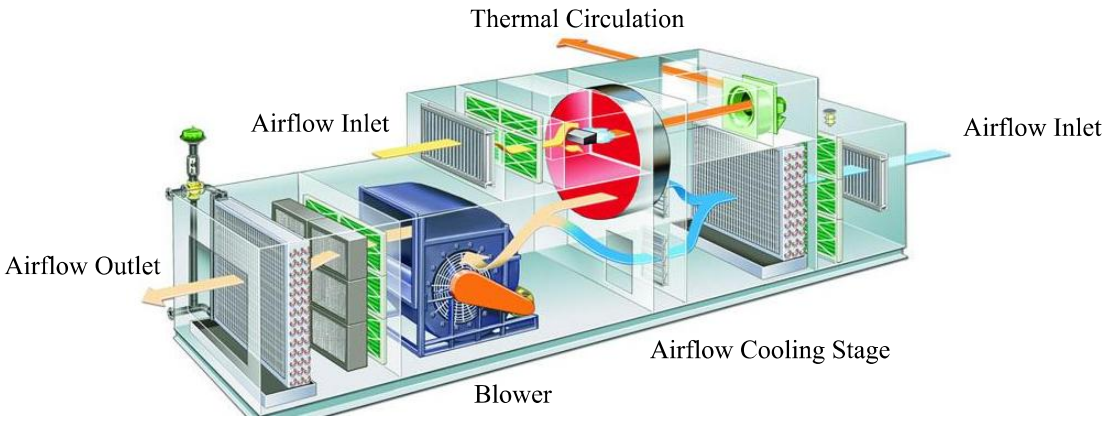

Figure 6.6 A typical AHU scheme.

An air handler is usually a large metal box containing a blower, heating or cooling elements and filter racks or chambers. Air handlers usually connect to a ductwork ventilation system that distributes the conditioned air through the building and returns it to the AHU.

Air from a room is sucked through the inlet and filtered to be dust-free, before passing

through the heating and cooling coil to adjust the temperature. Evaporator here is used to reduce the temperature. Finally, the air is accelerated by the centrifugal force from the wheel blade which propels the air continuously towards the outlet. The speed and quantity of the air is controlled by the blower, which can typically operate at a variety of set speeds allowing a wide range of airflow rates.

According to Chapter 1.2, the airflow blockage has become a significant problem in AHU. This section mainly focuses on the airflow blockage fault detection and the estimation of insufficient airflow. To accomplish the objectives, not only an exclusive index for the airflow rate is expected, but also a physical model that converts electrical signals to mechanical variables is required.

6.3.1 Airflow Fault Detection

It is an intuitive idea to study the influences of the airflow blockage on the motors. Actually, the airflow variation exists in the majority of the HVAC systems today. However the variation resulted from the blockage is no longer able to be overlooked, and definitely will affect the stator current of the induction motor based on the large amount of exiting studies on the load torque detection of induction motors [179, 180]. In general, these solutions take a frequency domain analysis by studying the spectrum of the stator current. The original idea of the proposed work comes from [181], the frequency component resulted from the torque oscillation will act as the major index for the airflow fault detection, as shown in Figure 6.7.

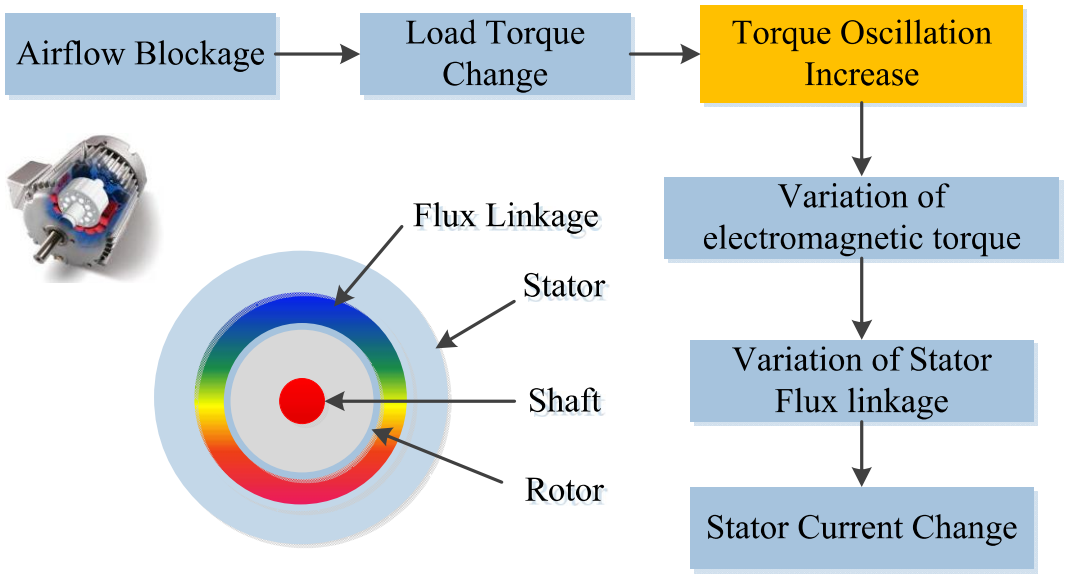

Figure 6.7 The illustration of the proposed solution.

In detail, the airflow blockage will result in the decrease of the airflow rate therefore will lead a torque oscillation of the blower due to the mechanical structure based on the aerodynamics. Usually the mechanical system is assumed linear, and then a torque oscillation in the steady state will generate a variation in the electromagnetic torque that contains all the frequency components of the oscillation. Moreover, the electromagnetic torque is the interaction between the stator flux linkage and rotor current in a *d-q* reference frame. Because the rotor current is not change, the stator flux linkage will keep all the variation information of the electromagnetic torque. As a result, any oscillation in the torque at a multiple of the rotational speed will produce a series of frequency sidebands with the line frequency as the center in an ideal machine where the flux linkage is purely sinusoidal. However, the sidebands are load-dependent, which needs to be tested for different case. This sideband signal actually will be used in this work to detect the airflow blockage. A typical FFT spectrum is shown in Figure 6.8.

As shown in Figure 6.8, to model the mechanical oscillation, the vibration power value

of the sideband frequency harmonics are utilized. The vibration power of the first 11^{th} order harmonic components is calculated considering the magnitude of the harmonics after 11^{th} order is too small. The equation is shown in (6.12).

$$P_{vibration} = \sqrt{\int_{0}^{+\infty} f(t)^2 \, dt} = \sqrt{\sum_{-11}^{+11} \emptyset(w_i)^2} \tag{6.12}$$

6.3.2 Airflow Estimation Method

In a blower, the air is propelled out of the wheel by the blades. When torque and speed are estimated, airflow is determined by the configuration and dimension of the blade. The curve denoting the volumetric airflow against mechanical power at different rotor speeds is called the fan curve, which demonstrates the intrinsic physical characteristic of the centrifugal fans, shown in Figure 6.9.

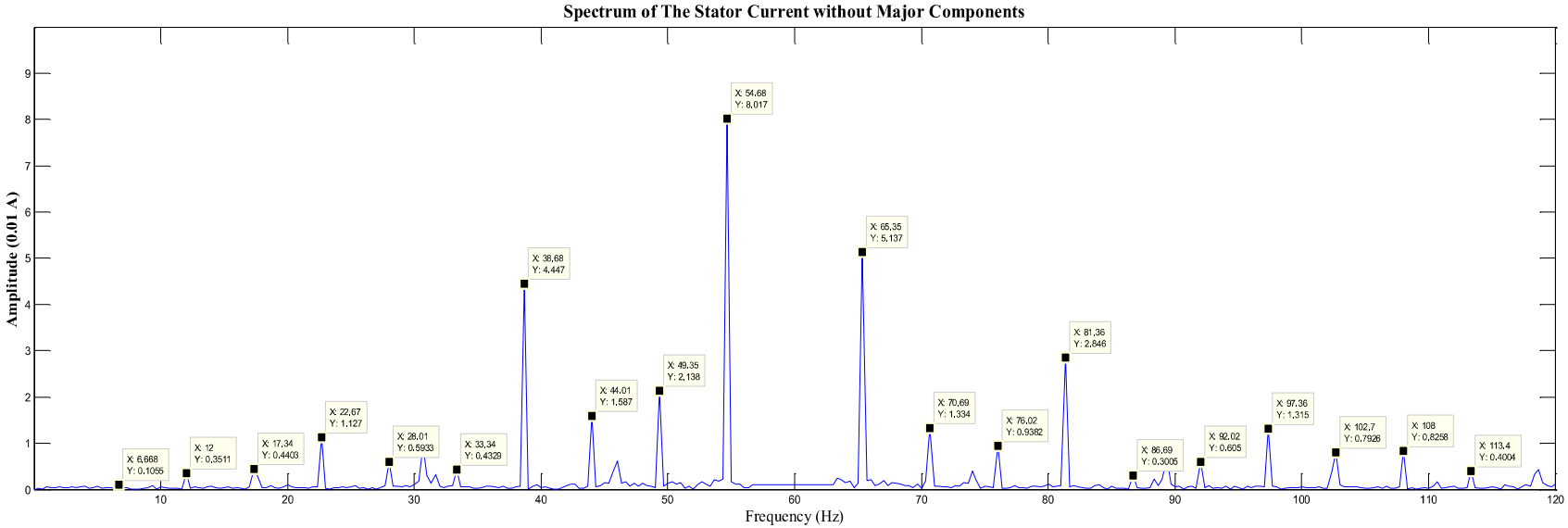

Figure 6.8 A typical FFT spectrum of AHU motor stator current waveform.

The basic derivation procedures for the fan curves are explained in [92]. The airflow is determined by the fan construction and mechanical power applied. Based on the equation of energy conversion and momentum equation, the relationship of mechanical power and airflow under certain speed can be expressed [92] by the following equation:

$$P_m = \rho_0 V[(\omega_r \frac{d}{2})^2 + \frac{V}{b \tan\theta}] \tag{6.13}$$

where P_m is the mechanical power, ρ_0 is the density of air, V is the airflow, ω_r is the rotor angular speed, d is the diameter of the wheel, b is the width of wheel and θ is the tangent angle of blade outer side, which in our case is 30 degrees.

With different rotation speeds, the airflow and mechanical power is expressed by different lines in Figure 6.9.

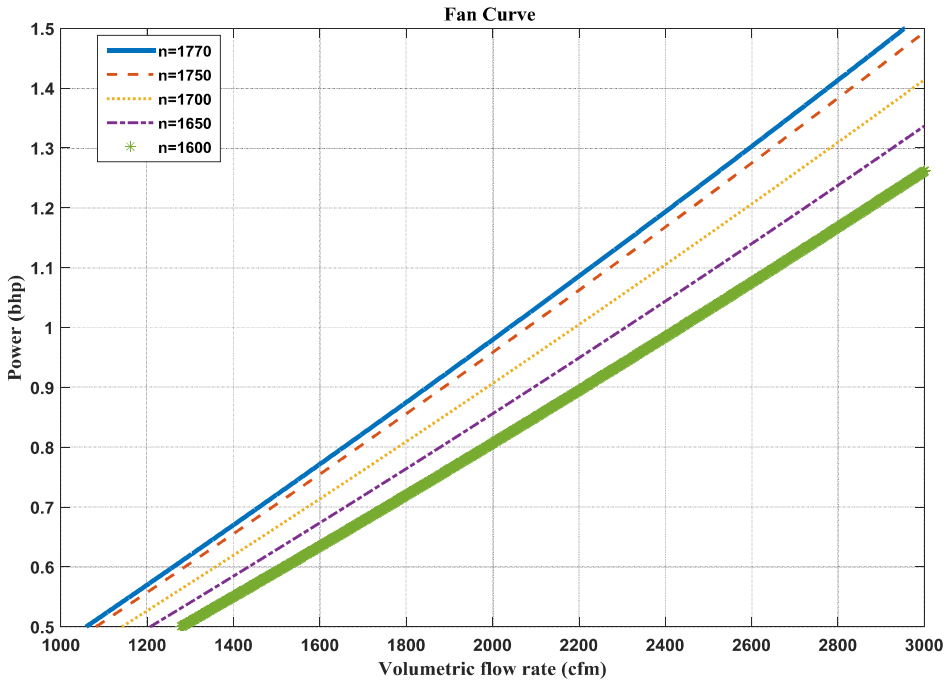

Figure 6.9 Fan curves of the AHU based on (6.13).

The airflow corresponding to a particular value of mechanical power can be found from

the series of curves. It needs to be clarified that (6.13) only works under certain assumptions and within a reasonable flow-rate range, dependent on different types of blowers. In this work, all the experiment and test are located in the reasonable range to guarantee the validity of (6.13).

6.3.3 Experiment Design and Instructions

The conceptual figure of the experimental AHU is shown in Figure 6.10. This unit was designed to be part of a split air-conditioning system, with an evaporator and filter holder located at the front side, and was configured as an "up-flow" mode, which means that the air was intake from below and output in the top of the air handler unit. The unit is equipped with a 54-blade forward-curved double duct centrifugal fan, which is ten inches in diameter and eleven inches wide, shown in Figure 6.11. This fan is directly attached to the motor shaft via a set screw. It is mounted in the middle of the air handler as shown in Figure 6.10. The air handler is equipped with a 3-phase induction motor, manufactured by BALDOR Electric Corp. and its Part Number is RM 3116A. It is a delta-connected 4-pole, 60 Hz, induction machine. The nameplate is shown in Figure 6.12. The measuring point of the system is shown in Figure 6.13, a 3-phase disconnection switch box. The motor is connected to the electric utility through a circuit breaker which is the installation point of the voltage and current sensors. One line to line voltage is monitored via a voltage probe (Tektronix P5205). Similarly, two current probes (Tektronix TCP303) are used to measure the phase currents I_A and I_B. Finally, these three signals are inputs to an oscilloscope via a computer interface (Tektronix TDS 5054). The voltage across each pair of stator windings, as well as the currents will be measured synchronously. The measuring devices are shown in Figure 6.14.

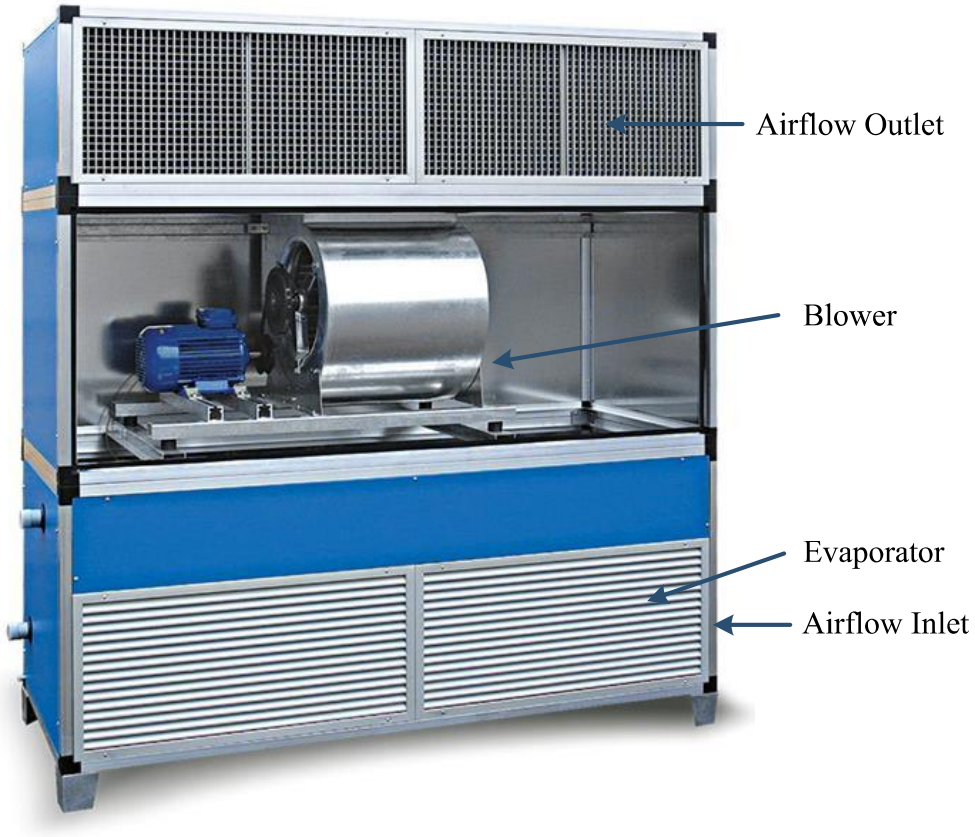

Figure 6.10 The experimental AHU in this dissertation.

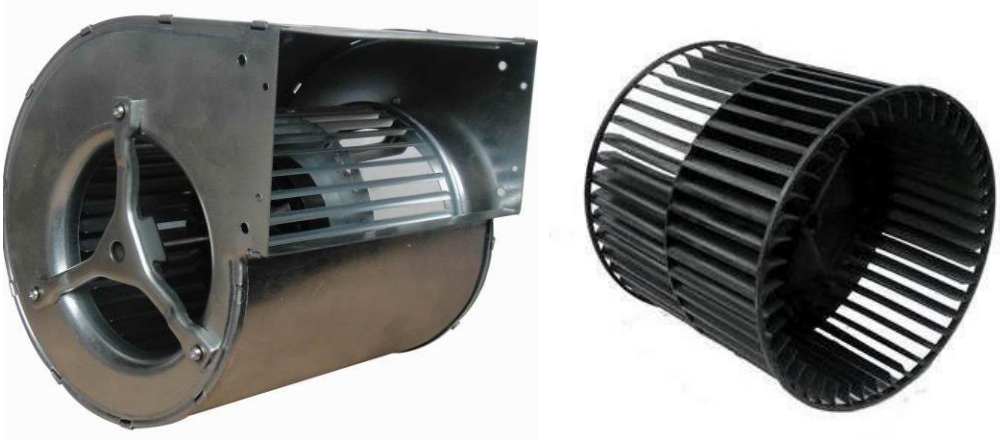

Figure 6.11 The internal structure of a blower.

Part Detail							
Revision:	-	Status:	PRD/A	Change #:		Proprietary:	No
Type:	AC	Prod. Type:	3516M	Elec. Spec:	35WGM137	CD Diagram:	
Enclosure:	OPEN	Mfg Plant:		Mech. Spec:	35E411	Layout:	
Frame:	56H	Mounting:	F1	Poles:	04	Created Date:	08-27-2010
Base:	RS	Rotation:	R	Insulation:	B	Eff. Date:	09-08-2010
Leads:	12#18	Literature:		Elec. Diagram:		Replaced By:	

Nameplate NP1257L							
CAT.NO.	RM3116A						
SPEC.	35E411M137G1						
HP	1						
VOLTS	208-230/460						
AMP	3.38-3.12/1.56						
RPM	1750						
FRAME	56H	HZ	60	PH	3		
SER.F.	1.15	CODE	M	DES	B	CL	B
NEMA-NOM-EFF	82.5	PF	73				
RATING	40C AMB-CONT						
CC		USABLE AT 208V					
DE	6203	ODE	6203				
ENCL	OPEN	SN					

Figure 6.12 The specs of the motor.

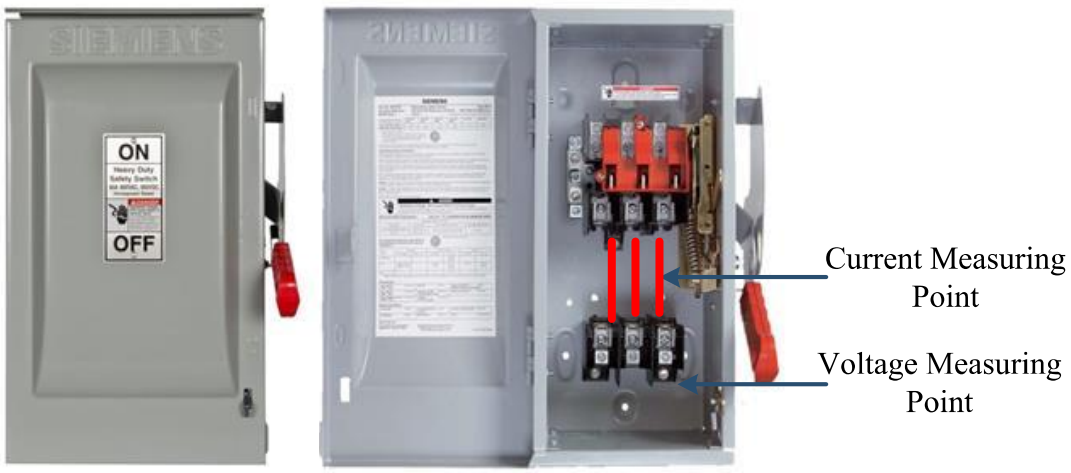

Figure 6.13 Measuring points at disconnected box.

Finally, the airflow speed is measured at the outlet, shown in Figure 6.15 by an air flow probe (TMA-21HW). The airflow measurement is repeated 5 times at different locations shown in Figure 6.15.

Figure 6.14 Data acquisition system, oscilloscope, current probe, and voltage probe from left to right.

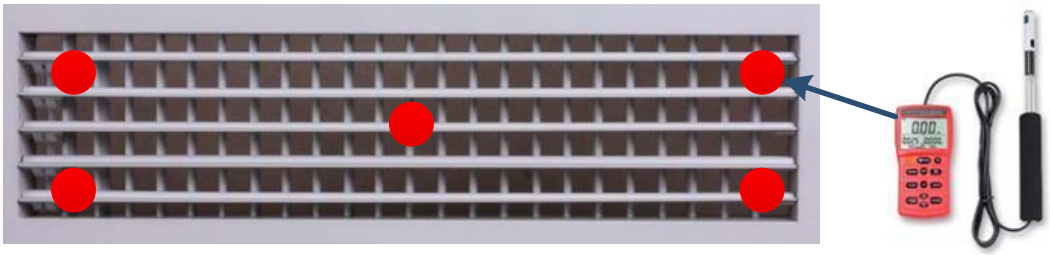

Figure 6.15 Airflow speed measurement points.

6.3.4 Experiment and Data Collection

To monitor the stator current under different airflow rate, the inlet of AHU will be blocked by a hard board simulating the dirty filters as shown in Figure 6.16. To assume the real situation, the experiment is conducted based on the blockage area. Five conditions will be implemented, i.e. open area, half of the open area, a quarter of the open area, 1/6 of the open area, and fully blocked. It is noted that the size of open area cannot represent the airflow rate and airflow input amount. The real airflow rate and input amount are monitored by the airflow probe simultaneously. Under each condition, three measurements are implemented with different sampling frequencies, i.e. 10 kHz, 5 kHz, and 2 kHz. Therefore there are 15 groups of datasets. Each dataset includes two stator currents and one line-to-line voltage of the induction motor. Table 6.2 summarizes the collected data.

Figure 6.16 The blockage method in the experiment.

Table 6.2 Summary of the measured data.

Sampling Frequency	Open Area
10 kHz	100%, 50%, 25%, 17%, and 0%
5 kHz	100%, 50%, 25%, 17%, and 0%
2 kHz	100%, 50%, 25%, 17%, and 0%

6.3.5 Simulation and Results Analysis

6.3.5.1 Torque Estimation

Based upon the above discussion, the constant motor loss C and rotor resistance R_s need to be provided before the torque estimation. They are typically provided by the manufacturer. However, they are not given directly on the nameplate in our experimental platform. A simple regression analysis is adopted here to estimate these two parameters. Table 6.3 gives the specs of the motor under different load condition which can be found in the datasheet of the motor. According to Table 6.3, a regression analysis for $p_0 - p_m$ against $3I^2$ is implemented based on (6.4). The regression analysis formulation can be expressed as (6.14) and the results are shown in Figure 6.17. In detail, the intercept denotes C (92.73) and the coefficient of the quadratic term denotes R_s (3.43). This regression analysis is only suitable for the range from 75% to 150% of the rated torque. Beyond this scope, the parameters are

not valid with a quadratic fitting line as given by the assumed model.

$$P_0 - P_{em} = 92.7255 + 3 \times 3.4343 I_s^2 \tag{6.14}$$

Table 6.3 Data Specification Under Different Load [29].

% of Rated Load	25	50	75	100	125	150	S.F.
Power Factor	34.0	53.0	66.0	75.0	80.0	84.0	78.0
Efficiency	69.7	79.8	83.1	83.9	83.7	82.5	83.8
Speed	1787.2	1775.3	1763.0	1749.5	1735.1	1715.8	1741.0
Line Amperes	1.01	1.13	1.31	1.51	1.75	2.09	1.65

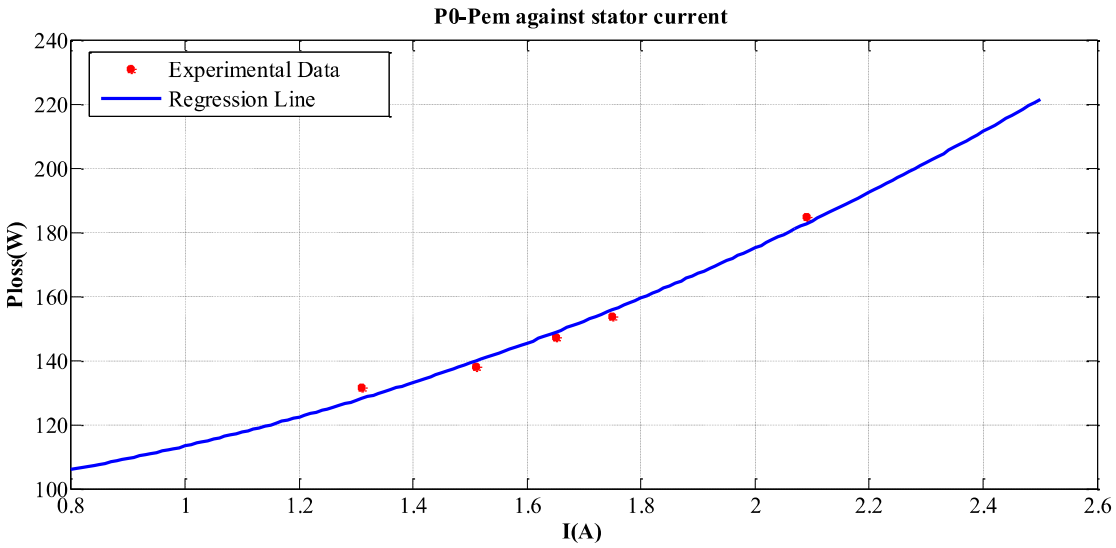

Figure 6.17 Regression Analysis of $p_0 - p_m$ against $3I^2$.

The results of torque estimation under different air blockage scenarios are listed in Table 6.4, where the electromagnetic power is deduced from (6.3), and the toque estimated from (6.4). The table shows an apparent torque decline as airflow blockage increases. As expected, when airflow decreases, less air is propelled from the blower, which reduces the air resistance and torque.

Table 6.4 Results of Torque Estimation.

Open Area	Electrical Power(W)	Electromagnetic Power(W)	Torque(N-m)
100%	1032.5	893.35	4.74
50%	1015.6	873.43	4.63
25%	990.32	854.56	4.53
17%	971.73	841.82	4.47
0%	841.38	719.33	3.82

6.3.5.2 Speed Estimation

The speed is estimated based on the eccentricity harmonics mentioned in the previous section. Five different scenarios are shown from Figure 6.18 to Figure 6.22. To make the spectrum recognizable, a band rejection filter is used to eliminate the main frequency component (60 Hz) and a notch filter is utilized to eliminate the irrelevant low frequency mechanical harmonics. The speeds at different scenarios are calculated based on (6.2). Table 6.5 summarizes the speed estimation results of the five scenarios. It is noted that error exists in the proposed solution due to the resolution of the stator current data. In this case, 1500 cycles are used for the FFT analysis, and the resolution is 0.04 Hz. According to (6.2), the relative error of speed estimation is calculated and listed in Table 6.5 as well. The relative errors are acceptable. Similarly, it shows that speed increases along with airflow as expected. However, the rotor speed is insensitive to air blockage scenarios, therefore is not a perfect indicator for the fault.

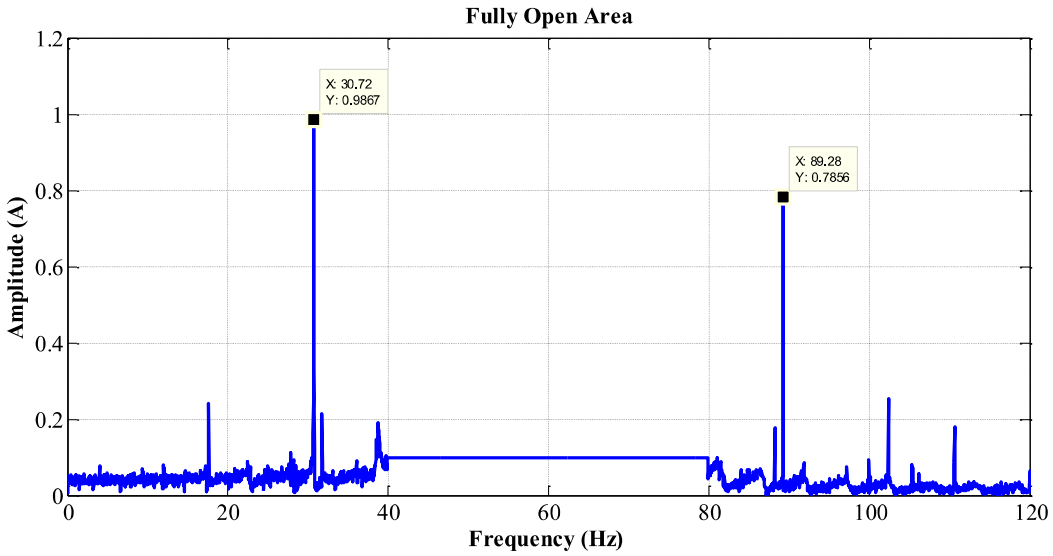

Figure 6.18 The eccentricity harmonics of AHU under the fully open area scenario.

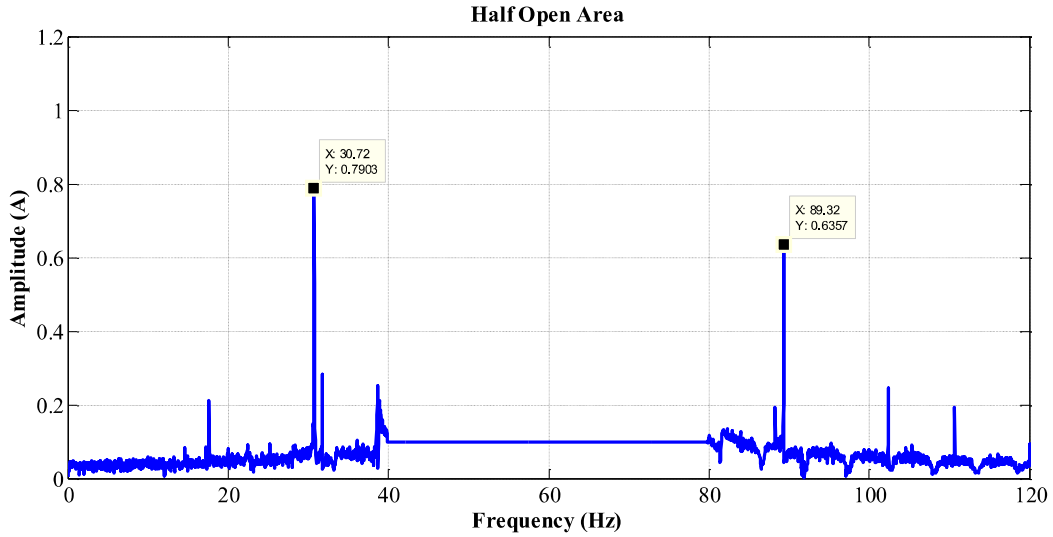

Figure 6.19 The eccentricity harmonics of AHU under the half open area scenario.

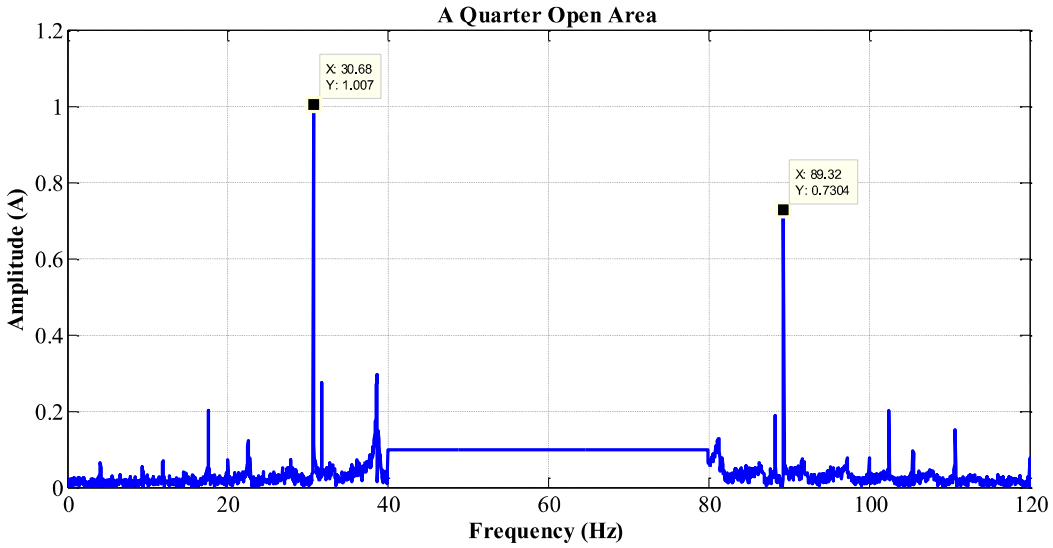

Figure 6.20 The eccentricity harmonics of AHU under the a quarter open area scenario.

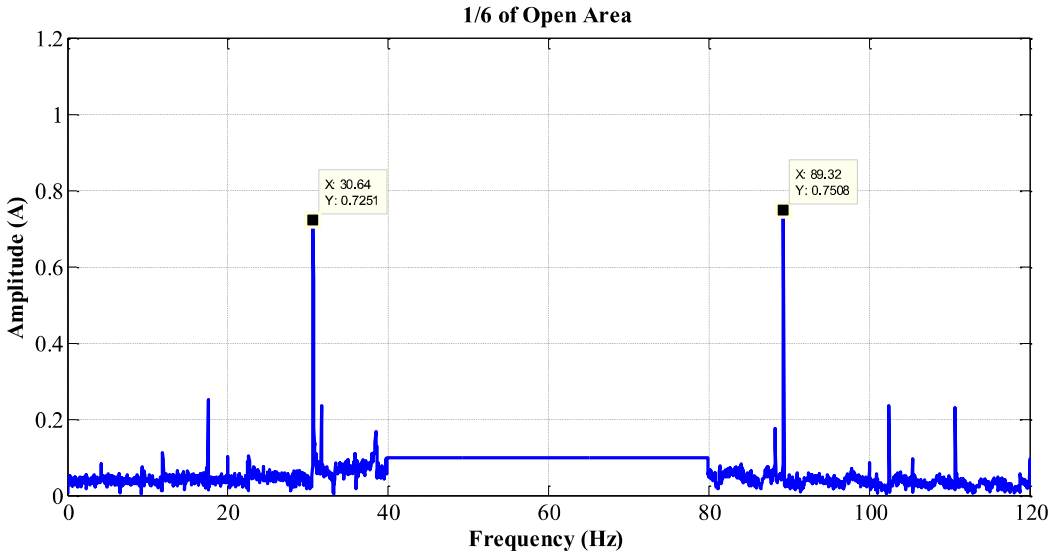

Figure 6.21 The eccentricity harmonics of AHU under the 1/6 of open area scenario.

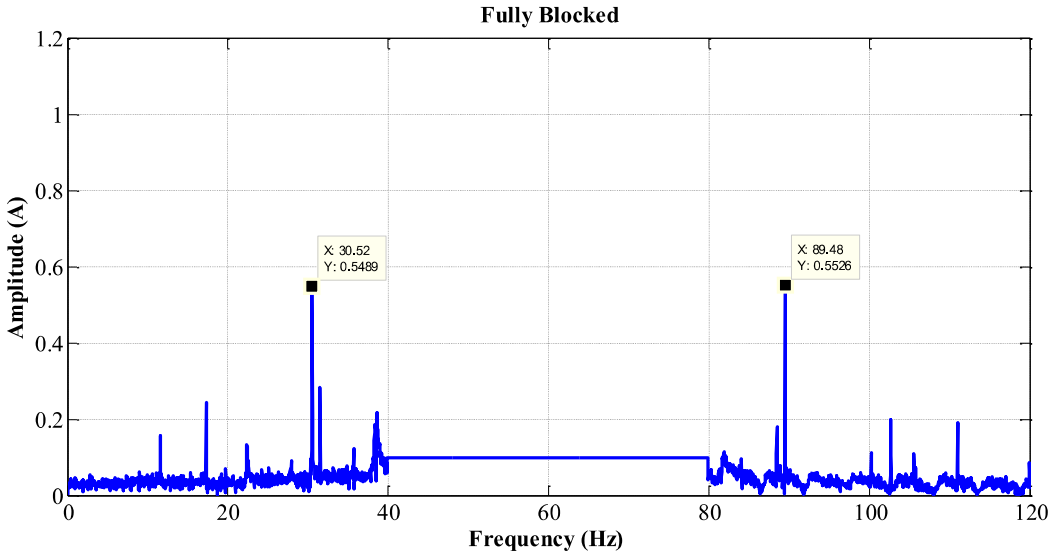

Figure 6.22 The eccentricity harmonics of AHU under the fully blocked scenario.

Table 6.5 Results of speed estimation.

Open Area	Slip (%)	Speed (rpm)	Relative Speed Error (%)
100%	2.44	1756	0.137
50%	2.39	1757	0.137
25%	2.39	1759	0.137
17%	2.27	1760	0.136
0%	1.72	1769	0.136

6.3.5.3 Airflow Fault Detection

To detect the airflow fault, the sideband frequency components needs to be extracted. Based on the (6.11), the value of vibration power can be calculated. Moreover, the airflow can also be estimated based on the (6.13) and the fun curve. To verify the experimental results, the real output airflow is also measured. All these data are shown in Table 6.6. The calculated airflow decreases along with the reduction of the airflow open area, and when the open area approaches fully blocked, the estimated airflow drops sharply as observed in the

real experimental conditions.

Table 6.6 Results of airflow estimation.

Open Area	Vibration Power ($\times 10^{-3}$)	Calculated Airflow (cfm)	Real Airflow (cfm)
100%	123.11	2583	1865
50%	119.37	2525	1819
25%	116.33	2468	1723
17%	114.05	2430	1699
0%	104.66	2070	1366

A regression analysis is implemented for the real and estimated airflow rate against the vibration power. Two quadratic functions are obtained as (6.15) as well as (6.16) and the fitted curve is shown in Figure 6.23. The vibration power is greatly dropped when the AHU is fully blocked. It may act as a good indicator for fault detection. Besides, the trends of estimated airflow rate is same as the real airflow rate, the reason why it higher than the real airflow may be because of the simple of the fan curve model and torque estimation methods. In the real application, instead of absolute value to the airflow rate, customer cares more about the relative change of the airflow rate comparing to the initial state after using certain of time. Therefore, the proposed electrical measurement based airflow rate estimation method is also a simple and cheap way to provide the condition monitoring services for the AHU.

$$V_{est} = -P_{vibration}^2 + 266P_{vibration} - 14293 \tag{6.15}$$

$$V_{real} = -P_{vibration}^2 + 203P_{vibration} - 11393 \tag{6.16}$$

6.3.5.4 Results Analysis

Based on the simulation results, several conclusions are presented below:

1. The mechanical vibration power is a good index to identify the airflow fault of the AHU.
2. The relationship between the mechanical oscillation components and air-flow rate is fitted as a quadratic curve.
3. The estimated airflow rate and motor speed is obviously higher than the actual speed, which is mainly due to the fact that only basic estimation methods are used in this work.
4. To use this method, a base measurement and airflow estimation are required when the AHU is in the commissioning stage.

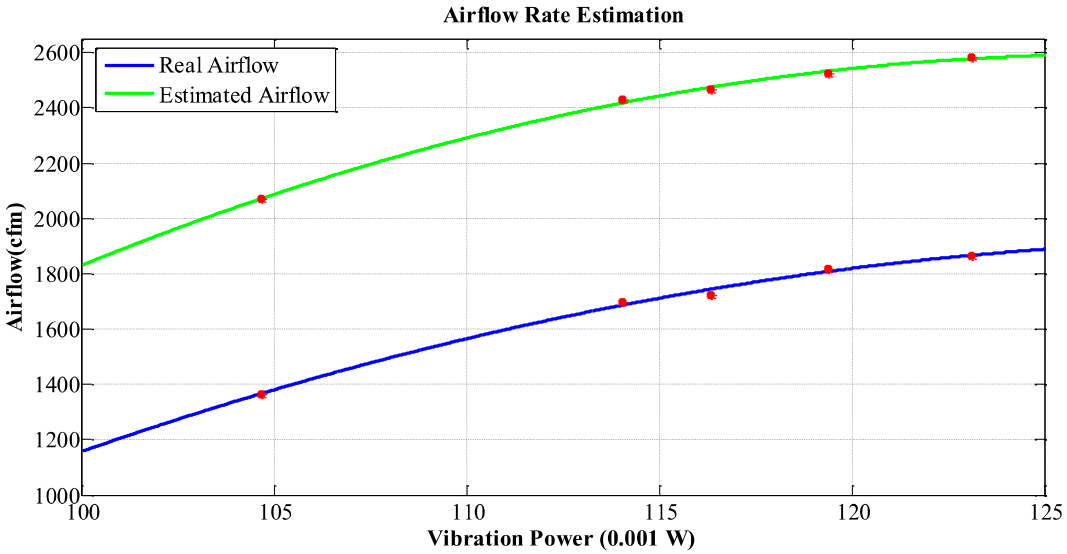

Figure 6.23 Regression analysis for airflow against the vibration power of AHU.

6.4 Refrigerant Fault Detection of an Enclosure Air Conditioner

In addition to the AHU, another important air-conditioning devices used in industry, especially in today's data center is the enclosure air conditioner. They are also known as the cabinet air conditioners [182], as shown in Figure 6.24. It is designed to dissipate heat from the enclosures by cooling the air inside to protect the temperature-sensitive components. They are usually built into the side or rear panel or into the door of the enclosure [183]. Air from the enclosure is sucked through the inlet, through the heating and cooling coil and then accelerated by the fan which propels the air continuously towards the outlet.

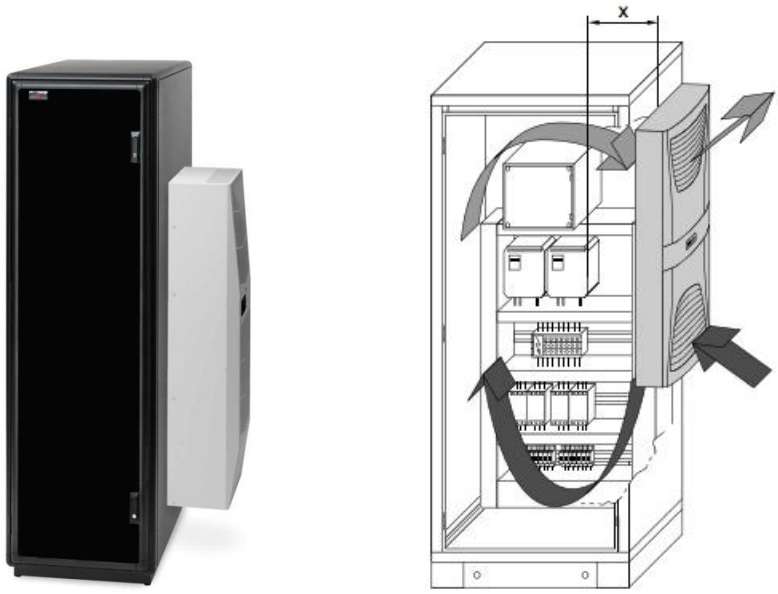

Figure 6.24 The concept figure of an enclosure air conditioner.

The air temperature is controlled by the refrigerant cycle, where the refrigerant transfers the thermal heat from the air around evaporator to the condenser [92]. Figure 6.25 shows the schematic diagram of the regular vapor compression air conditioner. The refrigerant flows clockwise along the arrow, changing the status from the liquid state in the condenser to the vapor state in the evaporator. After travelling through the compressor, the refrigerant is at a high temperature and a high pressure. Then it is cooled by the condenser where the heat is transferred to the air and makes the refrigerant become liquid. The expansion valve that the refrigerant encounters next is used to regulate the flow rate and reduce the pressure. Thus when the liquid flows to the evaporator, it starts to absorb heat like the slackening sponge absorbing water. The heat is therefore transmitted from the evaporator to the condenser [92].

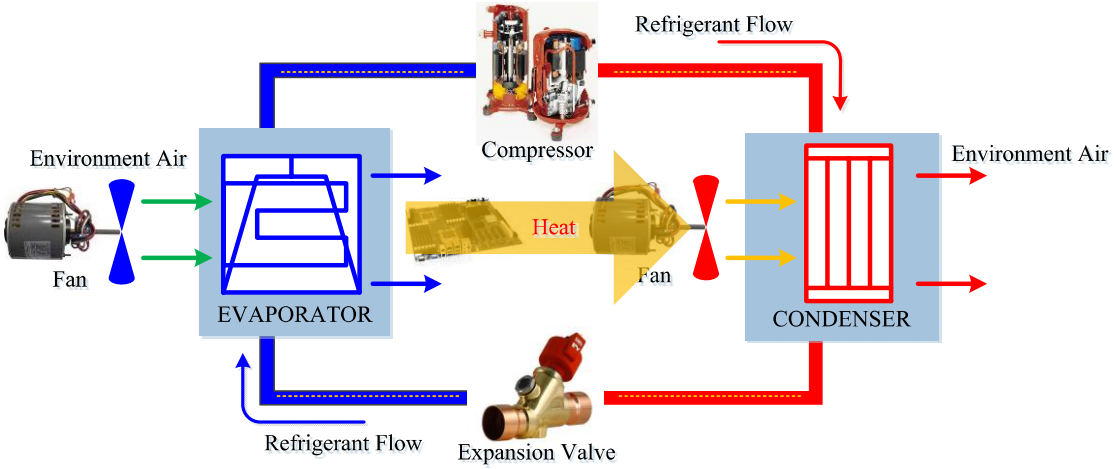

Figure 6.25 Air conditioning cycle schematic diagram.

Faults in the enclosure air conditioner occur in the different parts such as the ducts, fans, compressors and control systems. Among these faults, refrigerant undercharge or overcharge may cause severe effects on the compressor lifetime, the latent heat capacity or even the enclosure system.

The mass of refrigerant is specified for the expected cooling capacity. Too little refrigerant will cause the superheat of the evaporator, thus reduce the heat absorption capacity, while too much refrigerant will result in the higher pressure than rated, which will cause other undesirable effects on the motor. The possible causes for undercharge fault are leakage and mal-installation. The release of the chlorofluorocarbons is well-known for its destructive power to the ozone layer. Moreover the reduced cooling capacity will increase the power loss and thus lower the energy consumption efficiency.

This section describes a sensorless electrical measurement based study and mainly focuses on the refrigerant undercharge fault detection. It proposes a relatively simple fault detection method based on the temperature estimation.

6.4.1 Temperature Based Refrigerant Leakage Detection

As mentioned in above, the temperature of motor will be a good index for the refrigerant condition. Actually, when the refrigerant is insufficient, the cooling capacity is reduced. In order to adjust the temperature to the same level, more cooling cycles will be required for the undercharge condition comparing to the full charge condition, and the torque of compressor will also be higher than the rated value, thus more energy is utilized to drive the motor. As the current magnitude goes higher, the energy loss from the stator and the rotor resistance increases and more heat is produced inside the motor. Because the stator and rotor resistances are assumed to have a linear relationship with the temperature, as the time of use increase, the magnitude of the current of the undercharged air conditioner will be lower than then fully charged one. Therefore, the ultimate goal of this work is changed to the motor resistance estimation.

Much research has been done on the temperature estimation in induction machines during the past few decades [179, 180]. Most of them provided solutions by monitoring the spectrum of stator current. These literatures provide sufficient arguments for the nonintrusive sensorless detection method. Ref [169] is a generally adopted solution, which is greatly applied in the other works. The parameter estimation method based on both transient model and static model is also a generally adopted solution [184]. Recently, in the work did by Z. Gao [185], rotor resistance is used for motor temperature detection, which shows good robustness and accuracy. This work will refer to all these excellent work, and incorporated them into the enclosure air conditioner fault detection.

As shown in Figure 6.5, the parameters are estimated based on (6.11), therefore the rotor resistance can be calculated from the equivalent equation as:

$$R_r(\frac{L_m}{L_r})^2 = s\omega_e(1-\sigma)L_s\sqrt{\frac{\frac{V_s}{I_s}-\omega_e\sigma L_s}{\omega_e L_s-\frac{V_s}{I_s}}} \tag{6.17}$$

Although L_r is still unknown, it will not influence the temperature estimation since both L_m and L_r are not related to the temperature and can be regarded as a constant through the process. Therefore the relationship between the resistance ratio and the temperature can be expressed by (6.18).

$$\frac{R_r(t)}{R_0} = \frac{T(t)+k}{25+k} \tag{6.18}$$

Where, R_0 is the initial resistance value in the ambient temperature, which is 25℃, k is the temperature coefficient, which is preset as 225 here [186].

6.4.2 Experiment Design and Instructions

The structure of a typical enclosure air conditioner is shown in Figure 6.26 with the labeled components in each part. The measuring device printable circuit board (PCB) schematic is shown in Figure 6.27. It is composed of a current sensor, a voltage sensor, and a NI DAQ box. Beside the high frequency measurement (10 kHz), an oscilloscope based low frequency measurement (3600 Hz) is also implemented, which runs every 15 minutes and records only 3-5 minutes current and voltage data. The devices of the low frequency measurement are same as the ones used in the AHU experiment. The current and voltage probe will be applied to record the two-phase currents and one phase voltage information. Since the compressor is paralleled with two fans inside the air conditioner as shown in Figure 6.28, the current measurement data contains two components, i.e. the fan current and the compressor current. Even though both the fun motor currents take up a very small portion of the overall current, they still need to be filtered out to promise the accuracy of the

compressor performance analysis. Figure 6.29 gives a 12-minute startup current curve of the tested enclosure air conditioner. Since both fans run regularly without any fault, a constant phase difference is assumed for the fan current to simplify the filtering process.

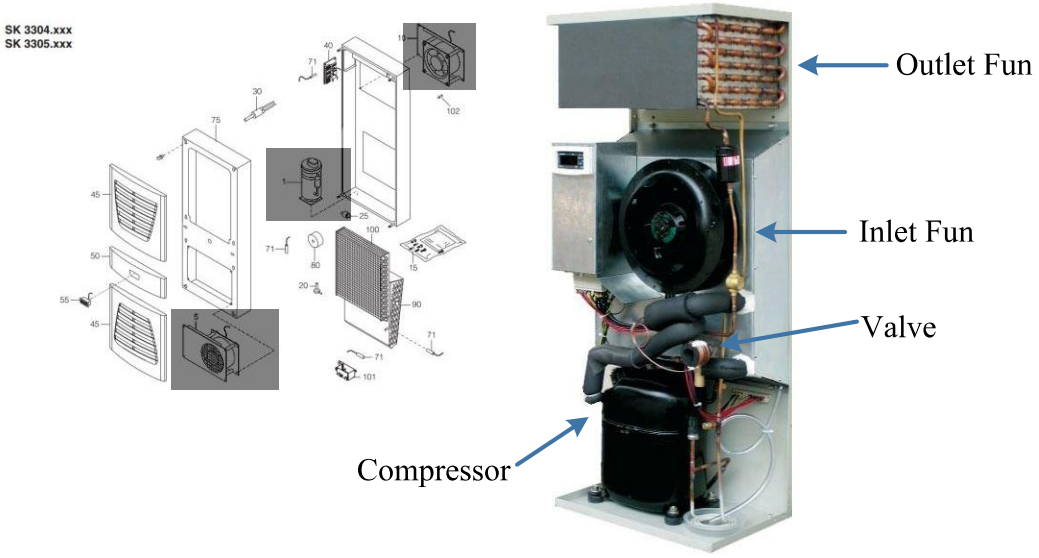

Figure 6.26 Structure of a typical enclosure air conditioner.

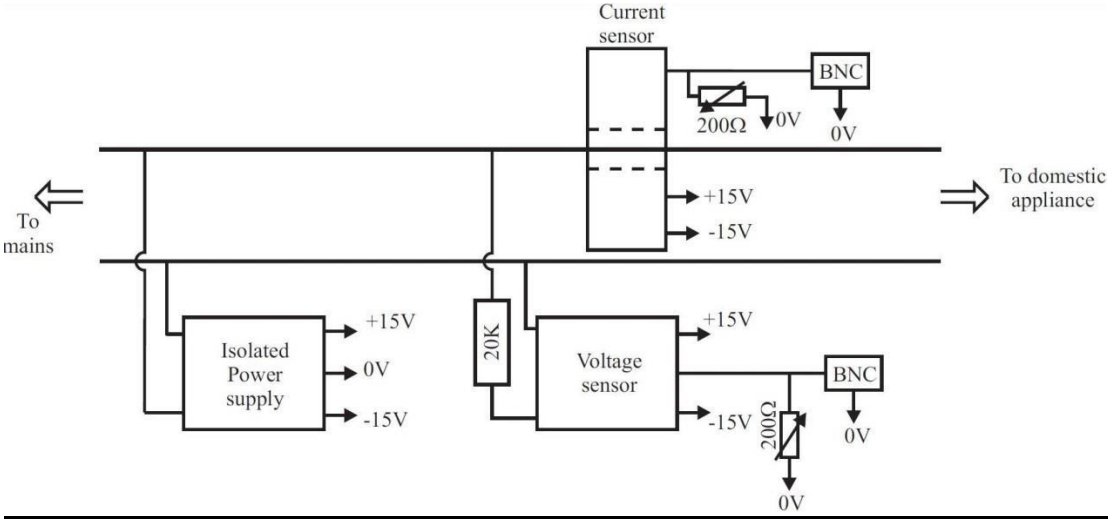

Figure 6.27 Data acquisition devices.

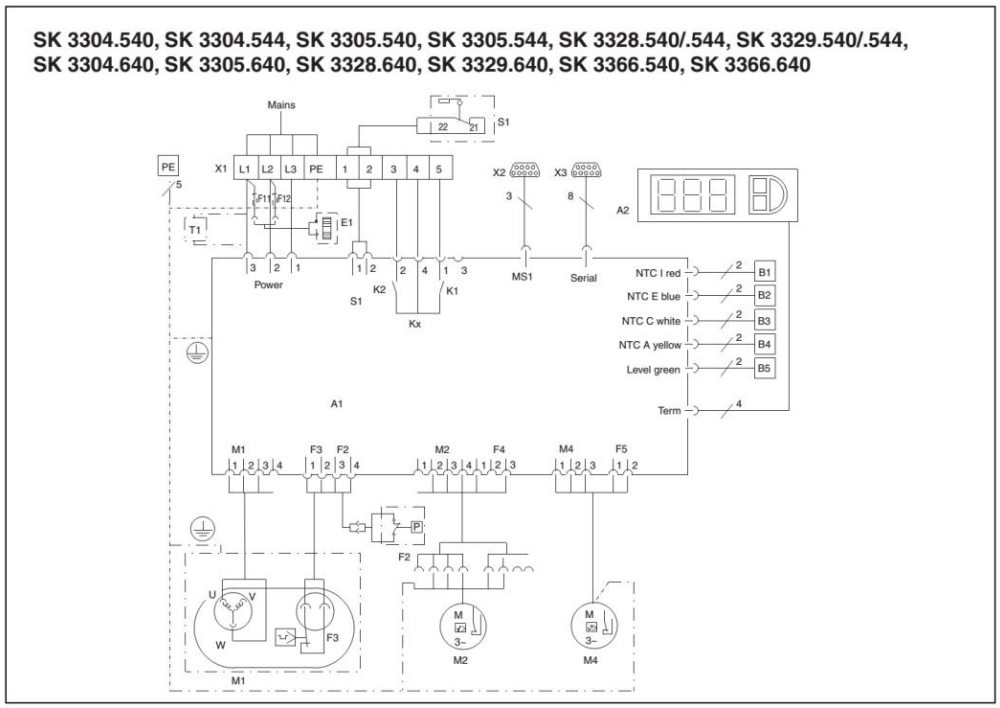

Figure 6.28 Electric circuit scheme of the air conditioner.

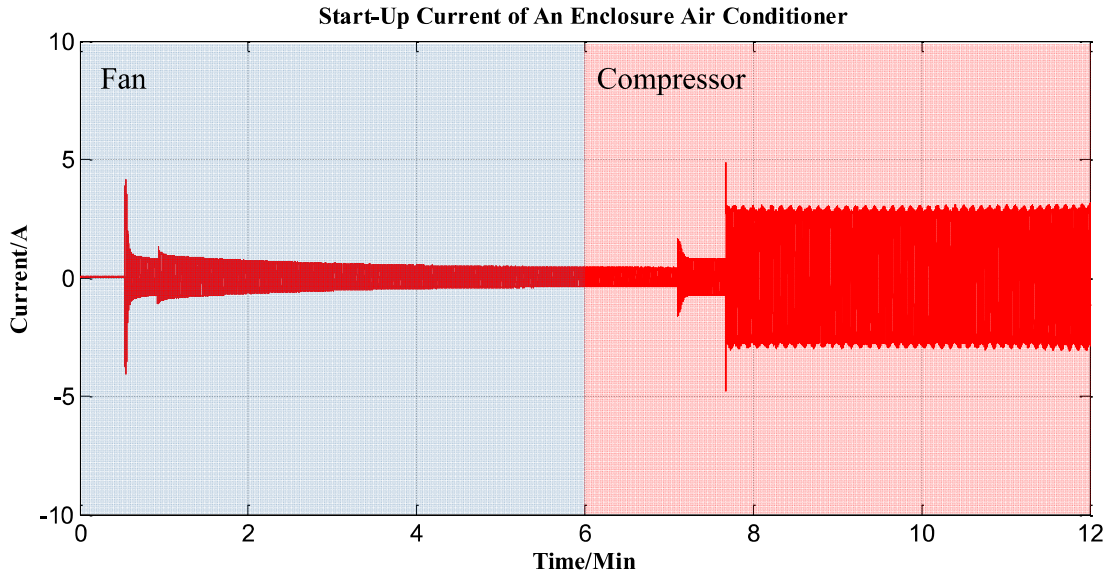

Figure 6.29 Start-up current of an enclosure air conditioner.

In the experiment, the air conditioner is preset to the 22℃ in a space with an initial

ambient temperature of 25℃. It is kept running for one hour. The refrigerant is adjusted to 100% full, 50% full and 25% full by using the scale weighting method [187], strictly consistent to the pressure-temperature chart of R134a. The detailed air conditioner information is shown in Table 6.7. The 10 kHz data are divided to many segments of 2.5s, after filtering out the fan currents. A total 800 datasets of (*Vs*, *Is*) are collected for each test. Table 6.8 gives the summary of the measured data.

Table 6.7 The nameplate of the tested air conditioner.

Nominate	**Number**
Rated current 60 Hz / A	2.9
Start-up current 60 Hz / A	12.7
Useful cooling output L35L35 60 Hz / W	1460
Air throughput, internal circuit / m3/h	600
Air throughput external circuit / m3/h	900
Operating pressure p. max	25 bar
Rated operating voltage V/Hz	400 50/460, 60 3~
Useful cooling output L35L50 60 Hz / W	890
Temperature range °C	+ 20 ° C to + 55 °
Refrigerant	R134a
Start-up current 50 Hz / A	11.5

Table 6.8 Summary of the measured data.

Sampling Frequency	Charging Condition
3.6 kHz	100%, 50%, and 25%
10 kHz	100%, 50%, and 25%

6.4.3 Simulation and Results Analysis

Based upon the models and theories, the required parameters are shown in Table 6.9. These parameters are derived from the 6.2.3. R_s was measured as 5.33 Ω and substituted into the (6.9) as an initial input of the parameter estimation algorithm. The least square method is applied to the (*Vs, Is*) datasets to obtain the parameters.

Table 6.9 Parameters under different conditions.

Condition	Ls	σLs
100%	3.69	0.083
50%	1.44	0.097
25%	0.88	0.112

The results of speed estimation are based on the slot frequency method demonstrated in 6.2.1. One example of the extracted slot harmonics from the undercharge scenario is shown in Figure 6.30. The slot frequency and slip are calculated for each segment, and the trend curves of the slip series under different refrigerant conditions are shown in Figure 6.31.

Given all the analysis above, the rotor resistance are estimated based on (6.17), where $R_r(\frac{L_m}{L_r})^2$ are calculated first. Assuming the initial rotor temperature is the same as the ambient temperature, i.e. 25℃. The time-series temperature curve calculated based on (6.18) can be drawn in Figure 6.32. Furthermore, the trend of temperature can be fitted by an exponential curve. It is clear to see the temperature of undercharge condition is higher than

that in full charge condition in the figure. This proves the theoretical analysis that the compressor has to work 'harder' to compensate the reduced heat capacity with insufficient refrigerant, thus the temperature rises higher than the normal condition.

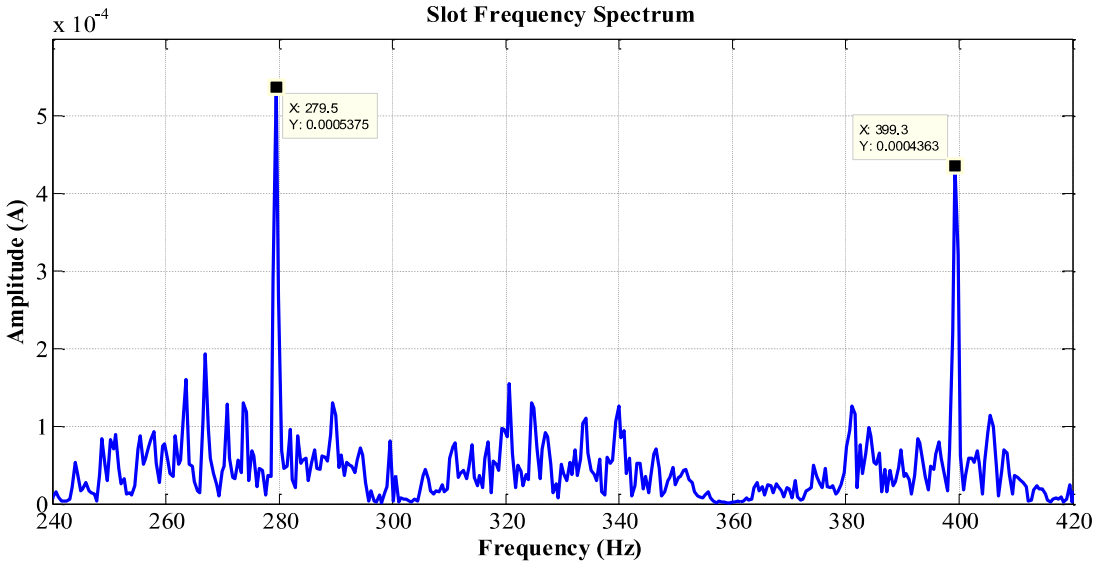

Figure 6.30 A sample slip frequency spectrum of the studied air conditioner.

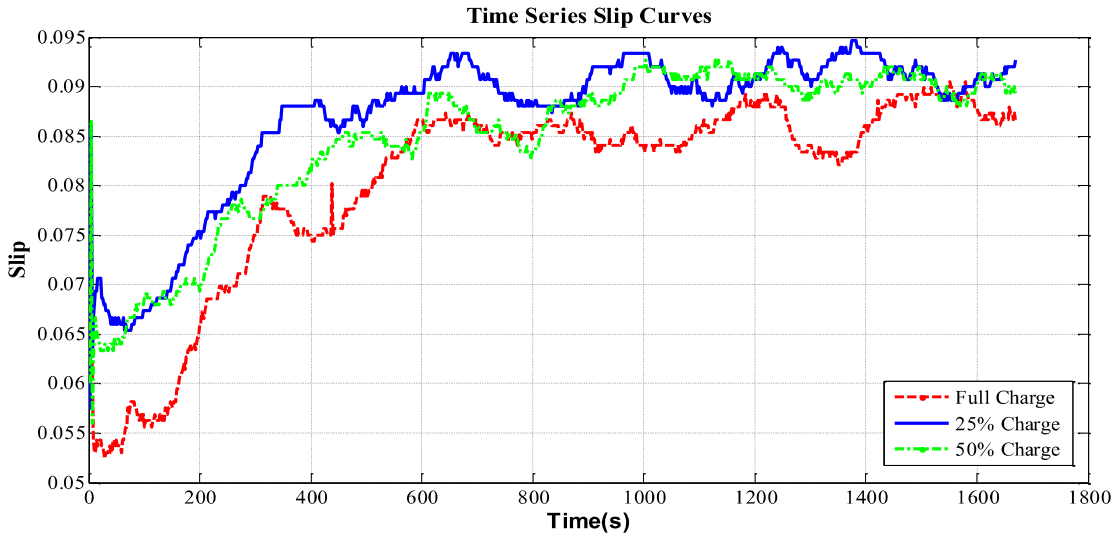

Figure 6.31 The time-series slip curves of the three studied refrigerant conditions.

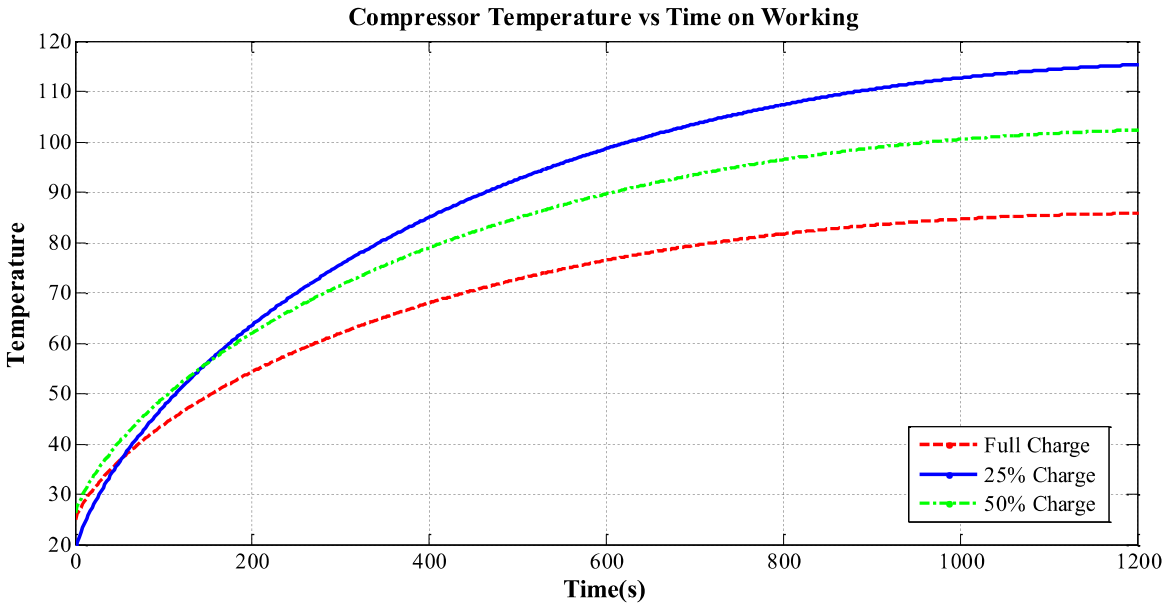

Figure 6.32 Estimated temperature curves of the three studied refrigerant conditions.

Based on the simulation results, several conclusions are presented below:

1. The estimated temperature curve is a good index to identify the refrigerant charge condition of air conditioners which can be used for non-intrusive fault detection.
2. The result is robust and evident to estimate the temperature. The less accuracy of data points in the figure is mainly due to some basic assumption of constant inductance and phase difference.
3. To use this method, the initial ambient temperature should be measured before running the algorithm, while no other input is needed for the method.

6.5 Chapter Summary

This chapter investigates the benefits of the electrically-based fault detection techniques used in the HVAC system. It is proved that the electrical instrumentation is often easier to install, more reliable, and less expensive than comparable mechanical instrumentation. Moreover, electrically-based FDD techniques can have inherent advantages over mechanical

sensors in some circumstances. It is also apparent from the results of this research that the electrical signals contain a significant amount of information about the mechanical state of the system, though many electrical processing methods discard this information, its effective use can provide an abundance of additional information about the state of the system.

To sum up, based on the discussion about the electrically-based FDD method for HVAC, it is believed that its merits and advantages over the conventional methods will make it popular, especially with the development of HEM and smart home.

CHAPTER 7 CONCLUSIONS, CONTRIBUTIONS, AND RECOMMENDATIONS FOR FUTURE WORK

7.1 Conclusions

Achieving a high efficiency and sustainable buildings is a challenge that has to be conquered. The smart building areas that have been developed for the past decades heavily rely on the massive mechanical sensors, offline monitoring and expensive retrofits. The large-scale deployment of small energy efficiency and sustainability techniques requires innovations of advanced monitoring technologies. The proposed research focuses on four aspects of building fault detection: proposing a model-driven feature selection and non-intrusive load monitoring framework, improving the end-device level load identification algorithm by introducing an online learning algorithm, proposing a circuit breaker level load disaggregation algorithm based on the 15-minute resolution smart meter data, and studying the potential of non-intrusive load monitoring technology employed in the fault detection of the air conditioning devices.

A robust feature selection is critical in the non-intrusive load monitoring study, however the available features used today cannot provide sufficient information. It is not even known whether these features are really useful and efficient. The proposed work introduces a new and pioneering prior-knowledge-based model-driven framework. The prior-knowledge includes front-end power supply circuit identification and electrical operating principles. This dissertation proposed a bi-level taxonomy for the load space from the power electronics' point of view. Moreover, a commercial power supply market survey guarantees that the proposed taxonomy represents the majority of appliance loads in the real world. Under the proposed taxonomy, a complete model-driven hierarchical feature extraction

method is presented, and the features extracted from this method prove much simpler and more feasible in differentiating the subtle differences between similar loads.

Even though a model driven solution can improve the identification efficiency and accuracy, it is still impossible to find an algorithm suitable for all the loads in the market, because the new types of load come to the market day by day. The proposed work comes up with an adaptive nonintrusive load identification model to address this problem. The proposed model is not dedicated to identify all the loads around the world, but it will grasp knowledge from samples that are not identified in the real application, and gradually form a new learning procedure so as to identify more and more new samples correctly. Random forest algorithm is introduced here to realize the objective and a case study is carried out to verify the effectiveness of the model. The adaptive model might present a practical and effective future of NILM.

In addition, the amount of data available for training is limited for the end device identification. It impedes the identifier to do a feasible learning. However, at the same time, the large amount of unused smart meter data comes to be the thumb problem for utilities. This work proposes a smart meter analyzer which can estimate the states and power consumptions of the individual load in a residential home, by only utilizing the power signals sampled by a smart meter, i.e., at a low sampling rate of 1 per 15 minutes. The Factorial Hidden Markov Model (FHMM) is adopted here and an adaptive unsupervised learning method, which does not require individual load waveforms or prior load knowledge, is also incorporated into the FHMM. All FHMM structures and parameters are learned automatically from the aggregated signal. A case study is conducted to verify the effectiveness of the proposed smart meter analyzer for those major high power loads in a residential house. Even though the information learnt from the 15-minute resolution smart

meter data cannot be equal to 1Hz data, it still can help utilities and load aggregators in many ways. Since the studied four loads are major demand responsive load. Demand responsive load modeling and DR capacity estimation is one of the very important applications for the proposed study. In addition, DR customer selection based on the statistical analysis of the disaggregated loads by providing the variance and average power of each load is also another important application. These statistic factors act as important metrics in the customer selection and the reward program.

Finally, most of the industrial members and the research institutes have been trying to find a more specific application for NILM with a more reasonable complexity for a long time. The fault detection of the air conditioning system proves to be a promising application area of NILM due to the reduced load space and the rich load data. This work proposes an electrical measurement based study and mainly focuses on the airflow blockage fault and the undercharge of refrigerant, which are two most important faults. The simple non-intrusive fault-detection method is based on the induction machine fault detection works. The fan torque and speed are estimated in order to get the relationship between the airflow variation and the stator current of the induction motor. A real AHU system as well as an enclosure air conditioner is built to validate the proposed solution. The obtained results show a great potential of the electrical measurement based method.

A lot more still need to be done to achieve a future smart building. The methods and discussions presented in this dissertation provide some insights into solving the challenged of the building energy monitoring technology.

7.2 Contributions

The contributions from this dissertation are summarized as follows:

The concept of “a Model-Driven Taxonomy” has been proposed by utilizing a priori

knowledge of appliances. This includes front-end electronic circuit topologies, electrical operation principles, and customer behaviors. This concept establishes a full load space, and provides a guideline to deal with the very wide diversity of the plug-in loads.

An extensive study on the power supply topology and the operation principles has been conducted to help establish a hierarchical structure taxonomy of appliances with a 95% coverage of present loads. The advantage of this multilevel structure taxonomy and the feasibility analysis of this multilevel structure have also been discussed in the dissertation.

The feature extraction has been driven by the understanding of the relationship between different steady state current waveforms and their corresponding circuit topologies and operation principles. The preliminary analysis has proved that this established relation is very helpful to optimize the feature space and to define simpler features.

Instead of introducing more features, an adaptive solution consisting of an unknown detection and an online identification are proposed for device level load identification. The adaptive solution proves to be able to recognize those easily misclassified loads as unknown loads first, and then correctly identify them after gaining knowledge. This adaptive model might present a practical and effective future for NILM in the energy auditing application.

A smart meter data disaggregation analysis is conducted and an unsupervised learning algorithm that can learn automatically without individual load waveforms or any other a priori load knowledge is proposed. The proposed algorithm estimates the number of loads and their parameters from only the aggregated signal.

An iterative learning framework as well as some new usage behavior features like usage duration and time stamp are introduced to overcome the challenge of low sampling frequency and further enhance the learning performance by greatly increasing the disaggregation rate of simultaneous events.

A new airflow fault detection method for the AHU is proposed. Based on the simulation results, a good indicator to detect the airflow fault of the AHU is introduced, which is the mechanical vibration power in the stator current spectrum. The relationship between the index and air-flow rate is fitted as a quadratic curve. The proposed non-intrusive solution outperforms in an online fault detection model and cost savings than the conventional mechanical measurement based solution.

A new refrigerant undercharge detection method for the enclosure air conditioner is proposed. It proposes a relatively simple fault detection method based on the rotor temperature estimation. Based on the simulation results, the rotor temperature in the undercharge condition is obviously higher than that in the full charge condition. The proposed non-intrusive solution outperforms in cost saving than the conventional mechanical measurement based solution as well.

Five journal papers, eight conference papers, and three patents have been published from the proposed dissertation research:

D. He, L. Du, Y. Yang, R. G. Harley, and T. G. Habetler, "Front-End Electronic Circuit Topology Analysis for Model-Driven Classification and Monitoring of Appliance Loads in Smart Buildings," *Smart Grid, IEEE Transactions on*, vol.3, no.4, pp.2286-2293, Dec. 2012.

D. He, W. Lin, N. Liu, R. G. Harley, and T. G. Habetler, "Incorporating Non-intrusive Load Monitoring into Building Level Demand Response," *Smart Grid, IEEE Transactions on,* vol.4, no.4, pp.1870,1877, Dec. 2013.

L. Du, Y. Yang, **D. He**, R. G. Harley, and T. G. Habetler, "Feature Extraction for Load Identification Using Long-Term Operating Waveforms," *Smart Grid, IEEE Transactions on*, vol.6, no.2, pp.1870,1877, Mar. 2015.

L. Du, **D. He**, R. G. Harley, and T. G. Habetler, "Electric Load Classification by Binary

Voltage-Current Trajectory Mapping," *Smart Grid, IEEE Transactions on*, accepted.

D. He, L. Du, Y. Yang, R. G. Harley, and T. G. Habetler, "Electronic Circuit Survey for Office Load Monitoring and Identification", *Energy Conversion Congress and Exposition (ECCE)*, 2012 IEEE , pp.1228-1232, 15-20 Sept. 2012

D. He, J. Mei, R. G. Harley, and T. G. Habetler," Utilizing Building-level Demand Response in Frequency Regulation of Actual Microgrids", *IECON 2013 – 39th Annual Conference on IEEE Industrial Electronics Society*.

L. Du, **D. He**, et.al, "Self-Organizing Classification and Identification of Miscellaneous Electric Loads", *Power and Energy Society General Meeting, 2012 IEEE*, pp.1,6, 22-26 July 2012, San Diego, CA, USA.

W. Lin, **D. He**, R. Xia, and T. G. Habetler, "The Impact of Demand Response on Rural Island Power System Operation," *IEEE PES GM 2013*, Vancouver, CA, July 2013.

L. Du, Y. Yang, **D. He**, R. G. Harley, T. G. Habetler, and B. Lu, "Support vector machine based methods for non-intrusive identification of miscellaneous electric loads", *IECON 2012 – 38th Annual Conference on IEEE Industrial Electronics Society*, pp.4866-4871, 25-28 Oct. 2012

D. He, J. Mei, R. G. Harley and T. G. Habetler, "A Study on Electrical Operation Principles of the Residential Loads for Building Monitoring," *IEEE PES GM 2014*, Washington DC, July 2013, under review.

Mei. J, S. Yan, G. Qu, and **D. He**, "Design Considerations for Non-Intrusive Load Monitoring Hardware Platforms in Smart Building," *Industry Applications Society Annual Meeting*, 2013 IEEE, pp. 1-6, 6-11 Oct, 2013

Mei. J, **D. He**, R. Harley, and T. Habetler, "Random Forest Based Adaptive Non-Intrusive Load Identification," *World Congress on Computational Intelligence*, 2014 IEEE,

pp.1978-1983, 6-11 Jul 2014

Y. Yang, L. Du, **D. He**, "Method And System Employing Graphical Electric Load Categorization to Identify One of A Plurality of Different Electric Load Types," US Patent 20,140,365,490.

Y. Yang, L. Du, **D. He**, "System and Method for Instantaneous Power Decomposition and Estimation," US Patent 20,140,371,932.

L. Du, Y. Yang, R. G. Harley, and T. G. Habetler, **D. He**, "Method And System Employing Finite State Machine Modeling To Identify One Of A Plurality Of Different Electric Load Types," US Patent 20,140,371,932.

7.3 Recommendations for Future Work

The following investigations are recommended for the continuing research based on the results presented in this dissertation work.

7.3.1 Data Acquisition and Feature Study

Since the load space and consumer electronics technology updates very quickly, new loads come to the market day by day. The knowledge database has to be updated time by time. Actually, as the development of the proposed self-adaptive and self-debugging algorithm in this work, a self-learning feature selection method corresponding to the identification algorithm is also expected. Besides, there are no criteria for data acquisition today. The data measured by different researchers cannot be applied by others due to the measuring discrepancy. Therefore, the algorithms are always exclusive to some specific data measured with certain frequency, certain duration at certain point of time, which makes peer evaluation of these algorithms impossible. Moreover, a uniform evaluation system of NILM is absent. A standard bench mark for data collection is also required.

7.3.2 Adaptive Online Learning for Plug-in Load Identification

Even though, the adaptive method can successfully solve the challenge of extreme large load space, the similarity problem is still not be touched at all. Future work should focus on the identification of very similar loads by introducing more features, such as the behavior information. In addition, the parameter selection of the GLR based solution is still empirical which impedes its widely application. A theoretical analysis on the trade-off between precision and recall for the binary classification should be further studied. Finally, the feature selection algorithm also needs to be updated to a self-learning algorithm to overcome the increasing load number.

7.3.3 15-minute Resolution Smart Meter Data Disaggregation

Even though the information learnt from the 15 minute smart meter data can help future utilities and load aggregators in many ways. There are lots of challenges to be solved. First, this work assumes that the load only change its operating modes in a sequential manner, while there always exists some loads with more complicated state transition structures. In addition, this model is based on an assumption that users' habits don't change much in up to three months. And the features of on-duration and starting time may be disturbed by the brown loads or newly-introduced appliances. Future work should be focused on these problems.

7.3.4 Airflow Fault Detection of AHUs

The main contribution of the proposed work is to present the potential application of electrical measurements for AHU fault detection. There are many problems to be solved. The estimated airflow rate and motor speed is obviously higher than the actual speed, which is mainly due to the fact that only basic estimation methods are used. Some more robust speed, torque and airflow estimation methods need to be developed. In addition, the thermal

influence analysis is mandatory before this research comes to an actual application, because some experimental phenomenas show that the change of stator winding temperature has some non-negligible influences on the results.

7.3.5 Refrigerant Fault Detection of Enclosure Air Conditioner

Same as airflow fault detection, this part of study is a preliminary exploration of the potential of NILM used in air-conditioner fault detection. Regarding the refrigerant undercharge detection, several assumptions like constant inductance and constant phase difference are made, which reduces the accuracy of the temperature estimation. Some more accurate parameter estimation method considering the skin effect of the rotor may be introduced. Error analysis is also needed to improve the validity of the proposed method. Finally, the proposed study is still in the concept stage, a detailed industrial application design is also expected.

REFERENCES

[1]. "Annual Energy Review 2011," Energy Information Administration, U.S. Department of Energy, Washington DC, DOC/EIA-0384(2011), 2012.

[2]. C. Haley, C. D. Barley, L. Pratsch, and R. Anderson, "Building America System Research Plan for Reduction of Miscellaneous Electrical Loads in Zero Energy Homes." National Renewable Energy Lab., Golden, CO. Tech. Rep. NREL/TP-550-43718. Nov 2008.

[3]. D. J. Hammerstrom, et al., “Pacific Northwest Grid-Wise Test-bed Projects: Part 1.” Pacific Northwest National Laboratory, PNNL-17167, Olympic Peninsula Project, Richland, WA, 2007.

[4]. S. Li, and A. Pandharipande, "Networked Illumination Control With Distributed Light-Harvesting Wireless Sensors," *Sensors Journal, IEEE* , vol.15, no.3, pp.1662,1669, March 2015.

[5]. A. Abdul Raheem, R.R.A. Issa, S. Olbina, "Energy and indoor comfort analysis of various window-shading assemblies INA hot and humid climate," *Simulation Conference (WSC), 2014 Winter* , pp.3200,3211, 7-10 Dec. 2014

[6]. M. Zeifman and K. Roth, "Nonintrusive Appliance Load Monitoring: Review and Outlook", IEEE Transactions on Consumer Electronics, vol. 57, no. 1, pp. 76-84, Feb 2011.

[7]. Google PowerMeter Press, “Google PowerMeter: A Google.org Project.” [Online Document], 2011, Available HTTP://www.google.com/powermeter/about/.

[8]. S. Lukovic, V. Congradac, and F. Kulic, "A System Level Model of Possible Integration of Building Management System in SmartGrid," in *Complexity in Engineering, 2010. COMPENG '10.*, 2010, pp. 58-60.

[9]. W. Kastner, G. Neugschwandtner, S. Soucek, and H. M. Newmann, "Communication Systems for Building Automation and Control," *Proceedings of the IEEE,* vol. 93, pp. 1178-1203, 2005.

[10]. W. Yunfei, I. R. Pordanjani, and W. Xu, "An Event-Driven Demand Response Scheme for Power System Security Enhancement," *Smart Grid, IEEE Transactions on,* vol. 2, pp. 23-29, 2011.

[11]. F. Genova, F. Bellifemine, M. Gaspardone, M. Beoni, A. Cuda, P. Gian, "Thermal and energy management system based on low cost Wireless Sensor Network Technology, to monitor, control and optimize energy consumption in," *Telecommunication - Energy Special Conference (TELESCON), 2009 4th International Conference on* , pp.1,8, 10-13 May 2009.

[12]. G. Koutitas, "Control of Flexible Smart Devices in the Smart Grid," *IEEE Transactions on Smart Grid,* vol. 3, pp. 1333-1343, 2012.

[13]. R. Brennan, T. Wei Tai, D. O'sullivan, M.S. Aslam, S. Rea, D. Pesch, "Open Framework Middleware for intelligent WSN topology adaption in smart buildings," *Ultra Modern Telecommunications & Workshops, 2009. ICUMT '09. International Conference on* , pp.1,7, 12-14 Oct. 2009.

[14]. N. Nhat-Hai, T. Quoc-Tuan, J. Leger, V. Tan-Phu, "A real-time control using wireless sensor network for intelligent energy management system in buildings," *Environmental Energy and Structural Monitoring Systems (EESMS), 2010 IEEE Workshop on* , pp.87,92, 9-9 Sept. 2010.

[15]. Intel Pressroom, “Telecom Service Providers Create New Revenue Source with Cloud-based IoT Platform for Smart Homes”, [Online Document], Available HTTP:// www.intel.com/content/dam/www/program/embedded/internet-of-things/blueprints/iot-cloud-based-platform-for-smart-homes-blueprint.pdf.

[16]. Belkin Web, [Online], Available HTTP://www.belkin.com/us/Products/home-automation/c/wemo-home-automation/.

[17]. A. M. Pasdar, I. H. Cavdar, Y. Sozer, "Power-Line Impedance Estimation at FCC Band Based on Intelligent Home Appliances Status Detection Algorithm Through Their Individual Energy and Impedance Signatures," *Power Delivery, IEEE Transactions on*, vol.29, no.3, pp.1407,1416, June 2014.

[18]. D. Kresta, “Non-intrusive Load Monitoring.” Emerging Technology Evaluation Process Report, Northwest Energy Efficiency Alliance, Portland, OR, 2012.

[19]. G. W. Hart, E. C. Kern, and F. C. Schweppe, "Non- intrusive appliance monitor apparatus," U.S. Patent 4 858 141, Aug. 15, 1989.

[20]. G.W. Hart, “Nonintrusive Appliance Load Monitoring,” *in Proc*. *IEEE PES General Meeting*, vol. 80, pp. 1870-1891, 1992.

[21]. Y. Du, L. Du, B. Lu, R. G. Harley, and T. G. Habetler, "A review of identification and monitoring methods for electric loads in commercial and residential buildings," in *Proc. 2010 IEEE Energy Conversion Conf. and Expo.*, Atlanta, GA, 2010, pp. 4527-4533.

[22]. "Annual Energy Outlook 2010: With Projections to 2035." Energy Information Administration, U.S. Department of Energy, Washington DC, DOC/EIA-0383(2010), 2010.

[23]. Siemens, *Demand Response Solutions for Commercial Buildings*, [Online], Available HTTP://w3.usa.siemens.com/buildingtechnologies/us/en.

[24]. Schneider Electric, *Building Energy Management Solution*, [Online], Available HTTP:// www.powerlogic.com/demos.cfm#.

[25]. Honeywell, *Intelligent Buildings: Automate, Communicate and Integrate* [Online], Available HTTP://buildingsolutions.honeywell.com/en-US/solutions.

[26]. Eaton press, “Eaton can help you building go green”, [Online Document], Available HTTP://www.eaton.com/ecm/idcplg?IdcService=GET_FILE&dID=412248.

[27]. United Technology, *Intelligent Buidling Technologies*, [Online], Available HTTP:// http://www.bis.utc.com/bis/en/worldwide/intelligent-building-technologies/.

[28]. R. Hendron and M. Eastment, "Development of an Energy-Savings Calculation Methodology for Residential Miscellaneous Electric Loads," in *ACEEE Summer Study on Energy Efficiency in Buildings*, Pacific Grove, California, 2006.

[29]. R. Hendron and M. Eastment, "Development of an Energy-Savings Calculation Methodology for Residential Miscellaneous Electric Loads," National Renewable Energy Laboratory, 2006.

[30]. Commertial and Residential Sector Miscellaneous Electricity Consumption: Y2005 and Projections to 2030," TIAX LLC2006.

[31]. J. Rivas. (2009). *Managing Plug Loads*. [Online Document], Available HTTP://www.epa.gov/climateleadership/documents/events/11feb_plugloads.pdf.

[32]. National Renewable Energy Laboratory. (2009). *Getting to Net Zero*. [Online Document], Available HTTP://www.nrel.gov/docs/fy09osti/46382.pdf.

[33]. C. D. Barley, C. Haley, R. Anderson, and L. Pratsch, Building america system research plan for reduction of miscellaneous electrical loads in zero energy homes: National Renewable Energy Laboratory, 2008.

[34]. S. Energy, "Energy Star®," ed, 2002. [Online], Available HTTP:// https://www.energystar.gov/.

[35]. *ENERGY STAR: Standby Power and Energy Vampires*. [Online], Available HTTP://www.energystar.gov/index.cfm?c=about.vampires.

[36]. Lawrence Berkeley National Laboratory: Standby Power Home Page. [Online], Available HTTP://standby.lbl.gov/.

[37]. C. D. Barley, C. Haley, R. Anderson, and L. Pratsch, Building america system research plan for reduction of miscellaneous electrical loads in zero energy homes: National Renewable Energy Laboratory, 2008.

[38]. *Building America: Resources for Energy Efficient Homes*. [Online], Available HTTP://www1.eere.energy.gov/buildings/building_america/.

[39]. National Renewable Energy Laboratory, “ARRA-Funded R&D Projects,” *Residential Building Energy Efficiency Meeting 2010*. [Online Document], Available HTTP://apps1.eere.energy.gov/buildings/publications/pdfs/building_america/ns/plenary_2_emerging_tech.pdf.

[40]. Apple HomeKit, [Online], Available HTTP://developer.apple.com/homekit/.

[41]. *What is Z-Wave home control*, [Online], Available http://www.z-wave.com/what_is_z-wave.

[42]. S. Lipoff, “Home Automation – the Unrealized Promise,” *IEEE Consumer Electronics Society Newsletter*, pp. 13-14, Fall 2010.

[43]. Apple Intelligence, “Review: Belkin Wemo Switch & Motion – home automation for the rest of us,” [Online Document], Available HTTP://9to5mac.com/2013/03/29/review-belkin-wemo-switch-motion-home-automation-for-the-rest-of-us/.

[44]. CAISO, “Demand Response and Energy Efficiency Roadmap”, [Online Document], Available HTTP:// http://www.caiso.com/documents/dr-eeroadmap.pdf.

[45]. S. Ira, et al., “Exploring Natural Gas and Renewables in ERCOT, Part III: The Role of Deemand Response, Energy Efficiency, and Combined Heat & Power”, *Consulting Report prepared for the Texas Clean Energy Coalition*, the Brattle Group, 2014.

[46]. “Assessment of Demand Response and Energy Efficiency Potential for Midwest ISO”, Consulting Report #1314, Global Energy Partners, LLC, July 2010. [Online Document], Available HTTP://elpc.org/wp-content/uploads/2010/09/GEP-Midwest-ISO-DR-and-EE-Potential-Assessment-Vol-1-DRAFT-_3_.pdf.

[47]. H. Christopher, “Integrating Energy Efficiency with Demand Response in NY,” *NYSERDA*, Sep, 2005. [Online Document], Available HTTP://aceee.org/files/pdf/conferences/eer/2005/05eer_chall.pdf.

[48]. P. Palensky and D. Dietrich, "Demand Side Management: Demand Response, Intelligent Energy Systems, and Smart Loads, " *IEEE Transactions on Industrial Informatics,* vol. 7, pp. 381 -388, 2011.

[49]. A. Mohsenian-Rad, V. W. S. Wong, J. Jatskevich, R. Schober, and A. LeonGarcia, "Autonomous Demand-Side Management Based on Game-Theoretic Energy Consumption Scheduling for the Future Smart Grid," *IEEE Transactions on Smart Grid,* vol. 1, pp. 320-331, 2010.

[50]. J. L. Mathieu, P. N. Price, S. Kiliccote, and M. A. Piette, "Quantifying Changes in Building Electricity Use, With Application to Demand Response," *IEEE Transactions on Smart Grid,* vol. 2, pp. 507-518, 2011.

[51]. Q. B. Dam, S. Mohagheghi, and J. Stoupis, "Intelligent Demand Response Scheme for Customer Side Load Management," in *Energy 2030 Conference, 2008. ENERGY 2008. IEEE*, 2008, pp. 1 -7.

[52]. T. Sousa, H. Morais, Z. Vale, P. Faria, and J. Soares, "Intelligent Energy Resource Management Considering Vehicle-to-Grid: A Simulated Annealing Approach," *IEEE Transactions on Smart Grid,* vol. 3, pp. 535-542, 2012.

[53]. A. Sepulveda, L. Paull, W. G. Morsi, H. Li, C. P. Diduch, and C. Liuchen, "A novel demand side management program using water heaters and particle swarm optimization," in *Electric Power and Energy Conference (EPEC), 2010 IEEE*, 2010, pp. 1-5.

[54]. S. Lee, Y. Chon, Y. Kim, R. Ha, and H. Cha, "Occupancy Prediction Algorithms for Thermostat Control Systems Using Mobile Devices," *IEEE Transactions on Smart Grid,* vol. 4, pp. 1332-1340, 2013.

[55]. Y. Guo, M. Pan, Y. Fang, and P. P. Khargonekar, "Decentralized Coordination of Energy Utilization for Residential Households in the Smart Grid," *IEEE Transactions on Smart Grid,* vol. 4, pp. 1341-1350, 2013.

[56]. C. Chen, J. Wang, Y. Heo, and S. Kishore, "MPC-Based Appliance Scheduling for Residential Building Energy Management Controller," *IEEE Transactions on Smart Grid,* vol. 4, pp. 1401 -1410, 2013.

[57]. T. Hubert and S. Grijalva, "Modeling for Residential Electricity Optimization in Dynamic Pricing Environments," *IEEE Transactions on Smart Grid,* vol. 3, pp. 2224-2231, 2012.

[58]. F. Corno and F. Razzak, "Intelligent Energy Optimization for User Intelligible Goals in Smart Home Environments," *IEEE Transactions on Smart Grid,* vol. 3, pp. 2128-2135, 2012.

[59]. I. Georgievski, V. Degeler, G. A. Pagani, N. Tuan Anh, A. Lazovik, and M. Aiello, "Optimizing Energy Costs for Offices Connected to the Smart Grid," *IEEE Transactions on Smart Grid,* vol. 3, pp. 2273-2285, 2012.

[60]. Y. Ozturk, D. Senthilkumar, S. Kumar, and G. Lee, "An Intelligent Home Energy Management System to Improve Demand Response," *IEEE Transactions on Smart Grid,* vol. 4, pp. 694-701, 2013.

[61]. M. Pipattanasomporn, M. Kuzlu, and S. Rahman, "An Algorithm for Intelligent Home Energy Management and Demand Response Analysis," *IEEE Transactions on Smart Grid,* vol. 3, pp. 2166-2173, 2012.

[62]. Y.-W. Chen, X. Chen, and N. Maxemchuk, "The Fair Allocation of Power to Air Conditioners on a Smart Grid," *IEEE Transactions on Smart Grid,* vol. 3, pp. 2188-2195, 2012.

[63]. N. Lu, "An Evaluation of the HVAC Load Potential for Providing Load Balancing Service," *IEEE Transactions on Smart Grid,* vol. 3, pp. 1263-1270, 2012.

[64]. N. Lu and Y. Zhang, "Design Considerations of a Centralized Load Controller Using Thermostatically Controlled Appliances for Continuous Regulation Reserves," *IEEE Transactions on Smart Grid,* vol. 4, pp. 914-921, 2013.

[65]. J. Page, S. Kiliccote, J. H. Dudley, M. A. Piette, A. K. Chiu, B. Kellow*, et al.*," Automated Demand Response Technology Demonstration for Small and Medium Commercial Buildings," Lawrence Berkeley National Laboratory,2011.

[66]. PNNL, *Decision-Making Software for Energy Efficiency*, [Online], Available HTTP://www.pnl.gov/feds/.

[67]. Con Edison, “Energy Efficiency And Demand Management Procedure – General, Calculating Customer Baseline Load,” Feb, 2013. [Online Document], Available HTTP://www.coned.com/energyefficiency/PDF/customer_baseline_load_procedure.pdf.

[68]. Google, *Project Brillo*, [Online], Available HTTP://developers.google.com/brillo/.

[69]. IBM, *Bluemix*, [Online], Available HTTP:// https://console.ng.bluemix.net/.

[70]. D. He; W. Lin; N. Liu, R.G. Harley, T.G. Habetler, "Incorporating Non-Intrusive Load Monitoring Into Building Level Demand Response," *Smart Grid, IEEE Transactions on* , vol.4, no.4, pp.1870,1877, Dec. 2013.

[71]. M. Milam, G. Kumar Venayagamoorthy, "Smart meter deployment: US initiatives," *Innovative Smart Grid Technologies Conference (ISGT), 2014 IEEE PES* , pp.1,5, 19-22 Feb. 2014

[72]. K. McKenney, M. Guernsey, R. Ponoum, and J. Rosenfeld, "Commercial Miscellaneous Electric Loads: Energy Consumption Characterization and Savings Potential in 2008 by Building Type," TIAX LLC, 35 Hartwell Ave. Lexington, MA 02421. Tech. Rep. D0498. May 2010.

[73]. J. Shugars, P. Coleman, C. Payne, and L.V.W. McGrory. “Bridging the efficiency gap: commercial packaged rooftop air conditioners.” *In ACEEE Summer Study*, 2000.

[74]. J. Wen and T.F. Smith. Development and validation of online parameter estimation for HVAC systems. *Journal of Solar Energy Engineering*, 125:324-330, August 2003.

[75]. S. Katipamula, and M. R. Brambley, “Methods for fault detection, diagnostics, and prognostics for building systems—a review, Part I,” *International Journal of Heating, Ventilating, Air Conditioning and Refrigerating Research*, Vol. 11, No. 1, 2005.

[76]. J. Hyvärinen, R. Kohonen, and I. E. Agency, IEA Annex 25 Real Time Simulation of HVAC Systems for Building Optimisation, Fault Detection and Diagnosis: Building Optimisation and Faul Diagnosis System Concept: Technical Research Centre of Finland, Laboratory of Heating and Ventilation, 1993.

[77]. R. Radhakrishnan, D. Nikovski, K. Peker, and A. Divakaran, "A Comparison between Polynomial and Locally Weighted Regression for Fault Detection and Diagnosis of HVAC Equipment," in *IEEE Industrial Electronics, IECON 2006 - 32nd Annual Conference on*, pp. 3668-3673, 2006.

[78]. J. Du and E. Meng-Joo, "An artificial intelligence approach towards fault diagnosis of an air-handling unit," in *Control Conference, 2004. 5th Asian*, pp. 1594-1601 Vol.3, 2004.

[79]. P. Fasolo and D. E. Seborg, "An SQC approach to monitoring and fault detection in HVAC control systems," in *American Control Conference, 1994*, pp. 3055-3059 vol.3, 1994.

[80]. H. Yonghong, L. Nianping, and S. Yangchun, "Automated Fault Detection and Diagnosis for an Air Handling Unit Based on a GA-Trained RBF Network," in *Communications, Circuits and Systems Proceedings, 2006 International Conference on*, pp. 2038-2041, 2006.

[81]. H. Altrabalsi, J. Liao, L. Stankovic, and V. Stankovic, “A low-complexity energy disaggregation method: Performance and robustness”, *IEEE Symposium on Computational Intelligence Applications in Smart Grid (CIASG),* 2014.

[82]. H. Kim, M. Marwah, M. F. Arlitt, G. Lyon and J. Han, “Unsupervised Disaggregation of Low Frequency Power Measurements,” *Proceedings of 11th International Conference on Data Mining*, pp. 747-758, Arizona, 2011.

[83]. J. Z. Kolter, and J. Tommi, "Approximate inference in additive factorial HMMs with application to energy disaggregation," *International Conference on Artificial Intelligence and Statistics*, pp. 1472-1482, 2012.

[84]. F. McQuiston, J. D. Parker, and J.D. Spitler. *Heating, Ventilating, and Air Conditioning: Analysis and Design*. John Wiley and Sons, sixth edition, 2005.

[85]. A. Bejan. *Advanced Engineering Thermodynamics*.(2nd ed.) Wiley Interscience,, 1997.

[86]. S. M. Namburu, M. S. Azam, J. Luo, K. Choi, and K. R. Pattipati, "Data-driven modeling, fault diagnosis and optimal sensor selection for HVAC chillers," *Automation Science and Engineering, IEEE Transactions on,* vol. 4, pp. 469-473, 2007.

[87]. K. Choi, M. Madhavi Namburu, M. Azam, J. Luo, K. Pattipati, and A. Patterson-Hine, "Fault diagnosis in HVAC chillers using data-driven techniques," in *AUTOTESTCON 2004. Proceedings*, 2004, pp. 407-413.

[88]. S. Sultan, T. Khan, and S. Khatoon, "Implementation of hvac system through wireless sensor network," in *Communication Software and Networks, 2010. ICCSN'10. Second International Conference on*, pp. 52-56, 2010.

[89]. S. Chun-Lien, Y. Kuen-Tyng, "Evaluation of Differential Pressure Setpoint of Chilled Water Pumps in Clean Room HVAC Systems for Energy Savings in High-Tech Industries," *Industry Applications, IEEE Transactions on* , vol.49, no.3, pp.1015,1022, May-June 2013.

[90]. R.J. Wiegerink, T.S.J. Lammerink, J. Haneveld, T.A.G. Hageman, J.C. Lötters, "Fully integrated micro coriolis mass flow sensor operating at atmospheric pressure," *Micro Electro Mechanical Systems (MEMS), 2011 IEEE 24th International Conference on* , pp.1135,1138, 23-27 Jan. 2011.

[91]. A.K. Sen, J. Darabi, "Modeling and Optimization of a Microscale Capacitive Humidity Sensor for HVAC Applications," *Sensors Journal, IEEE* , vol.8, no.4, pp.333,340, April 2008.

[92]. C. Laughman, “Fault Detection Methods for Vapor-Compression Air Conditioners Using Electrical Measurements,” Ph.D dissertation, Dept, Architecture, MIT, Cambridge, Boston, 2009

[93]. C. Fischer, “Feedback on household electricity consumption: a tool for saving energy?” *Energy Efficiency* 1 (1): 79-104, 2008.

[94]. A. Faruqui, S. Sergici, and A. Sharif, “The impact of informational feedback on energy consumption - a survey of the experimental evidence,” *Energy* 35 (4): 1598-1608, 2010.

[95]. Ehrhardt-Martinez, K., K. Donnelly, and J. Laitner, “Advanced metering initiatives and residential feedback programs: A meta-review for household electricity-saving opportunities,” Technical Report E105, American Council for an Energy Efficient Economy, Washington D.C., 2010.

[96]. I. Ayres, S. Raseman, and A. Shih, “Evidence from two large field experiments that peer comparison feedback can reduce residential energy usage,” Technical Report 15386, National Bureau of Economic Research, 2009.

[97]. D. Srinivasan, W. S. Ng, A. C. Liew, “Neural-Network-Based Signature Recognition for Harmonic Source Identification,” *IEEE Transactions on Power Delivery*, vol. 21, pp. 398-405, 2006.

[98]. W. Wichakool, A.-T. Avestruz, R. W. Cox, S. B. Leeb, “Modeling and Estimating Current Harmonics of Variable Electronic Loads,” *IEEE Transactions on Power Electronics*, vol. 24, pp. 2803-2811, 2009.

[99]. K. D. Lee, et al., “Estimation of Variable-Speed-Drive Power Consumption from Harmonic Content,” *IEEE Transactions on Energy Conversion*, vol. 20, pp. 566-574, 2005

[100]. S. B. Leeb, S. R. Shaw, J. L. Kirtley, Jr, “Transient Event Detection in Spectral Envelope Estimates for Nonintrusive Load Monitoring,” *IEEE Transactions on Power Delivery*, pp. 1200, 1995.

[101]. F. Sultanem, “Using Appliance Signatures for Monitoring Residential Loads at Meter Panel Level,” *IEEE Transactions on Power Delivery*, vol. 6, pp. 1380-1385, 1991.

[102]. S. N. Patel, et al., “At the Flick of a Switch: Detecting and Classifying Unique Electrical Events on the Residential Power Line,” *in Proc. Conference on Ubiquitous Computing*, 2007, pp. 271-288.

[103]. S. Gupta, M. S. Reynolds, S. N. Patel, “ElectriSense: Single-Point Sensing Using EMI for Electrical Event Detection and Classification in the Home,” *in Proc. Conference on Ubiquitous Computing*, 2010, pp. 139-148.

[104]. W. L. Chan, A. T. P. So, L. L. Lai, “Harmonics Load Signature Recognition by Wavelets Transforms,” *in Proc. International Conference on Electric Utility Deregulation and Restructuring and Power Technologies*, 2000, pp. 666-671.

[105]. W. K. Lee, G. S. K. Fung, H. Y. Lam, F. H. Y. Chan, M. Lucente, “Exploration on Load Signatures,” *in Proc. International Conference on Electrical Engineering (ICEE)*, 2004, ref. 725.

[106]. H.Y. Lam, G. S. K. Fung, W. K. Lee, “A Novel Method to Construct Taxonomy of Electrical Appliances Based on Load Signatures,” *IEEE Transaction on Consumer Electronics,* vol. 53, no. 2, pp. 653-660, May 2007.

[107]. J. Liang, S. K. K. Ng, G. Kendall, J. W. M. Cheng, “Load Signature Study—Part I: Basic Concept, Structure, and Methodology,” *IEEE Transactions on Power Delivery*, vol. 25, pp. 551-560, 2010.

[108]. G. W. Hart, and M. Schwartz, “Two Extensions of the Viterbi Algorithm,” *IEEE Transactions on Information Theory*, vol. 37, pp. 430-436, 1991.

[109]. G. W. Hart, “Correcting Dependent Errors in Sequences Generated by Finite-State Processes,” *IEEE Transactions on Information Theory*, vol. 39, pp. 1249-1260, 1993.

[110]. L. K. Norfold, S. B. Leeb, “Non-intrusive electrical load monitoring in commercial buildings based on steady-state and transient load-detection algorithms,” *Energy and Buildings*, vol. 24, pp. 51-64, 1996.

[111]. C. Laughman, et al., “Power Signature Analysis,” *IEEE Power & Energy Magazine*, pp. 56-63, March/April 2003.

[112]. W. Wichakool, Z. Remscrim, U.A. Orji, S. B. Leeb, "Smart Metering of Variable Power Loads," *Smart Grid, IEEE Transactions on* , vol.6, no.1, pp.189,198, Jan. 2015

[113]. A. I. Albicki and A. Cole, “Data Extraction for Effective Non-Intrusive Identification of Residential Power Loads,” *In Proc. IEEE Instrumentation and Measurement Technology Conference*, pp. 812-815, 1998.

[114]. A. I. Albicki, and A. Cole, “Algorithm for Non-Intrusive Identification of Residential Appliances,” *in Proc. IEEE International Symposium on Circuits and Systems*, vol. III, pp. 338-341, 1998.

[115]. Z. Ghahramani, M. I. Jordan, and P. Smyth, “Factorial hidden Markov models,” in Machine Learning. MIT Press, 1997.

[116]. L. Farinaccio, R. Zmeureanu, “Using a pattern recognition approach to disaggregate the total electricity consumption in a house into the major end-uses,” *Energy and Buildings*, vol. 30, pp. 245-259, 1999.

[117]. M. L. Marceau, R. Zmeureanu., “Nonintrusive Load Disaggregation Computer Program to Estimate the Energy Consumption of Major End Uses in Residential Buildings,” *Energy Conversion & Management*, vol. 41, pp. 1389-1403, 2000.

[118]. M. Baranski, J. Voss, “Non-Intrusive Appliance Load Monitoring Based on an Optical Sensor,” *in Proc. IEEE Power Tech Conference*, 2003.

[119]. M. Baranski, J. Voss, “Genetic Algorithm for Pattern Detection in NIALM Systems,” in Proc. *IEEE International Conference on Systems, Man and Cybernetics*, 2004, pp. 3462-3468.

[120]. M. Baranski, J. Voss, “Detecting Patterns of Appliances from Total Load Data Using a Dynamic Programming Approach,” *in Proc. Fourth IEEE International Conference on Data Mining (ICDM’04)*, 2004.

[121]. M. M. H. Kim, M. Arlitt, G. Lyon, and J. Han, "Unsupervised Disaggregation of Low Frequency Power Measurements," *in Proc. SIAM Conference on Data Mining*, 2011.

[122]. S. Pattem, "Unsupervised Disaggregation for Non-intrusive Load Monitoring," *in Proc. International Conference on Machine Learning and Applications*, 2012.

[123]. O. Parson, S. Ghosh, M. Weal and A. Rogers, “Using hidden markov models for iterative non-intrusive appliance monitoring,” *In Neural Information Processing Systems workshop on Machine Learning for Sustainability*, Sierra Nevada, Spain, 2011.

[124]. O. Parson, S. Ghosh, M. Weal and A. Rogers, “Non-Intrusive Load Monitoring Using Prior Models of General Appliance Types,” *Proceedings of the 26th AAAI Conference on Artificial Intelligence*, April 2012.

[125]. M. Berges, E. Goldman, H. S. Matthews, L. Soibelman, “Learning Systems for Electric Consumption of Buildings,” in Proc. ASCE International Workshop on Computing in Civil Engineering, Austin, Texas, 2009.

[126]. M. Berges, E. Goldman, H. S. Matthews, L. Soibelman, “Enhancing Electricity Audits in Residential Buildings with Nonintrusive Load Monitoring,” Journal of Industrial Ecology, vol. 14, no. 5, pp. 844-858, 2010

[127]. C. Laughman, “Fault Detection Methods for Vapor-Compression Air Conditioners Using Electrical Measurements,” Ph.D Thesis, MIT, Cambridge, Boston, 2009

[128]. U.A. Orji, Z. Remscrim, C. Laughman, S. B. Leeb, W. Wichakool, C. Schantz, R. Cox, J. Paris, J. L. Kirtley, L. K. Norford, "Fault detection and diagnostics for non-intrusive monitoring using motor harmonics," *Applied Power Electronics Conference and Exposition (APEC), 2010 Twenty-Fifth Annual IEEE* , pp.1547,1554, 21-25 Feb. 2010

[129]. K. Srinivasan, "Measurement of air leakage in air-handling units and air conditioning ducts," *Energy and Buildings,* vol. 37, pp. 273-277, 2005.

[130]. ASHRAE, "ASHRAE Handbook: Fundamentals," ed. Atlanta, GA,, 2001.

[131]. P. Francisco and L. Palmiter, "Field evaluation of a new device to measure air handler flow," *ASHRAE Transactions,* vol. 109, pp. 403-412, 2003.

[132]. K. R. D. Westphalen, and J. Brodrick, "Duct leakage fault detection," *ASHRAE Journal,* vol. 47, pp. 56-58, August 2005.

[133]. M. H. F. D. S. a. D. J. Oldham, "The development of a rapid single spectrum method for determining the blockage characteristics of a finite length duct," *Journal of Sound and Vibration,* vol. 243, pp. 625-640, June 2001.

[134]. R. W. Cox, "Minimally intrusive strategies for fault detection and energy monitoring," Ph D, Massachusetts Institute of Technology, 2006.

[135]. D. Y. Goswami*, et al.*, "Effect of refrigerant charge on the performance of air-conditioning systems," in *Energy Conversion Engineering Conference, 1997. IECEC-97., Proceedings of the 32nd Intersociety*, 1997, pp. 1635-1640 vol.3.

[136]. I. Grace*, et al.*, "Sensitivity of refrigeration system performance to charge levels and parameters for on-line leak detection," *Applied Thermal Engineering,* vol. 25, pp. 557-566, 2005.

[137]. K. Assawamartbunlue and M. J. Brandemuehl, "Refrigerant leakage detection and diagnosis for a distributed refrigeration system," *HVAC&R Research,* vol. 12, pp. 389-405, 2006.

[138]. C. Calwell, P. Ostendorp, "80 plus: a strategy for reducing the inherent environmental impacts of computers," *Electronics and the Environment, 2005. Proceedings of the 2005 IEEE International Symposium on* , pp.151,156, 16-19 May 2005.

[139]. K. N. Sakthivel, S. K. Das, K. R. Kini, "Importance of quality AC power distribution and understanding of EMC standards IEC 61000-3-2, IEC 61000-3-3 and IEC 61000-3-11," *Electromagnetic Interference and Compatibility, 2003. INCEMIC 2003. 8th International Conference on* , pp.423,430, 18-19 Dec. 2003

[140]. S. Burdett, J. Allan, B. Mellitt, and J. A. Taufiq, "A study of power factor correction techniques for high power AC locomotives," in *Main Line Railway Electrification, 1989., International Conference on*, 1989, pp. 363-367.

[141]. T. Saitoh, Y. Aota, T. Osaki, R. Konishi, and K. Sugahara, "Current Sensor based Non-intrusive Appliance Recognition for Intelligent Outlet," *presented at the ITC-CSCC,* 2008.

[142]. L. Du, D. He, Y. Yang, J. A. Restrepo, B. Lu, R. G. Harley, T. G. Habetler, "Self-organizing classification and identification of miscellaneous electric loads," *in Proc. IEEE Power and Energy Society General Meeting*, 2012, pp. 1-6.

[143]. L. Du, J. A. Restrepo, Y. Yang, R. G. Harley, T. G. Habetler, "Nonintrusive, Self-Organizing, and Probabilistic Classification and Identification of Plugged-In Electric Loads," *Smart Grid, IEEE Transactions on* , vol.4, no.3, pp.1371,1380, Sept. 2013.

[144]. L. Du, Y. Yang, D. He, R. G. Harley, T. G. Habetler, "Feature Extraction for Load Identification Using Long-Term Operating Waveforms," *Smart Grid, IEEE Transactions on* , vol.6, no.2, pp.819,826, March 2015.

[145]. L. Du, Y. Yang, D. He, R. G. Harley, T. G. Habetler, and B. Lu, "Support vector machine based methods for non-intrusive identification of miscellaneous electric loads", *IECON 2012 – 38th Annual Conference on IEEE Industrial Electronics Society*, pp.4866-4871, 25-28 Oct. 2012

[146]. J. Mei, D. He, R. Harley, and T. Habetler, "Random Forest Based Adaptive Non-Intrusive Load Identification," *World Congress on Computational Intelligence*, 2014 IEEE, pp.1978-1983, 6-11 Jul 2014.

[147]. D. Powers, "Evaluation: From Precision, Recall and F-Measure to ROC, Informedness, Markedness and Correlation". *Journal of Machine Learning Technologies* 2 (1): 37–63, 2011.

[148]. E. Bouyé, V. Durrleman, A. Nikeghbali, et al., "Copula for finance: a reading guide and some applications," *Working Paper of Financial Econometrics Research Centre*, City University Business School, London, 2000.

[149]. M. Akbar and D. Z. A. Khan, "Modified Nonintrusive Appliance Load Monitoring For Nonlinear Devices," *in Multitopic Conference, 2007. INMIC 2007. IEEE International*, 2007, pp. 1-5.

[150]. J. Liang, S. Ng, G. Kendall, and J. Cheng, "Load signature study – Part II: Disaggregation framework, simulation and applications," in Proc. 2010 IEEE Power and Energy Society General Meeting, Minneapolis, MN, July 2010.

[151]. A. Kjersti, "Modelling the dependence structure of financial assets: A survey of four copulas," SAMBA/22/04, December, 2004

[152]. E. Kole, K. Kees, and V. Marno, "Selecting copulas for risk management," *Journal of Banking & Finance* 31.8 (2007): 2405-2423, 2007.

[153]. T. Hastie, R. Tibshirani and J. Friedman, The Elements of Statistical Learning: data mining, inference, and prediction, 2nd edition. New York: Springer, Feb. 2009, p. 587-604.

[154]. L. Breiman, J. Friedman, R. Olshen, and C. Stone, “Classification and Regression Trees”, Wadsworth, 1984.

[155]. L. Breiman, “Bagging Predictors,” *in Machine Learning*, Springer, Volume 24, Issue 2, pp 123-140, August 2001.

[156]. Y. Amit, Y. and D. Geman, “Shape quantization and recognition with randomized trees,” *Neural Computation* 9, 1545-1588, 1997.

[157]. T. K. Ho, “The random subspace method for constructing decision forests,” *IEEE Trans. on Pattern Analysis and Machine Intelligence*, Vol.20, no.8, pp. 832, 844, 1998.

[158]. L. Breiman, “Random Forest,” *in Machine Learning*, Springer, Volume 45, Issue 1, pp 5-32, October 2001.

[159]. A. Saffari, C. Leistner, J. Santner, M. Godec and H. Bischof, “On-line random forests,” In *Computer Vision Workshops (ICCV Workshops), 2009 IEEE 12th International Conference on*, pp. 1393-1400, 2009.

[160]. R. J. Steele and A. E. Raftery, “Performance of Bayesian Model Selection Criteria for Gaussian Mixture Models,” Dept. of Statistics, University of Washington, Tech. Rep. No. 559, September 2009.

[161]. D. He, L. Du, Y. Yang, R. G. Harley, and T. G. Habetler, “Front-End Electronic Circuit Topology Analysis for Model-Driven Classification and Monitoring of Appliance Loads in Smart Buildings,” *IEEE Trans. on Smart Grid*, vol.3, no.4, pp.2286-2293, Dec. 2012.

[162]. A. Iwayemi, C. Zhou, “Leveraging Smart Meters for Residential Energy Disaggregation”, *PES General Meeting, 2014*.

[163]. Kolter, J. Z., Batra, S., and Ng, A. Y. “Energy Disaggregation via Discriminative Sparse Coding,” *In Proceedings of the 24th Annual Conference on Neural Information Processing Systems* (pp. 1153–1161). Vancouver, BC, Canada.

[164]. R. J. Tibshirani and T. B. Arnold, “Introduction to the genlasso package,” 2011.

[165]. A. N. Milioudis, G. T. Andreou, V. N. Katsanou, K. I. Sgouras, D. P. Labridis, "Event detection for load disaggregation in Smart Metering," *Innovative Smart Grid Technologies Europe (ISGT EUROPE), 2013 4th IEEE/PES* , pp.1,5, 6-9 Oct. 2013

[166]. CENTRON Smart Meter Type IIS Spec Sheet, [Online Document], Available HTTP://www.itron.com/na/productsAndServices/Pages/CENTRON.aspx.

[167]. The Demand Response Baseline, the white paper, EnerNoC, U.S., [Online Document], Available HTTP://www.enernoc.com/our-resources/white-papers/

[168]. S. Katipamula, and M. R. Brambley, "Methods for fault detection, diagnostics, and prognostics for building systems—a review, Part I," *International Journal of Heating, Ventilating, Air Conditioning and Refrigerating Research*, Vol. 11, No. 1, 2005.

[169]. K. D. Hurst and T. G. Habetler, "Sensorless speed measurement using current harmonic spectral estimation in induction machine drives," in *Power Electronics Specialists Conference, PESC '94 Record, 25th Annual IEEE*, 1994, pp. 10-15

[170]. K. J. B. H. Guldemir, "An improved approach to the prediction of line current spectrum in induction machines," *Electrical Engineering* vol. 86, pp. 17-24, November, 2003.

[171]. DOE, Improving Motor and Drive System Performance: A Sourcebook for Industry, 2008,Retrieved 31 December 2012.

[172]. T. G. Habetler, D. M. Divan, "Control strategies for direct torque control using discrete pulse modulation," *Industry Applications, IEEE Transactions on* , vol.27, no.5, pp.893,901, Sep/Oct 1991.

[173]. G. S. Buja, R. Menis, M.I. Valla, "Disturbance torque estimation in a sensorless DC drive," *Industrial Electronics, IEEE Transactions on* , vol.42, no.4, pp.351,357, Aug 1995.

[174]. H. Kubota and K. Matsuse, "Disturbance torque estimation for field oriented induction motor drives without rotational transducers," *Proc. IEEE IECON Ind. Electron. Conf.*, pp.336 -339 1992.

[175]. E. Vazquez-Sanchez, J. Gomez-Gil, J. C. Gamazo-Real, J. F. Diez-Higuera, “A New Method for Sensorless Estimation of the Speed and Position in Brushed DC Motors Using Support Vector Machines,” *Industrial Electronics, IEEE Transactions on,* On page(s): 1397 - 1408 Volume: 59, Issue: 3, March 2012.

[176]. C. Laughman, S.B. Leeb, L.K. Norford, S.R. Shaw, P.R. Armstrong, “A two-step method for estimating the parameters of induction machine models,” *Energy Conversion Congress and Exposition, 2009. ECCE 2009. IEEE* , pp.262,269, 20-24 Sept. 2009.

[177]. D. G. Luenberger *Introduction to Dynamic Systems*, 1979 :Wiley.

[178]. J. Cummings, C. Withers Jr. , "Problems Related to Air Handler Leakage," *ASHRAE,* vol. 50, pp. 36-46, Jan. 01, 2008.

[179]. R. R. Schoen*, et al.*, "Motor bearing damage detection using stator current monitoring,"*IEEE Transactions on Industry Applications,* vol. 31, pp. 1274-1279, 1995.

[180]. R. R. Schoen*, et al.*, "An unsupervised, on-line system for induction motor fault detection using stator current monitoring," in *Industry Applications Society Annual Meeting*, 1994, pp. 103-109

[181]. P. Capaldi*, et al.*, "Torque-oscillations damping in micro-cogeneration units with high brake mean pressure engines and PM-brushless generators," *2012 IEEE International Energy Conference and Exhibition (ENERGYCON)*, 2012, pp. 121-126.

[182]. Rittal Inc., [Online], Available HTTP://www.rittal.com/us-en.

[183]. Rittal System, "Cooling Unit Assembly and operating instructions," [Online Document], Available HTTP://www.manualslib.com/manual/835752/Rittal-Sk-3302-Series.html.

[184]. L. Sang-Bin*, et al.*, "An evaluation of model-based stator resistance estimation for induction motor stator winding temperature monitoring," in *Power Engineering Society Winter Meeting, 2002. IEEE*, 2002, p. 1233 vol.2.

[185]. G. Zhi*, et al.*, "A Sensorless Rotor Temperature Estimator for Induction Machines Based on a Current Harmonic Spectral Estimation Scheme," *Industrial Electronics, IEEE Transactions on,* vol. 55, pp. 407-416, 2008.

[186]. "IEEE Standard Test Procedure for Polyphase Induction Motors and Generators," *IEEE Std 112-2004 (Revision of IEEE Std 112-1996),* pp. 0_1-79, 2004.

[187]. *"Procedures for Charging Air Conditioning Systems with Refrigerant*," [Online], Available HTTP://www.trutechtools.com/RefrigerantCharging.

VITA

Dawei He was born in Jilin, China in 1987. He obtained his Bachelor's Degree in Electrical Engineering from Tsinghua University in Beijing, China in 2010. He then joined Georgia Institute of Technology in Atlanta, GA, USA in August 2010, where he obtained his Master's Degree in Electrical Engineering in 2013 and has been working towards his Ph.D. degree.

After he joined Georgia Tech, Dawei has been a graduate research assistant working on non-intrusive load monitoring project. His research interest lies in the broad field of power systems, smart buildings and smart grids, including modeling, control and optimization of power systems as well as electricity market, auditing and modeling energy usage of smart buildings, and employing advanced optimization and data mining knowledge into smart grid applications. During his study at Georgia Tech, he worked as a mentor for undergraduate research in the Opportunity Research Scholars program in the School of Electrical and Computer Engineering at Georgia Tech between 2011 and 2013. His industry experience includes a product development internship at Eaton Innovation Center in 2011, a R&D internship at ABB Corporate Research Center in 2012 and a costumer oriented product development internship at ALSTOM Grid in 2013.

Dawei He is the recipient of the American Public Power Associate Student Research Scholarship in 2013 and IEEE Computational Intelligence Society Student Research Award, in 2012.